Nonlinear Excitation of Photoactivated Molecules: Two-Photon Absorption Spectroscopy, Dynamics, and Quantum Yields

By

Amanda Lynn Houk

Submitted to the graduate degree program in the Department of Chemistry and the Graduate Faculty of the University of Kansas in partial fulfillment of the requirements for the degree of Doctor of Philosophy.

_____

Chairperson, Christopher G. Elles

_____

Ward H. Thompson

_____

Carey K. Johnson

_____

Robert C. Dunn

_____

Hui Zhao

Date Defended: October 21, 2015

The Dissertation Committee for Amanda Lynn Houk
certifies that this is the approved version of the following dissertation:

Nonlinear Excitation of Photoactivated Molecules: Two-Photon Absorption Spectroscopy, Dynamics, and Quantum Yields

_____

Chairperson, Christopher G. Elles

Date approved: October 21, 2015

Abstract

Higher-lying excited electronic states of model, photoactivated molecules are studied using nonlinear excitation to explore the electronic spectroscopy, excited-state dynamics, and reaction quantum yields. The photoactivated molecules studied in this dissertation include two photochromic molecules, stilbene and 1,2-bis(2,4-dimethyl-5-phenyl-3-thienyl)perfluoro-cyclopentene, that reversibly convert between different isomers following irradiation, as well as a photoactivated protecting group, *para*-hydroxyphenacyl, that photochemically releases a bound substrate. Studying higher-lying excited states above S_1 following nonlinear excitation provides information about the initially excited state, the subsequent excited-state dynamics, and the reaction quantum efficiency. Much less is known about the higher-lying excited states as compared to the well-studied ground and lowest-lying excited states, which motivates the work in this dissertation to investigate the higher-lying excited states of photoactivated molecules following nonlinear excitation.

The measurements of the higher-lying excited states reported here include a broadband pump-probe technique that is used to measure the two-photon absorption spectroscopy, as well as the excited-state dynamics following linear and nonlinear excitation of the studied photoactivated molecules. The broadband two-photon absorption spectroscopy measurements reveal the two-photon accessible states and their absolute two-photon absorption cross sections. Separate measurements of the excited-state dynamics and of the reaction quantum yields following nonlinear excitation collectively provide information about the behavior of the higher-lying excited-states, and how the identity of the excited states affect the outcome of the photochemical reactions. Probing the spectroscopy, dynamics, and quantum yields of the studied photoactivated molecules is important to develop a fundamental understanding of photochemical

reactions from higher-lying excited states. The spectroscopy, dynamics, and quantum yield measurements in this dissertation can also serve as new benchmarks for computational studies of these model molecules.

Dedication

To my husband, without your constant love, support, and encouragement I would not be where I am today and for that I am forever grateful.

Acknowledgements

First, I would like to thank my advisor, Chris Elles, for his mentorship, guidance, and encouragement over the past five years while a member of his group. I thank him for inspiring and encouraging me to always strive to be the best scientist I can be. I am appreciative of the time he has devoted to teaching me everything I know about ultrafast spectroscopy and nonlinear optics. Also, for giving me so many enriching opportunities to mentor students doing research in his laboratory and for the many opportunities to present our research to local, national, and international audiences from coast-to-coast. Chris has nourished my desire to continue to do meaningful scientific research, for that I am truly thankful for everything he has done for me!

I would also like to thank all of the past and present members of the Elles research group: Dr. Igor Zheldakov, Dr. Cassie Ward, Jenna Lindsey, Tim Quincy, Chris Otolski, Matt Barclay, Tyler Tommey, Samantha Allen, John Bliss, Will Cleek, and Emmaline Lorenzo. Thanks goes to all of them for their contributions to this research and stimulating discussions about research problems, as well as for their moral support over the past 5 years.

Special thank you to Dr. Richard Givens for being such an easygoing scientific collaborator and for supporting my research. I am also appreciative of our stimulating scientific conversations and of his willingness to share his scientific insight with me.

I would like to thank my friends near and far for their continued support throughout my graduate career. I would also like to thank my entire family for their unwavering love and support throughout my educational journey. Most importantly I would like to thank my husband Levi for being my rock through this entire journey, without him none of this would be possible! I am so blessed to have so many wonderful people in my life!

Finally, I would like to thank my committee, Dr. Christopher Elles, Dr. Ward Thompson, Dr. Carey Johnson, Dr. Robert Dunn, and Dr. Hui Zhao.

Table of Contents

List of Figures

List of Tables

1. Introduction

1.1 Nonlinear Excitation of Higher-Lying Excited States

This dissertation explores the electronic spectroscopy, excited-state dynamics, and reaction quantum yields of photoactivated molecules following nonlinear excitation. The insight we obtain from our nonlinear excitation measurements can be used to broaden our understanding of higher-lying excited states, which then can be used to control photochemical reactions by preferentially exciting states that may lead to favorable reaction pathways. These experiments also provide information about higher-lying excited states of several model compounds that can serve as benchmarks for experimental and computational studies of the excited-state energies, excited-state dynamics, and quantum yields.

Nonlinear excitation processes, namely two-photon excitation, can be used to selectively control reaction pathways and even the efficiency of photochemical reactions.[1-19] Studying the dynamics from higher-lying excited electronic states above S_1 following nonlinear excitation provides information about the initially excited state and also about the relaxation mechanism. Much less is known about the higher-lying excited states as compared to the well-studied ground and lowest-lying excited states for most molecules. Studying the excited-state dynamics from these higher-lying states is challenging because of the increasing density of states and strong configurational mixing, which leads to ultrafast electronic relaxation to the lowest excited state, S_1, consistent with Kasha's rule.[20] Computational measurements of higher-lying excited states are difficult, especially for two-photon accessible states that primarily have double-excitation character.[21-25] By studying higher-lying excited states that are accessed with nonlinear excitation we can gain a better fundamental understanding of these states, which can be utilized to control the outcome of photochemical reactions.

The work in this dissertation uses broadband two-photon absorption (2PA) spectroscopy to measure broadband 2PA spectra, absolute 2PA cross sections, and to determine the symmetry character of excited states. We use these 2PA measurements to assign specific electronic states to the observed 2PA transitions. We also measure the excited-state dynamics from highly excited two-photon accessible states to obtain information about the initially excited electronic states as well as about the relaxation pathway that can affect the reaction quantum yields.[26-29] Typically, highly-excited states relax on the order of hundreds of fs to lower-lying excited states through internal conversion[20] and once relaxed to lower-lying excited states the molecule can follow the same dynamics as with linear excitation.[1-4,6,12,15,17] Conversely, previous studies have also shown that some molecules excited to two-photon accessible states may undergo different excited-state dynamics and access reaction pathways that are inaccessible with one photon.[5,7-11,13,18,19] When different reaction pathways are accessed the efficiency of the reaction can be modified; particularly, the reaction dynamics and quantum yields following irradiation with one or more photons.[7-9,18,19]

1.2 Advantages of Using Two-Photon Excitation

Nonlinear excitation induces a photochemical reaction with two or more photons, unlike linear excitation with only a single photon. Usually, nonlinear excitation refers to a two-photon excitation, which occurs through the simultaneous absorption of two photons, where the total energy of the two photons is equal to a two-photon allowed transition. The decrease or loss of intensity, I, of the single laser beam passing through a sample path length in the z direction is proportional to the square of the intensity.

$$\frac{\partial I}{\partial z} = -\beta I^2 \qquad (1)$$

Here β is the two-photon absorption coefficient and I is the excitation pulse intensity. The right side of Equation 1 is dependent on the square of the intensity, which leads to the transmitted intensity from a single laser field having a quadratic dependence as a function of the incident intensity, indicating a two-photon absorption. Figure 1.1 shows the degenerate excitation as two red arrows. Generally, two-photon absorption is only observed at very high photon flux since the probability of a two-photon absorption is small compared to a linear absorption.

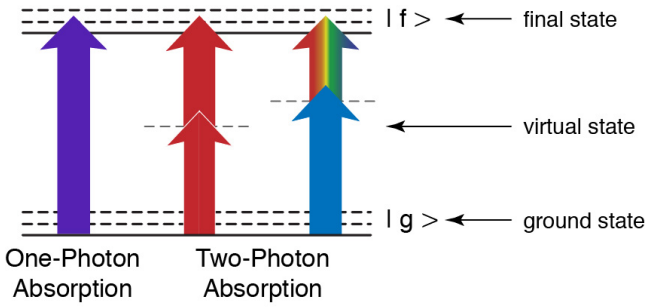

Figure 1.1 Energy level diagram of one- and two-photon absorption.

Two-photon excitation is also possible through the interaction of two different fields with intensity, I_{pump} and I_{probe}. For example, broadband 2PA spectroscopy measurement uses two fields to induce a two-photon excitation, one from a pump beam and another from a probe beam.

$$\frac{\partial I}{\partial z} = -\beta\, I_{\text{pump}}\, I_{\text{probe}} \qquad (2)$$

Here I_{pump} and I_{probe} are the excitation pulse intensities of pump and probe fields, respectively. The set of blue and multicolored arrows on the right side of Figure 1.1 represent the pump and probe pulses in the broadband 2PA spectroscopy measurement, respectively. The pump pulse is monochromatic light and the broadband probe pulse consists of a white-light continuum. Two-photon absorption is measured when the total energy of one pump and one probe photon are equal with a two-photon allowed transition.

Figure 1.1 shows that two-photon absorption proceeds through a nonresonant intermediate state (*i.e.* virtual state), which does not correspond to any electronic or vibrational energy eigenstate and has a short lifetime compared to eigenstates of the system. The virtual state can be represented as a sum-over-states, where the 2PA cross section (σ_{2PA}) is,

$$\sigma_{2PA} \propto \sum_k \left[\frac{\langle g|\mu\cdot\boldsymbol{\varepsilon}_{\text{pump}}|k\rangle\langle k|\mu\cdot\boldsymbol{\varepsilon}_{\text{probe}}|f\rangle}{\hbar\omega_{\text{pump}} - E_{\text{kg}}} + \frac{\langle g|\mu\cdot\boldsymbol{\varepsilon}_{\text{probe}}|k\rangle\langle k|\mu\cdot\boldsymbol{\varepsilon}_{\text{pump}}|f\rangle}{\hbar\omega_{\text{probe}} - E_{\text{kg}}} \right]^2 \quad (3)$$

Here μ is the dipole operator, $\boldsymbol{\varepsilon}_{\text{pump}}$ and $\boldsymbol{\varepsilon}_{\text{probe}}$ are the polarization vectors of the absorbed photons, ω_{pump} and ω_{probe} are the photon frequencies, and E_{kg} is the energy between the ground state *g* and the intermediate state *k*. The first term in Equation 3 represents the absorption of a pump photon from the ground electronic state *g* to an intermediate state *k*, followed by the absorption of a probe photon to reach the final electronic state *f*, and the second term in Equation 3 is the possibility of absorbing the probe photon first followed by the pump photon. The denominator of each term in Equation 3 is the energy difference between the excitation energy of one absorbing photon and the energy of the eigenstates of the system. The individual terms become large when the difference in energies in the denominator becomes small, meaning the absorbing photon becomes nearly resonant with an electronic transition.

The one- and two-photon absorption properties of molecules are dependent on the molecular symmetry of the system.[30-34] Molecules are assigned to point groups based on the molecular symmetry and the point group determines the parity selection rules of the system. For a molecule with an inversion center the parity selection rules are strict thus the one- and two-photon accessible states are different.[30-34] For example, excited states that are normally forbidden through one-photon transitions become allowed for two-photon absorption by centrosymmetric molecules.[30-34] Specifically, when the ground state of a centrosymmetric molecule is of *gerade* (even) symmetry two-photon transitions only access other *gerade* states, while *ungerade* (odd)

states are accessed by one-photon transitions.[30-34] For noncentrosymmetric molecules these parity selection rules are not mutually exclusive for one- and two-photon absorption but the symmetry of the final excited state and the polarization of the excitation beam determines which two-photon absorption transitions are preferentially excited.[32,34-36]

1.3 Nonlinear Excitation Measurements of Photoactivated Molecules

The molecular systems studied throughout this dissertation include two photochromic molecules, stilbene and 1,2-bis(2,4-dimethyl-5-phenyl-3-thienyl)perfluoro-cyclopentene (DMPT-PFCP), as well as a phototrigger molecule, *para*-hydroxyphenacyl (*p*HP). Photochromic molecules undergo reversible photochemical reactions, which include photoisomerization and photocyclization.[13,37-39] Phototriggers are a series of molecules that can be used to spatially and temporally control the release of bound substrates.[40-42] We use nonlinear excitation to study the electronic spectroscopy, excited-state dynamics, and reaction quantum yields of these photochromic and phototrigger molecules. The experimental and data analysis methods used throughout this dissertation are described in **Chapter 2**.

1.3.1 Photochromic Molecules

Photochromic molecules reversibly convert between different isomers following irradiation with light. These molecules can be used for materials science applications.[33,43,44] More specifically, the nonlinear absorption properties can be utilized for applications ranging from optical data storage[13,33,44,45] to three-dimensional microfabrication[33,44,46] to optical power limiting.[33,47] However, for photochromic molecules to be used in these applications the molecule must possess desirable properties that include thermal stability, fatigue resistance, rapid response

time, and high sensitivity.[13,38,48-52]

Stilbene is one of the simplest photochromic molecules and has been extensively studied, making stilbene an ideal model compound for exploring new techniques and dynamics.[37-39,48,53] Figure 1.2 shows that *trans*-stilbene undergoes photoisomerization to *cis*-stilbene and, following further irradiation, cyclizes to 4a,4b-dihydrophenanthrene, which irreversibly oxidizes to phenanthrene.

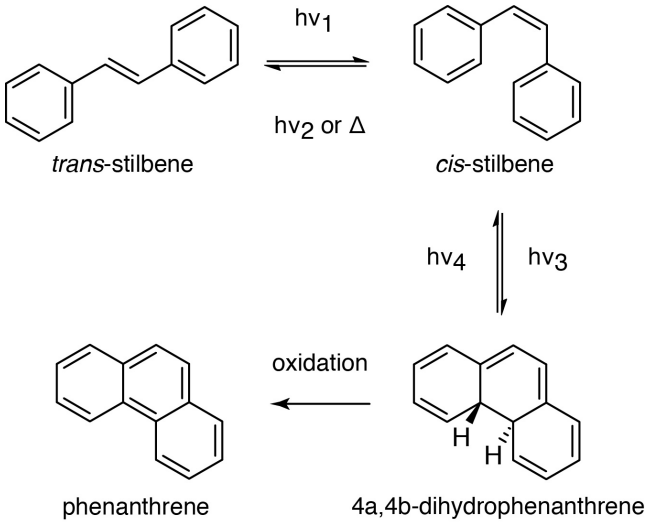

Figure 1.2 Stilbene photoisomerization and photocyclization reactions.

The excited-state dynamics of *trans*-stilbene from the lowest-lying excited state (S_1) to the ground state are well known.[37,39,53] However, much less is known about the two-photon accessible excited states for stilbene and additional measurements were necessary to measure the two-photon absorption properties. **Chapter 3** explores the two-photon accessible excited states of *trans*-stilbene through complimentary measurements of the broadband two-photon absorption (2PA) spectroscopy and of the excited-state dynamics following degenerate two-photon excitation. The broadband 2PA spectroscopy reveals distinct absorption bands near 5.1 and 6.4

eV. In separate measurements, the 2PA bands are excited with a degenerate two-photon excitation to probe the excited-state dynamics from those states. The dynamics reveal rapid relaxation from the initially excited states to S_1 in ~100 fs through internal conversion, which then lead to the same dynamics as linear excitation. The one- and two-photon absorption spectroscopy of the stilbene series, which includes *trans*-stilbene, *cis*-stilbene, and phenanthrene, are compared in **Chapter 4**. The experimentally measured excited-state transition energies and absolute 2PA cross sections are compared to computationally calculated transition energies and 2PA cross sections found in the literature. This series of molecules serves as a consistent benchmark for high-level computational measurements.

DMPT-PFCP (Figure 1.3) is a more complex photochromic molecule that is locked into a *cis* configuration due to the addition of a perfluorocyclopentene ring to the central C=C double bond, so the photocyclization reaction is preferentially selected over photoisomerization. Figure 1.3 shows that DMPT-PFCP undergoes reversible cyclization and cycloreversion when irradiated with light.

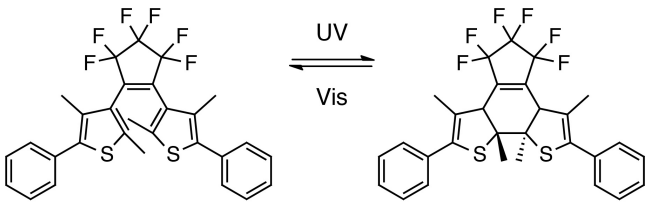

Figure 1.3 DMPT-PFCP photocyclization reaction.

DMPT-PFCP is thermally stable and fatigue resistant, making this molecule an ideal candidate to study higher-lying two-photon accessible excited states. **Chapter 5** examines the

spectroscopy and cycloreversion reaction quantum yields of DMPT-PFCP for one- and two-photon excitation. We report the absolute 2PA cross sections within the two lowest energy absorption bands of the closed-ring isomer. The cycloreversion reaction quantum yield is ~1.5% following excitation with one photon into the two lowest energy absorption bands, but a multi-photon excitation increases the quantum yield to ~16%. **Chapter 6** explores the cycloreversion mechanism of DMPT-PFCP with nonresonant high-intensity irradiation to investigate why the cycloreversion quantum yield increases under this irradiation condition. Evidence of a new reaction pathway following nonlinear excitation is presented, which is different from the known dynamics induced by linear excitation. The transient absorption following nonlinear excitation suggests an ionization pathway may be responsible for the increased cycloreversion quantum yield.

1.3.2 Phototrigger Molecules

Phototrigger molecules can selectively control the release of a bound substrate with light.[40-42] These molecules can be used for a wide variety of applications that use two-photon excitation to initiate release reactions ranging from medicine[33,54,55] to biology.[33,56-58] Specific applications include two-photon fluorescence microscopy,[33,56-58] drug delivery, [33,40-42] and two-photon photodynamic therapy.[33,54,55] *Para*-hydroxyphenacyl (*p*HP) is a phototrigger molecule that possesses desirable properties for these applications that include fast and efficient release of substrates, strong absorption in the visible to infrared, blue-shifted photoproduct absorption, and a biologically benign photoproduct. Figure 1.4 shows the release mechanism for *p*HP, which efficiently releases a substrate, X, when in aqueous media and produces only one significant byproduct, *para*-hydroxyphenylacetic acid (*p*HPAA).[40,41,59-63]

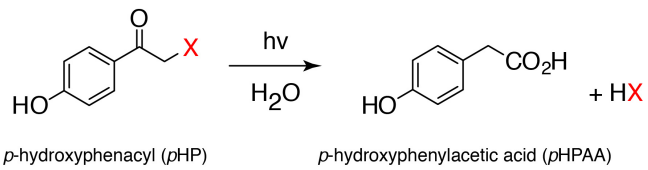

Figure 1.4 *para*-Hydroxyphenacyl (*p*HP) release reaction.

*p*HP photochemically releases a substrate with linear excitation and we have demonstrated the same release with two-photon excitation. **Chapter 7** compares the electronic spectroscopy and reaction quantum yields of substrate release from *p*HP following one- and two-photon excitation. The spectroscopy suggests the same excited electronic states are accessed with either one or two photons for both the protonated and deprotonated compounds, where the deprotonated compounds have the lowest energy absorption band shifted to the red. Two-photon induced release of phosphate groups from *p*HP is observed and likely undergoes the same release mechanism as with a one-photon excitation.

1.4 References

(1) Larson, E. J.; Friesen, L. A.; Johnson, C. K. An Ultrafast One-Photon and Two-Photon Transient Absorption Study of the Solvent-Dependent Photophysics in All-trans Retinal. *Chem. Phys. Lett.* **1997,** *265*, 161-168.

(2) Larson, E. J.; Pyszczynski, S. J.; Johnson, C. K. Solvent Dependence of Electronic Relaxation in All-trans Retinal Studied by One- and Two-Photon Induced Transient Absorption. *J. Phys. Chem. A* **2001,** *105*, 8136-8144.

(3) Linden, P. A.; Zimmermann, J.; Brixner, T.; Holt, N. E.; Vaswani, H. M.; Hiller, R. G.; Fleming, G. R. Transient Absorption Study of Peridinin and Peridinin−Chlorophyll a−Protein after Two-Photon Excitation. *J. Phys. Chem. B* **2004,** *108*, 10340-10345.

(4) Balkowski, G. M.; Groeneveld, M.; Zhang, H.; Hendrikx, C. C. J.; Polhuis, M.; Zuilhof, H.; Buma, W. J. Femtosecond Spectroscopic Studies of the One- and Two-Photon Excited-State Dynamics of 2,2,17,17-Tetramethyloctadeca-5,9,13-trien-3,7,11,15-tetrayne: A Trimeric Oligodiacetylene. *J. Phys. Chem. A* **2006,** *110*, 11435-11439.

(5) Corredor, C. C.; Belfield, K. D.; Bondar, M. V.; Przhonska, O. V.; Hernandez, F. E.; Kachkovsky, O. D. One- and Two-Photon Photochromism of 3,4-bis-(2,4,5-trimethyl-thiophen-3-yl)furan-2,5-dione. *J. Photochem. Photobiol. A* **2006,** *184*, 177-183.

(6) Kosumi, D.; Kusumoto, T.; Fujii, R.; Sugisaki, M.; Iinuma, Y.; Oka, N.; Takaesu, Y.; Taira, T.; Iha, M.; Frank, H. A.; Hashimoto, H. One- and Two-Photon Pump–Probe Optical Spectroscopic Measurements Reveal the S_1 and Intramolecular Charge Transfer States are Distinct in Fucoxanthin. *Chem. Phys. Lett.* **2009,** *483*, 95-100.

(7) Pang, Y.; Prantil, M. A.; Van Tassle, A. J.; Jones, G. A.; Fleming, G. R. Excited-State Dynamics of 8′-Apo-β-caroten-8′-al and 7′,7′-Dicyano-7′-apo-β-carotene Studied by Femtosecond Time-Resolved Infrared Spectroscopy. *J. Phys. Chem. B* **2009,** *113*, 13086-13095.

(8) Pang, Y.; Jones, G. A.; Prantil, M. A.; Fleming, G. R. Unusual Relaxation Pathway from the Two-Photon Excited First Singlet State of Carotenoids. *J. Am. Chem. Soc.* **2010,** *132*, 2264-2273.

(9) Buckup, T.; Weigel, A.; Hauer, J.; Motzkus, M. Ultrafast Multiphoton Transient Absorption of β-Carotene. *Chem. Phys.* **2010,** *373*, 38-44.

(10) Ishibashi, Y.; Okuno, K.; Ota, C.; Umesato, T.; Katayama, T.; Murakami, M.; Kobatake, S.; Irie, M.; Miyasaka, H. Multiphoton-Gated Cycloreversion Reactions of Photochromic Diarylethene Derivatives with Low Reaction Yields Upon One-Photon Visible Excitation. *Photochem. Photobiol. Sci.* **2010,** *9*, 172-180.

(11) Mori, K.; Ishibashi, Y.; Matsuda, H.; Ito, S.; Nagasawa, Y.; Nakagawa, H.; Uchida, K.; Yokojima, S.; Nakamura, S.; Irie, M.; Miyasaka, H. One-Color Reversible Control of Photochromic Reactions in a Diarylethene Derivative: Three-Photon Cyclization and Two-Photon Cycloreversion by a Near-Infrared Femtosecond Laser Pulse at 1.28 μm. *J. Am. Chem. Soc.* **2011,** *133*, 2621-2625.

(12) Kosumi, D.; Kusumoto, T.; Fujii, R.; Sugisaki, M.; Iinuma, Y.; Oka, N.; Takaesu, Y.; Taira, T.; Iha, M.; Frank, H. A.; Hashimoto, H. Ultrafast S_1 and ICT State Dynamics of a Marine Carotenoid Probed by Femtosecond One- and Two-Photon Pump-Probe Spectroscopy. *J. Lumin.* **2011,** *131*, 515-518.

(13) Irie, M.; Fukaminato, T.; Matsuda, K.; Kobatake, S. Photochromism of Diarylethene Molecules and Crystals: Memories, Switches, and Actuators. *Chem. Rev.* **2014,** *114*, 12174-12277.

(14) Ward, C. L.; Elles, C. G. Controlling the Excited-State Reaction Dynamics of a Photochromic Molecular Switch with Sequential Two-Photon Excitation. *J. Phys. Chem. Lett.* **2012,** *3*, 2995-3000.

(15) Ma, L.; Galstyan, G.; Zhang, K.; Kloc, C.; Sun, H.; Soci, C.; Michel-Beyerle, M. E.; Gurzadyan, G. G. Two-Photon-Induced Singlet Fission in Rubrene Single Crystal. *J. Chem. Phys.* **2013,** *138*, 184508.

(16) Ward, C. L.; Elles, C. G. Cycloreversion Dynamics of a Photochromic Molecular Switch via One-Photon and Sequential Two-Photon Excitation. *J. Phys. Chem. A* **2014,** *118*, 10011-10019.

(17) Houk, A. L.; Zheldakov, I. L.; Tommey, T. A.; Elles, C. G. Two-Photon Excitation of *trans*-Stilbene: Spectroscopy and Dynamics of Electronically Excited States Above S_1. *J. Phys. Chem. B* **2015,** *119*, 9335-9344.

(18) Moreno, J.; Dobryakov, A. L.; Ioffe, I. N.; Granovsky, A. A.; Hecht, S.; Kovalenko, S. A. Broadband Transient Absorption Spectroscopy with 1- and 2-Photon Excitations: Relaxation Paths and Cross Sections of a Triphenylamine Dye in Solution. *J. Chem. Phys.* **2015,** *143*, 024311.

(19) Moreno, J.; Gerecke, M.; Dobryakov, A. L.; Ioffe, I. N.; Granovsky, A. A.; Bléger, D.; Hecht, S.; Kovalenko, S. A. Two-Photon-Induced versus One-Photon-Induced Isomerization Dynamics of a Bistable Azobenzene Derivative in Solution. *J. Phys. Chem. B* **2015,** *119*, 12281-12288.

(20) Kasha, M. Characterization of Electronic Transitions in Complex Molecules. *Discuss. Faraday Soc.* **1950,** *9*, 14-19.

(21) Hsu, C.-P.; Hirata, S.; Head-Gordon, M. Excitation Energies from Time-Dependent Density Functional Theory for Linear Polyene Oligomers: Butadiene to Decapentaene. *J. Phys. Chem. A* **2001,** *105*, 451-458.

(22) Maitra, N. T.; Zhang, F.; Cave, R. J.; Burke, K. Double Excitations Within Time-Dependent Density Functional Theory Linear Response. *J. Chem. Phys.* **2004,** *120*, 5932-5937.

(23) Cave, R. J.; Zhang, F.; Maitra, N. T.; Burke, K. A Dressed TDDFT Treatment of the 2^1A_g States of Butadiene and Hexatriene. *Chem. Phys. Lett.* **2004,** *389*, 39-42.

(24) Levine, B. G.; Ko, C.; Quenneville, J.; MartÍnez, T. J. Conical Intersections and Double Excitations in Time-Dependent Density Functional Theory. *Molec. Phys.* **2006,** *104*, 1039-1051.

(25) Mikhailov, I. A.; Tafur, S.; Masunov, A. E. Double Excitations and State-to-State Transition Dipoles in π-π* Excited Singlet States of Linear Polyenes: Time-Dependent Density-Functional Theory Versus Multiconfigurational Methods. *Phys. Rev. A* **2008,** *77*, 012510.

(26) Zewail, A. H. Laser-Selective Chemistry and Vibrational Energy Redistribution in Molecules. *J. Photochem.* **1981,** *17*, 269-279.

(27) Felker, P. M.; Zewail, A. H. Direct Picosecond Time Resolution of Dissipative Intramolecular Vibrational-Energy Redistribution (IVR) in Isolated Molecules. *Chem. Phys. Lett.* **1984,** *108*, 303-310.

(28) Felker, P. M.; Lambert, W. R.; Zewail, A. H. Dynamics of Intramolecular Vibrational-Energy Redistribution (IVR). IV. Excess Energy Dependence, *t*-Stilbene. *J. Chem. Phys.* **1985,** *82*, 3003-3010.

(29) Zewail, A. H. Femtochemistry: Recent Progress in Studies of Dynamics and Control of Reactions and Their Transition States. *J. Phys. Chem.* **1996,** *100*, 12701-12724.

(30) Peticolas, W. L. Multiphoton Spectroscopy. *Annu. Rev. Phys. Chem.* **1967,** *18*, 233-260.

(31) McClain, W. M. Two-Photon Molecular Spectroscopy. *Acc. Chem. Res.* **1974,** *7*, 129-135.

(32) Wirth, M. J.; Koskelo, A.; Sanders, M. J. Molecular Symmetry and Two-Photon Spectroscopy. *Appl. Spectrosc.* **1981,** *35*, 14-21.

(33) Pawlicki, M.; Collins, H. A.; Denning, R. G.; Anderson, H. L. Two-Photon Absorption and the Design of Two-Photon Dyes. *Angew. Chem. Int. Ed.* **2009,** *48*, 3244-3266.

(34) Rumi, M.; Perry, J. W. Two-Photon Absorption: An Overview of Measurements and Principles. *Adv. Opt. Photonics* **2010,** *2*, 451-518.

(35) Monson, P. R.; McClain, W. M. Polarization Dependence of the Two-Photon Absorption of Tumbling Molecules with Application to Liquid 1-Chloronaphthalene and Benzene. *J. Chem. Phys.* **1970,** *53*, 29-37.

(36) McClain, W. M. Excited State Symmetry Assignment Through Polarized Two-Photon Absorption Studies of Fluids. *J. Chem. Phys.* **1971,** *55*, 2789-2796.

(37) Meier, H. The Photochemistry of Stilbenoid Compounds and Their Role in Materials Technology. *Angew. Chem. Int. Ed. Engl.* **1992,** *31*, 1399-1420.

(38) Irie, M. Diarylethenes for Memories and Switches. *Chem. Rev.* **2000,** *100*, 1685-1716.

(39) Budyka, M. F. Diarylethylene Photoisomerization and Photocyclization Mechanisms. *Russ. Chem. Rev.* **2012,** *81*, 477-493.

(40) Goeldner, M.; Givens, R. S., *Dynamics Studies in Biology*. Wiley-VCH: Weinheim, Germany, 2006.

(41) Klán, P.; Ŝolomek, T.; Bochet, C. G.; Blanc, A.; Givens, R.; Rubina, M.; Popik, V.; Kostikov, A.; Wirz, J. Photoremovable Protecting Groups in Chemistry and Biology: Reaction Mechanisms and Efficacy. *Chem. Rev.* **2013,** *113*, 119-191.

(42) Bort, G.; Gallavardin, T.; Ogden, D.; Dalko, P. I. From One-Photon to Two-Photon Probes: "Caged" Compounds, Actuators, and Photoswitches. *Angew. Chem. Int. Ed.* **2013,** *52*, 4526-4537.

(43) Albota, M.; Beljonne, D.; Brédas, J.-L.; Ehrlich, J. E.; Fu, J.-Y.; Heikal, A. A.; Hess, S. E.; Kogej, T.; Levin, M. D.; Marder, S. R.; McCord-Maughon, D.; Perry, J. W.; Röckel, H.; Rumi, M.; Subramaniam, G.; Webb, W. W.; Wu, X.-L.; Xu, C. Design of Organic Molecules with Large Two-Photon Absorption Cross Sections. *Science* **1998,** *281*, 1653-1656.

(44) Cumpston, B. H.; Ananthavel, S. P.; Barlow, S.; Dyer, D. L.; Ehrlich, J. E.; Erskine, L. L.; Heikal, A. A.; Kuebler, S. M.; Lee, I. Y. S.; McCord-Maughon, D.; Qin, J.; Rockel, H.; Rumi, M.; Wu, X.-L.; Marder, S. R.; Perry, J. W. Two-Photon Polymerization Initiators for Three-Dimensional Optical Data Storage and Microfabrication. *Nature* **1999,** *398*, 51-54.

(45) Walker, E.; Rentzepis, P. M. Two-Photon Technology: A New Dimension. *Nat. Photon.* **2008,** *2*, 406-408.

(46) LaFratta, C. N.; Fourkas, J. T.; Baldacchini, T.; Farrer, R. A. Multiphoton Fabrication. *Angew. Chem. Int. Ed.* **2007,** *46*, 6238-6258.

(47) Ehrlich, J. E.; Wu, X. L.; Lee, I. Y. S.; Hu, Z. Y.; Röckel, H.; Marder, S. R.; Perry, J. W. Two-Photon Absorption and Broadband Optical Limiting with Bis-Donor Stilbenes. *Opt. Lett.* **1997,** *22*, 1843-1845.

(48) Kay, E. R.; Leigh, D. A.; Zerbetto, F. Synthetic Molecular Motors and Mechanical Machines. *Angew. Chem. Int. Ed.* **2007,** *46*, 72-191.

(49) Piao, X.; Zou, Y.; Wu, J.; Li, C.; Yi, T. Multiresponsive Switchable Diarylethene and Its Application in Bioimaging. *Org. Lett.* **2009,** *11*, 3818-3821.

(50) Yun, C.; You, J.; Kim, J.; Huh, J.; Kim, E. Photochromic Fluorescence Switching From Diarylethenes and Its Applications. *J. Photochem. Photobiol. C* **2009,** *10*, 111-129.

(51) Liu, H.; Chen, Y.; Yao, B. Two-Photon Absorption of Photochromic Diarylethene and Its Application to Rewritable Holographic Recording. *Front. Chem. China* **2010,** *5*, 221-225.

(52) Irie, M. Photochromism of Diarylethene Molecules and Crystals. *P. Jpn. Acad. B-Phys.* **2010,** *86*, 472-483.

(53) Waldeck, D. H. Photoisomerization Dynamics of Stilbenes. *Chem. Rev.* **1991,** *91*, 415-436.

(54) Brown, S. B.; Brown, E. A.; Walker, I. The Present and Future Role of Photodynamic Therapy in Cancer Treatment. *Lancet Oncol.* **2004,** *5*, 497-508.

(55) Collins, H. A.; Khurana, M.; Moriyama, E. H.; Mariampillai, A.; Dahlstedt, E.; Balaz, M.; Kuimova, M. K.; Drobizhev, M.; YangVictor, X. D.; Phillips, D.; Rebane, A.; Wilson, B. C.; Anderson, H. L. Blood-Vessel Closure Using Photosensitizers Engineered for Two-Photon Excitation. *Nat. Photon.* **2008,** *2*, 420-424.

(56) Zipfel, W. R.; Williams, R. M.; Webb, W. W. Nonlinear Magic: Multiphoton Microscopy in the Biosciences. *Nat. Biotech.* **2003,** *21*, 1369-1377.

(57) Helmchen, F.; Denk, W. Deep Tissue Two-Photon Microscopy. *Nat. Meth.* **2005,** *2*, 932-940.

(58) Kim, H. M.; Cho, B. R. Small-Molecule Two-Photon Probes for Bioimaging Applications. *Chem. Rev.* **2015,** *115*, 5014-5055.

(59) Park, C.-H.; Givens, R. S. New Photoactivated Protecting Groups. 6. *p*-Hydroxyphenacyl: A Phototrigger for Chemical and Biochemical Probes. *J. Am. Chem. Soc.* **1997,** *119*, 2453-2463.

(60) Conrad, P. G.; Givens, R. S.; Hellrung, B.; Rajesh, C. S.; Ramseier, M.; Wirz, J. *p*-Hydroxyphenacyl Phototriggers: The Reactive Excited State of Phosphate Photorelease. *J. Am. Chem. Soc.* **2000,** *122*, 9346-9347.

(61) Givens, R. S.; Heger, D.; Hellrung, B.; Kamdzhilov, Y.; Mac, M.; Conrad, P. G.; Cope, E.; Lee, J. I.; Mata-Segreda, J. F.; Schowen, R. L.; Wirz, J. The Photo-Favorskii Reaction of *p*-Hydroxyphenacyl Compounds is Initiated by Water-Assisted, Adiabatic Extrusion of a Triplet Biradical. *J. Am. Chem. Soc.* **2008,** *130*, 3307-3309.

(62) Givens, R. S.; Stensrud, K.; Conrad, P. G.; Yousef, A. L.; Perera, C.; Senadheera, S. N.; Heger, D.; Wirz, J. *p*-Hydroxyphenacyl Photoremovable Protecting Groups - Robust Photochemistry Despite Substituent Diversity. *Can. J. Chem.* **2011,** *89*, 364-384.

(63) Klíčová, Ĺ.; Šebej, P.; Šolomek, T.; Hellrung, B.; Slavíček, P.; Klán, P.; Heger, D.; Wirz, J. Adiabatic Triplet State Tautomerization of p-Hydroxyacetophenone in Aqueous Solution. *J. Phys. Chem. A* **2012,** *116*, 2935-2944.

2. Experimental Methods

2.1 Overview

The spectroscopy, dynamics, and quantum yields of various photoactivated molecules in solution have been measured using laser-based techniques. Primarily, nonlinear excitation processes were investigated, with an emphasis on excitations with two photons. A two-photon transition occurs through the simultaneous absorption of two photons, which the absorbed photons are either degenerate or nondegenerate. The total energy of the two absorbed photons also needs to be resonant with a two-photon allowed transition. Exciting molecules with two photons can access different excited states, induce different excited-state dynamics, and change the efficiency of reactions as compared to exciting with only a single photon.

This chapter describes the experimental pump-probe setup we use to measure the excited-state dynamics following one- and two-photon excitation. The pump-probe setup is also used to measure the broadband two-photon absorption (2PA) spectroscopy, which is used to determine the absolute 2PA cross section and the polarization ratio of the 2PA spectra, measured at parallel and perpendicular relative polarization of the pump and probe beams. The 2PA measurement provides information about the symmetry of the two-photon accessible states. Reaction quantum yields were measured following a one-photon excitation and also a degenerate two-photon excitation within a single beam, to determine the efficiency of photochemical reactions. Exciting molecules to higher-lying excited states that are two-photon accessible can open up different reaction pathways, which can induce different excited-state dynamics, electronic spectroscopy, and reaction quantum yields as compared to linear excitation.

2.2 Transient Absorption Spectroscopy Following One- and Two-Photon Excitation

A pump-probe technique was used to measure the excited-state dynamics following one- and two-photon excitation. The sample is irradiated with an intense pump pulse that excites the sample to an excited electronic state. The pump pulse excites the sample and a broadband probe pulse is overlapped spatially and temporally to measure the transient absorption spectra. The pump and probe pulses were derived from a regeneratively amplified Ti:Sapphire laser (Legend Elite, Coherent), with <35 fs pulses at a repetition rate of 1 kHz.

The pump beam is generated from a tunable optical parametric amplifier (TOPAS-C, Light Conversion). The fundamental 800 nm light is sent into the TOPAS-C and produces tunable pump light in the range of 2600–240 nm. The TOPAS-C software (WinTOPAS) controls the pump wavelength by using a wavelength calibration installed in the software and the actual wavelength is verified with a spectrometer (BLUE-Wave, StellarNet). A sychronized optical chopper (NewFocus, 3501) blocks every other pulse of the pump beam for active background subtraction when calculating the transient absorption signal. The pump beam has a repetition rate of 1 kHz and the chopper is set at 500 Hz. The polarization of the pump beam is controlled by a $\lambda/2$ waveplate to have control over the relative polarization of the pump and probe at the sample. The pump beam is slightly focused into the sample with a beam diameter of ~200–300 μm for one-photon excitation and the beam is tightly focused to ~50–100 μm within the sample to induce a degenerate two-photon excitation within a single pump pulse. The transmitted pump light through the sample is blocked to minimize excess scattered light at the detector.

The broadband probe beam is generated by focusing either the fundamental 800 nm light or a small portion of infrared pump light from the TOPAS-C into a material to produce a white light continuum (WLC). The material for WLC generation can be a translating 2 mm calcium

fluoride (CaF_2) crystal, a 2 mm sapphire crystal, or a 1 cm quartz cuvette filled with water. For the dynamics measurements the WLC is generated exclusively in CaF_2 to minimize the amount of material the beam passes through prior to reaching the sample, since dispersion stretches the probe pulse as it passes through material. The WLC usually extends from 750–350 nm, but the WLC generated in CaF_2 can extend further to the UV to ~300 nm. When using infrared pump light to generate WLC, the usable probe range is extended to the red to ~1000 nm by eliminating interference effects between the intense fundamental 800 nm and the WLC. The polarization of the probe beam is also controlled with a λ/2 waveplate that is placed prior to the generation of WLC. The WLC maintains the same polarization as the incident beam, as long as the WLC is generated in an isotropic material.[1,2] The CaF_2 crystal is not isotropic, so the crystal is also rotated to maintain the proper polarization of the WLC. A Glan-Taylor polarizer can be used to measure the polarization purity. Further details for generating WLC have been described previously.[1-3] The probe beam is focused at the sample to a diameter of ~50–100 μm and overlapped spatially with the pump beam within the sample.

The probe light transmitted through the sample is passed through a transmission grating that disperses the different wavelengths onto a 256-element photodiode array (Hamamatsu, S3901-256Q). Excess fundamental 800 nm or infrared light was filtered out of the probe beam by either using two 2 mm KG3 colored glass bandpass filter (transmits 710–315 nm), one 2 mm BG38 colored glass bandpass filter (580–335 nm), one 2 mm BG39 colored glass bandpass filter (580–360 nm), or one 2 mm BG40 colored glass bandpass filter (610–335 nm). For the dynamics measurements the bandpass and longpass filters are placed after the sample to reduce material the probe beam passed through prior to the sample. These filters eliminate excess fundamental 800 nm and the second-harmonic generation of the fundamental, respectively. In some cases a

407 nm colored glass longpass filter is used after the sample as well to eliminate any second-harmonic generation from the residual 800 nm fundamental in the probe beam.

To measure the excited-state dynamics following one- and two-photon excitation the pump and probe beams are spatially and temporally overlapped in the sample. The sample for the one- and two-photon excitation measurements is a liquid solution that is forced through a sapphire slit nozzle (Kyburz) to produce a windowless, liquid jet with a path length of 300 μm.[3] Using the windowless jet eliminates material (*i.e.* glass) from the sample, thus reducing material dispersion through the sample. Typically, the relative polarization of the pump and probe beams is set to magic angle (54.7°), to only measure the isotropic signal.[4,5] For the two-photon excitation measurement the relative angle between the pump and probe beams is also set to magic angle. There are equal contributions from parallel and perpendicular polarization components of the transient absorption signal at magic angle, which eliminates any anisotropic effects from the transient absorption.[4,5]

The transient absorption spectra following one- and two-photon excitation can be analyzed to extract time constants to then understand the excited-state dynamics. Specifically the time constants can be determined through global and target analyses, details of these analyses are described elsewhere.[3,6,7] Briefly, the global analysis fits a sum of exponentials simultaneously to all probe wavelengths in the transient absorption signal while fixing the time constants and allowing only the amplitudes of the fits to change. Global analysis produces decay-associated spectra (DAS) and the shape and amplitudes of the DAS provide information about the kinetic evolution of the system. The target analysis imposes a physical model onto the measured transient absorption signal to extract species-associated spectra (SAS) of the evolving excited state.[3,6,7]

All of the data analysis is performed using custom data analysis and modeling software written in IGOR Pro 6.37 (WaveMetrics) and Maple 17 (Maplesoft). The technical details of the pump-probe setup, including the electronics and LabVIEW programs used to run measurements are in the Ph.D. dissertation of Cassandra Ward.[3]

2.3 Broadband Two-Photon Absorption Spectroscopy

The experimental setup to measure the broadband two-photon absorption (2PA) spectra of liquid solutions is essentially the same as the transient absorption spectroscopy measurements, with a few differences.[8-15] The broadband 2PA spectrum of the sample is measured when the pump and probe beams are overlapped spatially and temporally. Two-photon absorption occurs through the simultaneous absorption of one pump and one probe photon. A 2PA is observed when the total energy of the pump and probe photons is resonant with a two-photon allowed transition. Other more traditional methods that measure the 2PA at single wavelengths are susceptible to point-to-point variations along the spectrum due to changes of the pump beam at each wavelength, while the broadband method we use is less sensitive to variations across the spectrum because all wavelengths are measured simultaneously.

The broadband two-photon absorption (2PA) spectrum is measured when the pump and probe beams cross at a small angle to one another and are overlapped in time and space in the sample. The sample is typically a 1 mm quartz cuvette filled with a concentrated liquid solution, usually >0.1 M. The energy of the pump beam needs to be low enough (usually <5 μJ) to not observe measurable transient absorption signal outside of the pump-probe overlap due to nonlinear excitation of the sample. The optimum energy of the pump beam for the 2PA measurement depends on the diameter of the pump beam, the overlap of the pump and probe

beams, the 2PA signal, and the concentration of the sample. The relative delays between the pump and probe pulses are scanned to account for the temporal dispersion of the linearly chirped probe pulse. The 2PA spectrum is usually measured by scanning a 2–3 ps range with a step size of 10 fs to ensure no additional signals are measured before and after the temporal overlap of the pump and probe pulses. Representative 2D contour plots are shown in Figure 2.1A–B. The first 300 fs prior to the overlap of the pump and probe pulses are averaged at each probe wavelength and are used for baseline correction across the entire spectrum. The maximum overlap of the pump and probe pulses in time are fit to a polynomial as function of probe wavelength to represent the "time zero" or "τ=0" to account for the temporal dispersion of the probe pulse (Figure 2.1A). A range of usually about ±0.3 ps around the "time zero" is integrated at each wavelength to obtain the 2PA signal. The integration also eliminates dispersive effects, such as cross-phase modulation, therefore only absorptive features are measured, such as 2PA and stimulated Raman scattering. [14,16] We use a numerical integration method, specifically Simpson's rule, to obtain the 2PA spectrum. The integration range around "time zero" is varied to ensure there are no signals from photoproduct transient absorption and extending the integration range confirms there is no effect on the integrated signal (Figure 2.1B). Figure 2.1 pictorially shows the process for analyzing the 2PA signal. Figure 2.1C shows the 2PA signals plotted as a function of the probe wavelength.

2.3.1 Two-Photon Absorption (2PA) Cross Section

The absolute 2PA cross sections at each probe wavelength can be determined from the 2PA signal at that wavelength. The 2PA cross section is measured in units of GM (1 GM = 10^{-50} $cm^4 \cdot s \cdot molecule^{-1} \cdot photon^{-1}$). The 2PA cross section (σ_{2PA}) is determined using Equation 1.[14]

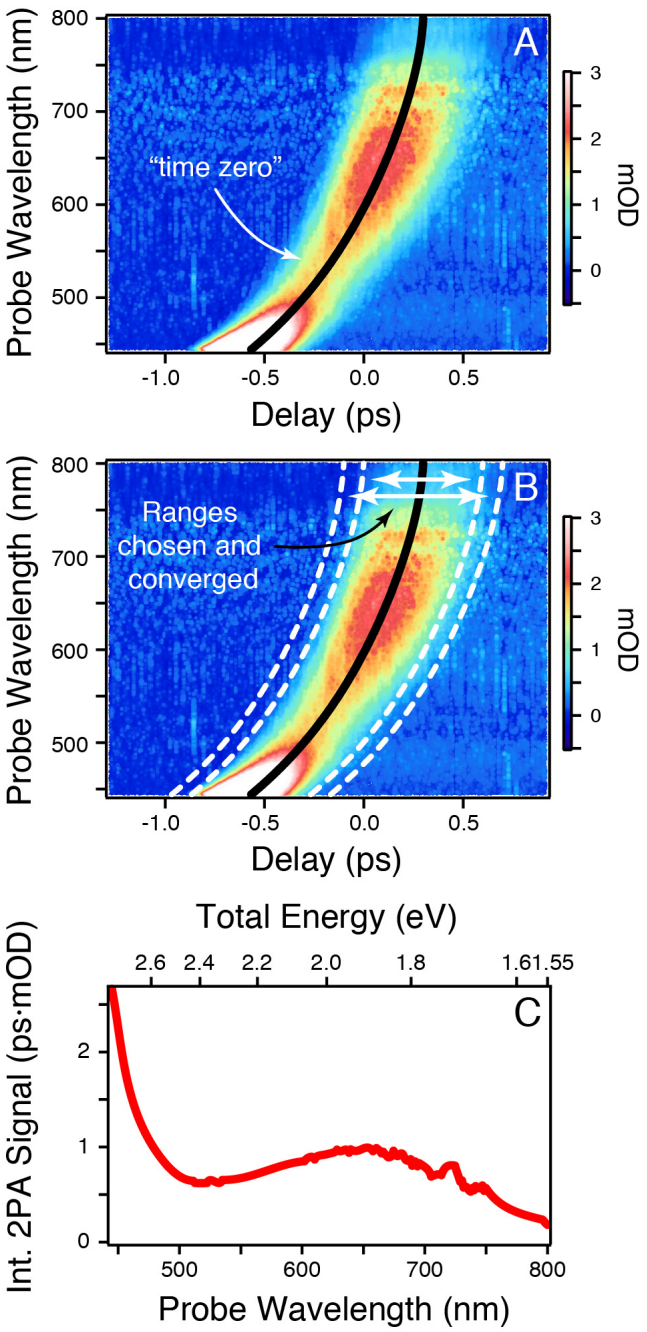

Figure 2.1 Obtaining the two-photon absorption spectrum from pump-probe measurements. (A) 2D contour plot of measured 2PA signal with a "time zero" fit, (B) 2D contour plot showing the variation of integration ranges around "time zero" to obtain the 2PA signal, and (C) integrated 2PA signal plotted against probe wavelength. Pump wavelength = 370 nm.

$$\sigma_{2PA} = \frac{\ln(10)}{E_{pump}\,\ell\,GF}\,\frac{h\,c}{\lambda_{pump}\,N}\int \Delta A(\tau)d\tau_{2PA} \quad (1)$$

E_{pump} is the energy of the pump pulse, ℓ is the path length of the sample, GF is a Gaussian overlap factor, h is Planck's constant, c is the speed of light, λ_{pump} is the pump wavelength, N is the number density of the sample, and $\int\Delta A(\tau)d\tau_{2PA}$ is the time-integrated 2PA signal at each probe wavelength. The spatial overlap GF is determined from the spatial overlap of the pump and probe beams at the sample, assuming both beams are Gaussian.[14]

$$GF = \frac{1}{\sqrt{2\pi\left[(\omega_{x,pump})^2+(\omega_{x,probe})^2\right]}}\,\frac{1}{\sqrt{2\pi\left[(\omega_{y,pump})^2+(\omega_{y,probe})^2\right]}} \quad (2)$$

The $\omega_{x,pump}$ and $\omega_{y,pump}$ are the widths of pump beam in the x and y direction, respectively, and $\omega_{x,probe}$ and $\omega_{y,probe}$ are the widths of the probe beam in the x and y direction, respectively. The widths of the two beams are determined by placing a razor blade at the same location as the sample, on an XYZ linear translation stage and then move the razor blade into the beam while measuring the transmitted energy as a function of the razor blade position. The measured energy as a function of distance is fit to an error function, which gives the beam widths for the pump and probe beams that can be input into Equation 2.

We calculate the constant value on the right side of Equation 1 based on experimental parameters and the 2PA signal, $\int\Delta A(\tau)d\tau_{2PA}$, is the measured value from the analysis above. The broadband 2PA spectrum can be plotted as a function of total energy (pump+probe energy) in eV.

2.3.2 Stimulated Raman as an Internal Standard

In addition to the 2PA signal, resonant stimulated Raman scattering signals can also be observed when the pump and probe beams are temporally and spatially overlapped. The stimulated Raman signal is due to the coherent interaction of the pump and probe light, where

the difference in energy between the pump wavelength and probe wavelength is resonant with a vibrational transition. The stimulated Raman signal of the solvent or solute can be used as an internal standard to more accurately determine the 2PA cross section of the studied molecules.[17] The spatial overlap of the pump and probe beams is the main source of uncertainty in the 2PA cross section measurement (*i.e. GF*). However, the stimulated Raman and 2PA signals have the same dependence on the spatial overlap of the pump and probe beams, which means the Raman signal can be used to calibrate the 2PA cross section measurement without needing to know the spatial overlap of the beams.[17]

Figure 2.2 shows an example of the 2PA spectra integrated in time, $\int \Delta A(\tau) d\tau_{2PA}$, of a solute and of a pure solvent (methanol), where both have contributions from stimulated Raman scattering.

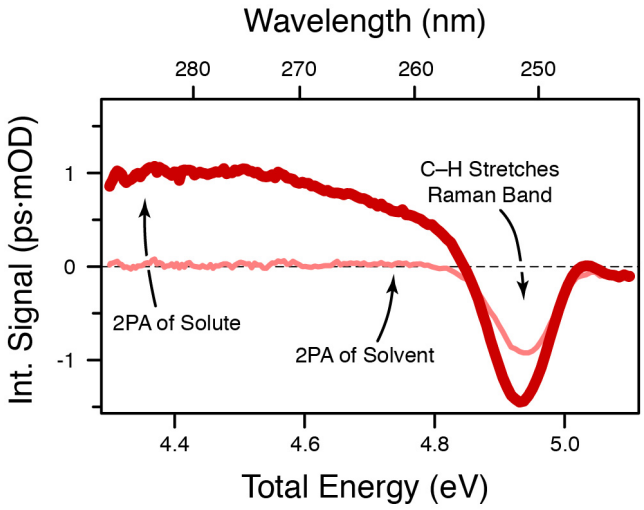

Figure 2.2 An example of the combined two-photon absorption (2PA) and stimulated Raman spectra for a solution (red line), as compared with the stimulated Raman spectrum of the pure solvent (methanol; pink line).

The stimulated Raman band for the C–H stretching vibrations of the solvent (pink line) is plotted as a function of frequency in Figure 2.3. The black dotted line in Figure 2.3 is a Gaussian fit to the stimulated Raman spectrum and the fit is integrated in the frequency domain over the entire Raman band, which gives the total stimulated Raman signal integrated in time and frequency, $\iint \Delta A(\tau,\omega) d\tau_{2PA} d\omega_{Raman}$ that is proportional to the spontaneous Raman scattering cross section ($d\sigma/d\Omega$), where $d\Omega$ is the differential scattering solid angle. The stimulated Raman signal in Figure 2.3 is negative in the anti-Stokes region of the spectrum and the signal would be positive in the Stokes region of Raman scattering spectrum. We are unable to resolve the individual Raman transitions of methanol because we are using fs pulses that have spectral bandwidths of ~10 nm. Due to the Fourier-transform-limit the spectral broadening is typically ~350 cm^{-1} for ~45 fs pulses.

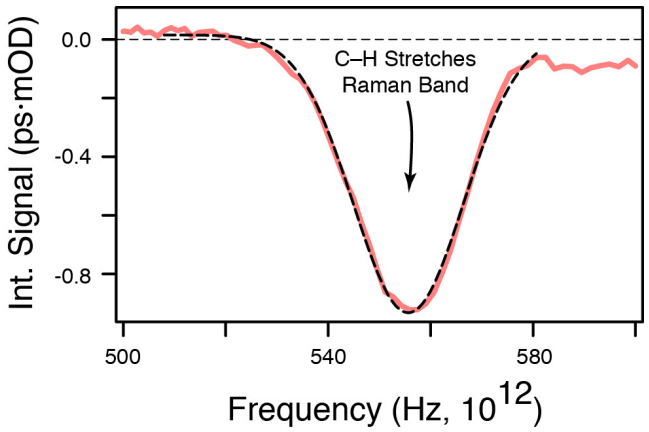

Figure 2.3 Integrated stimulated Raman spectrum of C–H stretches in methanol plotted as a function of frequency.

The stimulated Raman scattering signal of a pure solvent integrated in the time and frequency domain is proportional to the spontaneous Raman scattering cross section ($d\sigma/d\Omega$) of that solvent.[17]

$$\frac{d\sigma}{d\Omega} = -\frac{\ln(10)}{E_{pump}\,\ell\,GF}\,\frac{\hbar\,\omega_{pump}\,\omega_{probe}^{2}}{8\,\pi^{3}\,c^{2}\,N_{solvent}}\iint \Delta A(\tau,\omega)d\tau_{2PA}d\omega_{Raman} \qquad (3)$$

The integral, $\iint\Delta A(\tau,\omega)d\tau d\omega_{Raman}$, is the pump-probe signal integrated over all delay times and across the entire stimulated Raman band , the ω_{pump} is the angular frequency of the pump beam, ω_{probe} is the angular frequency of the probe beam, and $N_{solvent}$ is the number density of the solvent.

The spontaneous Raman scattering cross section and absolute 2PA cross section (σ_{2PA})[14] are both given as a function of the spatial overlap of the pump and probe beams (*GF*).[17]

$$\sigma_{2PA} = \frac{\ln(10)}{E_{pump}\,\ell\,GF}\,\frac{\hbar\,\omega_{pump}}{N_{solute}}\int \Delta A(\tau)d\tau_{2PA} \qquad (4)$$

The spatial overlap of the pump and probe beams have the same effect on the 2PA and stimulated Raman cross section measurements. Since the Gaussian overlap factor (*GF*) for the 2PA and stimulated Raman cross section measurements are the same, the *GF* value in Equation 3 for the stimulated Raman cross section can be used with Equation 4 for the 2PA cross section. A more accurate measurement of the absolute 2PA cross section of the solute is determined by using the integrated Raman band of the solvent as an internal standard. Using the integrated Raman band eliminates the need to use the spatial overlap of the pump and probe beams to determine the 2PA cross section and is given by,

$$\sigma_{2PA} = -\frac{8\,\pi^{3}\,c^{2}\,N_{solvent}}{N_{solute}\,\omega_{probe}^{2}}\left(\frac{d\sigma}{d\Omega}\right)\frac{\int \Delta A(\tau)d\tau_{2PA}}{\int \Delta A(\tau,w)d\tau d\omega_{Raman}} \qquad (5)$$

All of the constants on the right side of Equation 5 are known from experimental parameters except for the differential spontaneous Raman cross section, $d\sigma/d\Omega$, which is from the literature. The 2PA cross section in Equation 5 is calibrated using the Raman band as an internal standard at each probe wavelength, which also incorporates the experimentally determined constants from the right side of Equation 5, including the 2PA signal ($\int \Delta A(\tau) d\tau_{2PA}$) from the pump-probe experiment described previously. This procedure gives the broadband 2PA spectrum with the calibrated absolute 2PA cross sections, which can be plotted as a function of total energy in eV.

2.3.3 Two-Photon Absorption Polarization Ratios

The 2PA spectra are measured separately for relative polarizations of the pump and probe beams that are parallel ($\sigma_{2PA}(\|)$) and perpendicular ($\sigma_{2PA}(\perp)$). The separate 2PA polarization measurements are compared and used to determine a polarization ratio,[18-21]

$$r = \frac{\sigma_{2PA}(\|)}{\sigma_{2PA}(\perp)} \tag{6}$$

The polarization ratio provides information about the symmetry of the two-photon allowed electronic transitions of the molecules. For any point group, totally symmetric transitions have $r \geq 4/3$ when using linearly polarized light and for nontotally symmetric transitions $r < 4/3$. Table 2.1 gives the polarization ratios for two-photon allowed transitions under general conditions and also in two limiting cases, as discussed by McClain and coworkers.[18-20] The limiting case of degenerate excitation is when the two absorbed photons have the same energy and the near-resonance limiting case refers to one of the absorbed photons being close in energy to a one-photon allowed transition of the molecule.

Table 2.1 Polarization ratio limits for parallel and perpendicular linearly polarized light for molecules belonging to any point group.

Symmetry		General	Degenerate	Near-resonance
Totally symmetric	$\delta_{para}/\delta_{perp}$	$4/3 \leftrightarrow \infty$	$4/3 \leftrightarrow \infty$	3
Nontotally symmetric	$\delta_{para}/\delta_{perp}$	$1/2 \leftrightarrow 4/3$	4/3	1/2

2.4 Degenerate Two-Photon Absorption Cross Sections

More traditional measurements of the 2PA cross section typically use degenerate excitation with a single laser beam. We use degenerate excitation within a single pump pulse to measure the absolute 2PA cross section to compare with our broadband absolute 2PA cross section. Figure 2.4 shows the experimental setup to measure the absolute 2PA cross section at a single wavelength. The pump beam is split into two different beams, one that is used as a reference and another that passes through the sample. The intensity of every incident and transmitted pump pulse is measured simultaneously on two different photodiodes (PD) in order to account for laser fluctuations. The two large-area silicon PDs (~13 mm^2; Hamamatsu, S1336-44BQ) record the integrated intensity of each laser pulse at the 1 kHz repetition rate of the laser.[3] These UV-enhanced silicon PDs have a spectral response from 1100–190 nm. The attenuation of the beam passing through the sample as a function of incident intensity reveals the two-photon absorption coefficient (β).

A telescope decreases the diameter of the pump beam to ensure a high enough photon flux to induce a simultaneous two-photon absorption in the sample. Diameter of the beam is typically ~300 μm and the intensity is usually within 10–1000 GW/cm^2 to induce a degenerate two-photon excitation. The collimated pump beam after being passed through the sample is then slightly focused on the PD to ensure all the light reaches the PD and the beam is also attenuated

so the PD does not saturate. The sample in this experiment consists of a 1 cm quartz cuvette filled with 1 mL of a solution and stirred continuously with a magnetic stir bar.

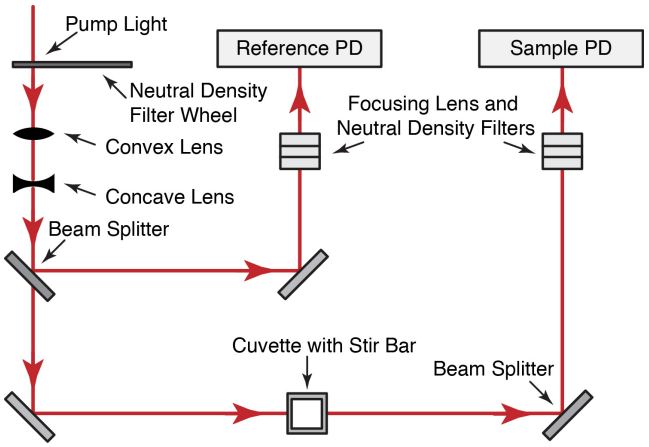

Figure 2.4 Degenerate two-photon absorption and quantum yield measurement at a single energy.

The decrease or loss of intensity, I, of the single laser beam passing through a path length in the z direction is given as,

$$\frac{\partial I}{\partial z} = -\alpha\, I - \beta\, I^2 \qquad (7)$$

Here α is the one-photon absorption coefficient and β is the two-photon absorption coefficient. The second term on the right side of Equation 7 is dependent on the square of the intensity and thus the transmitted light as a function of the incident light has a quadratic dependence indicating a two-photon allowed transition. To determine the absolute 2PA cross section for degenerate excitation the transmittance through the sample as a function of the incident intensity is measured to determine the two-photon coefficient, β. In the limit of no linear absorption, *i.e.* α = 0, solving the differential equation in Equation 7 gives,

$$\text{transmittance} = \frac{I}{I_0} = \frac{1}{1+\beta\,\ell\,I_0} \tag{8}$$

Here I is the transmitted intensity, I_0 is the incident intensity, and ℓ is the path length. The absolute 2PA cross section (σ_{2PA}) is proportional to β as a function of the number density of the sample, N.

$$\sigma_{2PA} = \frac{\beta}{N}\left(\frac{h\,c}{\lambda}\right) \tag{9}$$

When the excitation wavelength is resonant with both a one- and two-photon allowed transition the additional one-photon absorption contribution needs to be accounted for when measuring β. Including the one- and two-photon absorption components when solving the differential equation in Equation 7 gives,[22-26]

$$\text{transmittance} = \frac{I}{I_0} = \frac{e^{-\alpha\ell}}{1+\beta\,I_0\left(\frac{1-e^{-\alpha\ell}}{\alpha}\right)} \tag{10}$$

The one-photon absorption coefficient, α, is related to the one-photon extinction coefficient (ε) with the concentration (c_0) of the sample, *i.e.* $\alpha = \ln(10)\,\varepsilon{\cdot}c_0$. The absolute 2PA cross sections measured with a degenerate two-photon excitation within a single beam can include additional intensity losses from one-photon absorption and from solvent losses, but these losses are accounted for when using Equation 10 to extract the two-photon absorption coefficient, β.

2.5 Quantum Yield Measurements

The number of molecules converted per absorption event is the quantum yield.

$$\Phi = \frac{\text{molecules converted}}{\text{absorption event}} \tag{11}$$

We measure the quantum yields by monitoring the photochemical conversion reactions of photochromic and phototrigger molecules. A single laser beam at one wavelength is used to induce the photochemical reaction with linear or nonlinear excitation. We monitor the changing

concentration per laser pulse via the absorption of incident light, where the absorbance of the incident light is also responsible for inducing the conversion reaction. Throughout this dissertation the quantum yield is reported as the number of molecules converted per absorption event. For example, a two-photon absorption event means two photons were simultaneous absorbed and is equated to one event, while for a one-photon absorption only one photon is absorbed per event.

2.5.1 One-Photon Excitation

Figure 2.5 shows the general setup of the one-photon absorption (1PA) quantum yield (Φ_{1PA}) measurement. The spot size of the pump beam is usually >1 mm to ensure the pump beam irradiates as much of the sample volume as possible. The single pump beam is divided into two different beams by a beamsplitter. One beam acts as a reference to track laser fluctuations, and the beam is attenuated and gently focused onto the PD in the same way as before. The other PD measures the transmitted energy through the sample. Again the transmitted beam is slightly focused onto a different PD and neutral density (ND) filters attenuate the beam so as not to saturate the PD. The sample is in a 1 cm quartz cuvette filled with 1 mL of the sample and is constantly stirred with a magnetic stir bar.

The PDs measure the energy per pulse and the energies are collected with the LabVIEW program "Run Quantum Yield Experiment", which has been described in detail previously.[3] Typically, pump light irradiates the sample on the order of tens of minutes to induce a measureable change to the molecules, while recording every pulse of light that reaches the PDs. A calibration is implemented to convert the measured PD voltages to laser pulse energies.

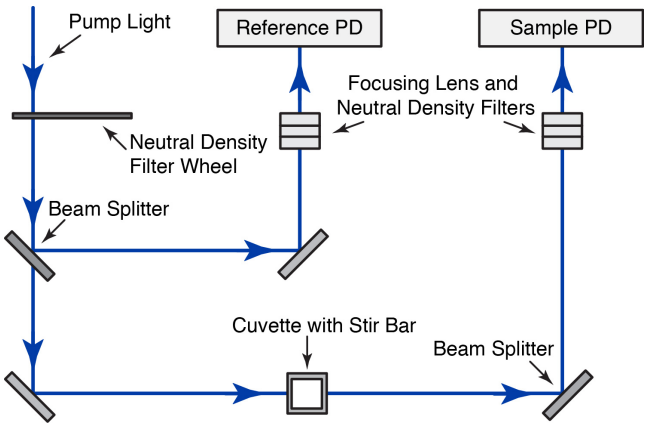

Figure 2.5 One-photon absorption quantum yield measurement at a single energy.

Sometimes when allowing a sample to completely convert through a photochemical reaction, the energies at the reference and sample PDs do not converge, as shown in Figure 2.6. In other words, the measured reference energies are shifted by a constant offset, which may arise from reflection losses that were not accounted for during calibration or if the sample was moved after the calibration. To account for this offset the transmitted energy through the sample as a function of laser pulses (thin red line) is fit to an exponential function and the energy at the reference PD (thin green line) averaged. The difference between the asymptotic limit of the signal and the average value of the reference is used to shift the energy of the reference PD (thick blue line) to match the offset from the exponential fit of the sample energy.

The difference in pulse energy between the reference (thick blue line) and sample (thin red line) PDs, is proportional to the number of photons absorbed by the sample for any given laser pulse (Figure 2.6). To determine the total number of photons absorbed throughout the experiment, the energy differences between the reference and sample PDs are summed over all laser pulses (m).

$$\text{photons absorbed} = \frac{\Delta E}{E/\text{photon}} = \frac{\lambda}{h\,c} \cdot n_p \cdot \sum_m \left(E_0(m) - E(m)\right) \tag{12}$$

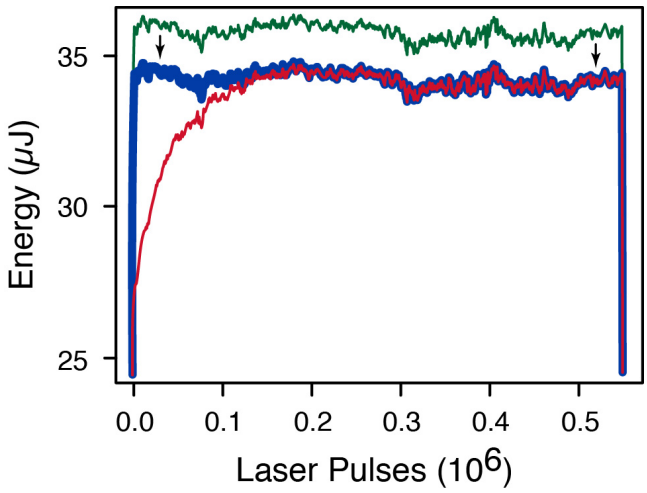

Figure 2.6 Representative one-photon absorption quantum yield measurement. The thick green line is the measured reference energy per laser pulse, the thick blue line is the reference energy shifted to account for additional losses, and the thin red line is the measured transmitted energy.

The excitation wavelength is λ, Planck's constant is h, the speed of light is c, the incident energy measured at time/laser pulse (m) is $E_0(m)$, the transmitted energy measured at the same time/laser pulse is $E(m)$, and each collected data point is the sum of a number of laser pulses, n_p. This method works best in the limit of complete conversion of the sample because this method uses the accumulated signal of the entire measurement so this measurement is less sensitive to shot-to-shot variations, but is sensitive to the initial measurement of incident energy.

The number of molecules converted is determined by first using Beer's Law to calculate the concentration of the sample before (c_0) and after (c_f) irradiation from the measured absorbances with a UV-vis spectrophotometer. The number of molecules in the sample is determined using the volume (V) of sample.

$$\text{Molecules converted} = \left(c_0 - c_f\right) \cdot V \cdot N_A = \Delta c \cdot V \cdot N_A = \frac{\Delta A}{\varepsilon\, \ell} \cdot V \cdot N_A$$

$$= \frac{V}{\varepsilon\, \ell} \cdot \left(A_0 - A_f\right) \cdot N_A \qquad (13)$$

Where A_0 is the absorbance of the sample prior to irradiation, A_f is the absorbance after irradiation, N_A is Avogadro's number, ε is the extinction coefficient of the target molecule, and ℓ is the path length of the sample. The 1PA quantum yield is obtained by substituting Equations 12 and 13 into Equation 11.

$$\Phi_{1\mathrm{PA}} = \frac{\frac{V}{\varepsilon\,\ell}\cdot\left(A_0 - A_f\right)\cdot N_A}{\frac{\lambda}{h\,c}\cdot n_p\cdot\sum_m\left(E_0(m)-E(m)\right)} = \frac{V}{\varepsilon\,\ell}\frac{h\,c}{\lambda}\frac{N_A}{n_p}\frac{A_0 - A_f}{\sum_m\left(E_0(m)-E(m)\right)} \tag{14}$$

The 1PA quantum yield is reported as the number of molecules converted per absorption event, which is also equal to the number of molecules converted per absorbed photon of light.

2.5.2 Two-Photon Excitation

The experimental setup used to measure the quantum yield following two-photon excitation ($\Phi_{2\mathrm{PA}}$) is the same as the degenerate two-photon absorption measurement in Figure 2.4, except that we do not vary the intensity of the beam during the experiment. We use a high intensity laser beam to simultaneously induce and measure nonlinear absorption. The spot size of the pump beam is reduced with a telescope to ensure a high enough photon flux at the sample. The two reference and pump beams are then slightly focused on two different PDs, one used for a reference to measure the incident energy and another to measure the transmitted energy through a sample. In the same way as the quantum yield measurements following one-photon excitation, every pulse of light that reaches the PDs is recorded as a voltage and is converted to laser pulse energy through a calibration. The sample is irradiated for up to several hours to measure a distinguishable change in the nonlinear transmittance of the sample. A measureable change of the sample occurs on the order of many hours but complete conversion can take much longer, so we typically only measure the initial conversion rate. The sample again is a 1 mL solution placed in a 1 cm quartz cuvette that is constantly stirred with a magnetic stir bar.

For consistency and ease of comparison the 2PA and 1PA quantum yields are reported as molecules converted per absorption event. In the case of the 2PA quantum yield, one absorption event occurs when two photons are simultaneously absorbed by the sample.

To determine the 2PA quantum yield we first need to know the absolute 2PA cross section (σ_{2PA}) because we actually measure a two-photon action cross section ($\sigma_{2PA}\Phi_{2PA}$), which is the product of the two-photon absorption quantum yield and the absolute 2PA cross section. When measuring the two-photon action cross section with this single wavelength method our observable with the large-area silicon PDs is the intensity of the laser pulse integrated in the radial coordinate r and in time t, as well as through the path length z, $I(r,t,z)$, which is used to determine the 2PA action cross section and then the 2PA quantum yield. The differential intensity, I, of the single laser beam passing through a path length in the z direction, as a function of the radial coordinate r and time t, assuming only a two-photon absorption process is given as,

$$\frac{\partial I(r,t,z)}{\partial z} = -\beta\, I(r,t,z)^2 = -\sigma_{2\mathrm{PA}}\, N \left(\frac{\lambda}{hc}\right) I(r,t,z)^2 \qquad (15)$$

The irradiance in the r radial coordinate, through the path length in the z coordinate, and in time, t, is $I(r,t,z)$ and the integrated intensity is proportional to the energy, the 2PA coefficient is β, the number density of the sample is N, and the pump wavelength is λ. Where the 2PA coefficient is proportional to the absolute 2PA cross section and the irradiance has a quadratic dependence for a two-photon absorption process. The transmitted irradiance in time and in the r coordinate, $I(r,t)$, is obtained by integrating over the path length of the sample in the z direction, for an incident irradiance, I_0, to give the measured transmittance through the sample that is related to the absorbance by the sample,

$$I(r,t) = \frac{I_0(r,t)}{1+\beta\, \ell\, I_0(r,t)} \qquad (16)$$

In the limit $\beta \ell I_0(r,t) \ll 1$, which occurs when the incident irradiance is small while still producing a measureable β, the change of irradiance before and after the sample, ΔI, can be represented as,

$$\Delta I = I_0(r,t) - I(r,t) \cong \beta \, \ell \, I_0^2(r,t) \tag{17}$$

The incident pulse $I_0(r,t)$ is approximated as a Gaussian function both radially and in time,

$$I_0(r,t) = I_0 \, e^{-r^2/2\rho^2} e^{-t^2/2\tau^2} \tag{18}$$

Here the pulse diameter is ρ, the pulse duration is τ, and the peak irradiance is I_0,

$$I_0 = \frac{E}{(2\pi)^{3/2} \, \rho^2 \, \tau} \tag{19}$$

Here the integrated laser pulse energy is E. We do not measure I_0 directly, but we are able to measure E, to then relate laser pulse energy to irradiance through the pulse parameters in Equation 19. We measure the change in energy of the laser pulse, ΔE, that can be determined from the difference of the incident energy, E_0, and the energy as a function of position in the path length of the sample, $E(z)$. The change in energy is determined by integrating the difference in irradiance in time t and in the radial coordinate r, over the entire laser pulse.

$$\Delta E = E_0 - E(z) = \iint \Delta I \, dr \, dt \tag{20}$$

The change in energy ΔE becomes,

$$\Delta E = \frac{\sigma_{2\mathrm{PA}} \, N \, \ell \, E^2}{8\pi^{3/2} \, \rho^2 \, \tau} \left(\frac{\lambda}{h \, c}\right) \tag{21}$$

This change in energy ΔE is related to number of molecules converted, which is also proportional to the two-photon excitation conversion rate (Rate). The Rate is the measure of molecules converted per laser pulse, which is proportional to the 2PA quantum yield $\Phi_{2\mathrm{PA}}$.

$$\mathrm{Rate} = \frac{\Delta E}{\left(\frac{h \, c}{\lambda}\right)} \, \Phi_{2\mathrm{PA}} = \frac{N \, \ell}{8\pi^{3/2} \, \rho^2 \, \tau} \left(\frac{\lambda}{h \, c}\right)^2 E^2 \, \sigma_{2\mathrm{PA}} \Phi_{2\mathrm{PA}} \tag{22}$$

By substituting Equation 21 into Equation 22, the Rate is given in terms of our experimental parameters, which becomes,

$$\text{Rate} = \frac{N\,\ell}{8\pi^{3/2}\,\rho^2\,\tau}\left(\frac{\lambda}{h\,c}\right)^2 E^2\,\sigma_{2\text{PA}}\Phi_{2\text{PA}} \tag{23}$$

Rearranging Equation 23 gives the 2PA quantum yield,

$$\Phi_{2PA} = 8\pi^{3/2}\frac{\rho^2\,\tau}{N\,\ell}\left(\frac{h\,c}{\lambda}\right)^2\frac{1}{E^2}\frac{1}{\sigma_{2\text{PA}}} \tag{24}$$

The absolute 2PA cross section can be determined more accurately by measuring the β as a function of number density N and fitting a line to the β versus N data. The slope of the linear regression is proportional to the absolute 2PA cross section,

$$\beta(N) = \frac{\sigma_{2\text{PA}}\,\lambda}{h\,c}\,N + \text{offset} \tag{25}$$

Here the offset is related to any other intensity losses besides from a two-photon absorption. The slope of Equation 25 gives a more accurate absolute 2PA cross section and thus can give a more accurate 2PA quantum yield in Equation 24 because fluctuations between each 2PA measurement are averaged out.

To account for one- and two-photon absorption processes occurring simultaneously within the sample, as well as any offset to β due to solvent losses (scattering or absorption), we include the one-photon absorption term in Equation 15 and becomes,

$$\frac{\partial I(r,t,z)}{\partial z} = -\alpha\,I(r,t,z) - \beta\,I(r,t,z)^2 \tag{26}$$

Here α is the 1PA coefficient. In the same way as above, the transmitted irradiance in time and in the r coordinate, $I(r,t)$, is obtained by integrating over the path length of the sample in the z direction, to obtain the transmittance through the sample,

$$I(r,t) = \frac{\alpha}{\alpha\,e^{\alpha\ell} + \beta\,I_0(r,t)\,e^{\alpha\ell} - \beta\,I_0(r,t)} \tag{27}$$

As above, the two-photon absorption quantum yield is obtained by calculating the difference between incident energy and transmitted energy as a function of position in the path length of the sample along the z direction energy, ΔE, that includes the one-photon absorption coefficient, α,

that becomes $\Delta E'$. Including the change in energy that includes the one- and two-photon absorption contributions in the Rate equation in Equation 22 and then solving for just the 2PA quantum yield gives,

$$\Phi_{2PA} = \frac{\text{Rate}}{\Delta E'}\frac{h\,c}{\lambda} - \Phi_{1PA} \tag{28}$$

This 2PA quantum yield equation is only necessary when the excitation wavelength is resonant with one-photon absorption; otherwise, when only a two-photon absorption is resonant with the excitation wavelength then Equation 24 is used to determine the 2PA quantum yield.

2.6 References

(1) Nagura, C.; Suda, A.; Kawano, H.; Obara, M.; Midorikawa, K. Generation and Characterization of Ultrafast White-Light Continuum in Condensed Media. *Appl. Opt.* **2002,** *41*, 3735-3742.

(2) Buchvarov, I.; Trifonov, A.; Fiebig, T. Toward an Understanding of White-Light Generation in Cubic Media-Polarization Properties Across the Entire Spectral Range. *Opt. Lett.* **2007,** *32*, 1539-1541.

(3) Ward, C. L. Controlling the Cycloreversion Reaction of a Diarylethene Derivative Using Sequential Two- Photon Excitation. Ph.D. Dissertation, University of Kansas, 2014.

(4) Kummel, A. C.; Sitz, G. O.; Zare, R. N. Determination of Population and Alignment of the Ground State Using Two-Photon Nonresonant Excitation. *J. Chem. Phys.* **1986,** *85*, 6874-6897.

(5) Lakowicz, J. R.; Gryczynski, I.; Gryczynski, Z.; Danielsen, E.; Wirth, M. J. Time-Resolved Fluorescence Intensity and Anisotropy Decays of 2,5-diphenyloxazole by Two-Photon Excitation and Frequency-Domain Fluorometry. *J. Phys. Chem.* **1992,** *96*, 3000-3006.

(6) van Wilderen, L. J. G. W.; Lincoln, C. N.; van Thor, J. J. Modelling Multi-Pulse Population Dynamics from Ultrafast Spectroscopy. *PLoS ONE* **2011,** *6*, e17373.

(7) Holzwarth, A. R., Data Analysis of Time-Resolved Measurements. In *Biophysical Techniques in Photosynthesis*, Amesz, J.; Hoff, A. J., Eds. Springer Netherlands: 1996; Vol. 3, pp 75-92.

(8) Negres, R. A.; Hales, J. M.; Hagan, D. J.; Van Stryland, E. W. Experiment and Analysis of Two-Photon Absorption Spectroscopy Using a White-Light Continuum Probe. *IEEE J. Quantum Elect.* **2002,** *38*, 1205-1216.

(9) Negres, R. A.; Hales, J. M.; Kobyakov, A.; Hagan, D. J.; Van Stryland, E. W. Two-Photon Spectroscopy and Analysis with a White-Light Continuum Probe. *Opt. Lett.* **2002,** *27*, 270-272.

(10) Yamaguchi, S.; Tahara, T. Two-Photon Absorption Spectrum of all-*trans* Retinal. *Chem. Phys. Lett.* **2003,** *376*, 237-243.

(11) Yamaguchi, S.; Tahara, T. Observation of an Optically Forbidden State of C_{60} by Nondegenerate Two-Photon Absorption Spectroscopy. *Chem. Phys. Lett.* **2004,** *390*, 136-139.

(12) Hosoi, H.; Yamaguchi, S.; Mizuno, H.; Miyawaki, A.; Tahara, T. Hidden Electronic Excited State of Enhanced Green Fluorescent Protein. *The Journal of Physical Chemistry B* **2008,** *112*, 2761-2763.

(13) Makarov, N. S.; Drobizhev, M.; Rebane, A. Two-Photon Absorption Standards in the 550-1600 nm Excitation Wavelength Range. *Opt. Express* **2008,** *16*, 4029-4047.

(14) Elles, C. G.; Rivera, C. A.; Zhang, Y.; Pieniazek, P. A.; Bradforth, S. E. Electronic Structure of Liquid Water from Polarization-Dependent Two-Photon Absorption Spectroscopy. *J. Chem. Phys.* **2009,** *130*, 084501.

(15) Houk, A. L.; Zheldakov, I. L.; Tommey, T. A.; Elles, C. G. Two-Photon Excitation of *trans*-Stilbene: Spectroscopy and Dynamics of Electronically Excited States Above S_1. *J. Phys. Chem. B* **2015,** *119*, 9335-9344.

(16) Kovalenko, S. A.; Dobryakov, A. L.; Ruthmann, J.; Ernsting, N. P. Femtosecond Spectroscopy of Condensed Phases with Chirped Supercontinuum Probing. *Phys. Rev. A* **1999,** *59*, 2369-2384.

(17) Isobe, K.; Kawano, H.; Suda, A.; Kumagai, A.; Miyawaki, A.; Midorikawa, K. Simultaneous Imaging of Two-Photon Absorption and Stimulated Raman Scattering by Spatial Overlap Modulation Nonlinear Optical Microscopy. *Biomed. Opt. Express* **2013,** *4*, 1548-1558.

(18) Monson, P. R.; McClain, W. M. Polarization Dependence of the Two-Photon Absorption of Tumbling Molecules with Application to Liquid 1-Chloronaphthalene and Benzene. *J. Chem. Phys.* **1970,** *53*, 29-37.

(19) McClain, W. M. Excited State Symmetry Assignment Through Polarized Two-Photon Absorption Studies of Fluids. *J. Chem. Phys.* **1971,** *55*, 2789-2796.

(20) Monson, P. R.; McClain, W. M. Complete Polarization Study of the Two-Photon Absorption of Liquid 1-Chloronaphthalene. *J. Chem. Phys.* **1972,** *56*, 4817-4825.

(21) Wirth, M. J.; Koskelo, A.; Sanders, M. J. Molecular Symmetry and Two-Photon Spectroscopy. *Appl. Spectrosc.* **1981,** *35*, 14-21.

(22) Bechtel, J. H.; Smith, W. L. Two-Photon Absorption in Semiconductors with Picosecond Laser Pulses. *Phys. Rev. B* **1976,** *13*, 3515-3522.

(23) Liu, P.; Smith, W. L.; Lotem, H.; Bechtel, J. H.; Bloembergen, N.; Adhav, R. S. Absolute Two-Photon Absorption Coefficients at 355 and 266 nm. *Phys. Rev. B* **1978,** *17*, 4620-4632.

(24) Dragonmir, A.; McInerney, J. G.; Nikogosyan, D. N. Femtosecond Measurements of Two-Photon Absorption Coefficients at λ = 264 nm in Glasses, Crystals, and Liquids. *Appl. Opt.* **2002,** *41*, 4365-4376.

(25) Dragomir, A.; McInerney, J. G.; Nikogosyan, D. N.; Ruth, A. A. Two-Photon Absorption Coefficients of Several Liquids at 264 nm. *IEEE J. Quantum Electron.* **2002,** *38*, 31-36.

(26) Dragomir, A.; McInerney, J. G.; Nikogosyan, D. N.; Kazansky, P. G. Two-Photon Absorption Properties of Commercial Fused Silica and Germanosilicate Glass at 264 nm. *Appl. Phys. Lett.* **2002,** *80*, 1114-1116.

3. Two-Photon Excitation of *trans*-Stilbene: Spectroscopy and Dynamics of Electronically Excited States above S_1

(Published previously by Houk, *et al.* in The Journal of Physical Chemistry B)[1]

3.1 Introduction

Probing the ultrafast dynamics of molecules in electronically excited states above S_1 represents an important frontier in the field of chemical reaction dynamics that challenges the current limits of both experiment and theory.[2] Among other complications, the rapidly increasing density of electronic states leads to strong configurational mixing and very short excited-state lifetimes for even the smallest of molecules, as manifest in Kasha's rule.[3] Nevertheless, probing the behavior of these highly excited systems is important for developing a predictive and general understanding of the nonadiabatic dynamics that govern chemical reactions under a wide range of conditions.

Extensive work over the past 70 years provides significant insight into the photoisomerization dynamics of stilbene, making this compound an ideal prototype for studying excited-state dynamics.[4-8] Experimental[9-19] and theoretical[20-28] studies reveal a mechanism in which torsional rotation around the central C=C double bond carries the molecule over a small barrier in the S_1 excited state before passing through a conical intersection (CI) that returns the molecule to S_0. The CI connecting the ground and excited electronic states is located near the minimum of the S_1 excited-state potential energy surface, where the phenyl rings have perpendicular orientation, but also requires some degree of pyramidalization at one of the ethylene carbon atoms.[25,27] Passage through the CI results in a roughly 1:1 ratio of *cis*- and *trans*-stilbene.[4]

One-photon excitation of the lowest excited state of *trans*-stilbene initially accesses a singly excited state with $\pi\pi^*$ character. However, the electronic configuration that correlates diabatically with the ground electronic state of the product, and therefore participates in the CI, is a doubly excited state with $\pi^*\pi^*$ character (becoming $\pi\pi$ in the ground state).[21,29] This two-electron excited state of *trans*-stilbene has been observed previously using two-photon absorption spectroscopy,[29-35] which is suitable for accessing doubly excited states because of the propensity for two-photon–two-electron interactions.[36] Two-photon excitation also satisfies the symmetry selection rules for accessing the totally symmetric (A_g) $\pi^*\pi^*$ state; therefore, the electronic configuration that correlates diabatically with the product ground state is accessible directly via a symmetry-allowed two-photon $(HOMO)^2 \rightarrow (LUMO)^2$ transition from a equilibrium ground state of the *trans* isomer. Although there have been no direct reports of the excited-state dynamics following two-photon excitation, competing kinetics measurements for both isomers indicate that the *cis–trans* isomerization process is more efficient following two-photon excitation than for one-photon excitation.[37-39]

Despite the detailed picture that emerges for dynamics on the lowest $\pi\pi^*$ excited state of stilbene, and even for the $\pi^*\pi^*$ excited state, much less is known about the dynamics in the higher-lying excited states, or how excitation to these levels might be used to selectively control the photoisomerization reaction. Recently, Bao and Weber probed the dynamics of *cis*- and *trans*-stilbene in the gas phase following excitation of one-photon-accessible excited-states lying roughly 6 eV above the respective ground-state minima, and observed distinctly different dynamics than the well-known torsional isomerization pathway that occurs on S_1.[17,18,40] In particular, coherent oscillations in the higher-lying excited-state (S_5) of *trans*-stilbene were attributed to an antisymmetric twisting motion of the phenyl groups about the C–C single bonds,

which suggests that excitation to higher excited-states gives rise to different initial motions of *trans*-stilbene than on the S_1 surface. Similarly, Kovalenko and coworkers[13] probed the solution-phase photoisomerization dynamics of stilbene following one-photon excitation to the second absorption band at 226 nm, from which they observed rapid (sub-100 fs) internal conversion followed by vibrational cooling on the lowest excited state.

The experiments presented in this chapter examine the spectroscopy and dynamics of two-photon-accessible excited-states of *trans*-stilbene in solution. Mutually exclusive selection rules due to the inversion center of *trans*-stilbene ensure that one- and two-photon excitation access different excited states of the molecule. Here, we present the first *continuous* 2PA spectrum of *trans*-stilbene up to 6.5 eV, and then compare the excited-state dynamics following one- and two-photon excitation. Our results provide new benchmarks for computational studies of the electronic structure and excited-state dynamics of *trans*-stilbene above S_1.

3.2 Experimental Methods

We use ultrafast pump-probe techniques to examine the spectroscopy and dynamics of *trans*-stilbene in solution. Briefly, the two-photon absorption (2PA) spectrum is obtained from the wavelength-dependent attenuation of a broadband probe pulse that is temporally and spatially overlapped in the sample with a nonresonant pump pulse,[41-45] whereas the excited-state dynamics are monitored via the evolution of the transient absorption (TA) spectrum as a function of time following one- or two-photon excitation.[46,47] In both experiments, pump and probe pulses are derived from the output of a regeneratively amplified Ti:Sapphire laser (Legend Elite, Coherent). Nonlinear frequency conversion produces pump pulses that are tunable across the visible-UV, and continuum generation in a 2 mm CaF_2 crystal produces broadband probe pulses covering the

range 750-350 nm. We control the relative polarization of the linearly polarized pump and probe light by rotating a λ/2 waveplate in the 800 nm fundamental prior to continuum generation, while also rotating the CaF_2 crystal to maintain the polarization purity of the probe beam.[48,49] After passing through the sample, the probe light is dispersed with a UV transmission grating onto a 256 element photodiode array for shot-to-shot detection. A chopper wheel blocks alternating pump pulses before the sample for active background subtraction. We typically average 6×10^3 laser pulses per delay for the 2PA measurements and 10^4 laser pulses per delay for the TA measurements, as described below.

In the 2PA experiments, the simultaneous absorption of one pump and one probe photon occurs when the combined energy of the two photons is resonant with a two-photon-allowed transition, but neither photon is absorbed individually.[41-45] Using three different pump wavelengths (370, 390, and 420 nm) and a continuum probe in the range 750–400 nm gives overlapping spectra that cover the full range of 2PA transition energies from 4.6 to 6.5 eV. We scan the relative delay of the two pulses in order to account for temporal dispersion of the probe and then integrate the transient signal at each probe wavelength over a range of delay times (typically ±0.3 ps relative to the optimum temporal overlap) to obtain the relative 2PA cross section as a function of the total pump + probe transition energy.[41] The integrated signal is independent of nonresonant effects, such as cross-phase modulation of the probe light.[41,50] Varying the integration range confirms that there are no contributions to the signal from photoproduct transient absorption, because the integrated signal does not change when increasing the integration window outside of the region of pulse overlap. The diameters of the overlapping pump and probe beams are ~300 μm and ~100 μm at the sample, respectively, and the average energy of the pump pulse is typically 35 nJ/pulse. The sample for the 2PA measurements

consists of a 1 mm path length quartz cuvette filled with a 0.5 M solution of *trans*-stilbene (Aldrich, 96%) in chloroform (Sigma-Aldrich, ≥99%). We are unable to measure the 2PA spectrum of *trans*-stilbene in cyclohexane due to low solubility in that solvent.

Separate TA experiments probe the excited-state dynamics of *trans*-stilbene following one- and two-photon excitation.[47,48] One-photon excitation (1PE) experiments use pump pulses at 310 nm (4.0 eV) that are resonant with the lowest absorption band of *trans*-stilbene. The ~0.5 μJ pulses are weakly focused to a diameter of ~300 μm at the sample, where they intersect the ~100 μm diameter probe beam. Nonresonant two-photon excitation (2PE) requires higher-intensity pump pulses, therefore we reduce the beam diameter to ~100 μm at the sample and increase the pulse energy (~2 μJ at 475 nm, or ~3 μJ at 380 nm). The intense, nonresonant pump beam induces degenerate two-photon excitation at a total transition energy equal to twice the photon energy, which is 5.2 eV for 475-nm irradiation and 6.5 eV for 380-nm irradiation. The TA measurements cover a range of delays on a quasi-logarithmic scale from –1 to 800 ps, with the relative polarization of the pump and probe set to the magic angle (54.7°) in order to exclude anisotropic effects. Samples of *trans*-stilbene in cyclohexane (Sigma-Aldrich, >99%) were prepared with concentrations of 1.2 mM for the 1PE measurements and 6.5 mM for the 2PE measurements. The sample solution passes through a slit nozzle to form a windowless liquid stream with a path length of 300 μm.

3.3 Results and Analysis

3.3.1 One- and Two-Photon Absorption Spectroscopy

The top panel of Figure 3.1 shows the one-photon absorption (1PA) spectrum of *trans*-stilbene in solution. The spectrum is essentially the same in both cyclohexane and chloroform,

except for a weak bathochromic shift of 4 nm. Solvent absorption below 260 nm prevents us from measuring the full 1PA spectrum of *trans*-stilbene in chloroform. The three prominent bands in the 1PA spectrum, located near 4.1, 5.4, and 6.1 eV, have been discussed extensively in the literature.[29,34,51,52] The solid vertical bars in the figure represent transition energies and oscillator strengths for one-photon allowed transitions that were calculated by Molina et al.[52] using CASPT2. The calculated energies are in good agreement with our experimental spectrum (see Table 3.1).

The bottom panel of Figure 3.1 shows the two-photon absorption (2PA) spectrum of *trans*-stilbene in chloroform. We measure the broadband 2PA spectrum using both parallel and perpendicular relative polarization of the pump and probe light. In both cases, the spectrum has distinct bands centered near 5.1 and 6.4 eV, with the only difference being a cross section (σ) that is smaller by about a factor of 3 for perpendicular polarization. The inset shows that the polarization ratio, $\sigma_{para}/\sigma_{perp}$, is constant across the entire spectrum. The figure also shows the baseline signal obtained under identical conditions for pure chloroform, and confirms that 2PA by the solvent is insignificant below 6.5 eV. The hollow vertical bars in the figure mark the calculated (CASPT2) transition energies for two-photon accessible states of *trans*-stilbene from Molina et al.[52] All of the bars have the same height in this case because those authors did not report two-photon absorption intensities.

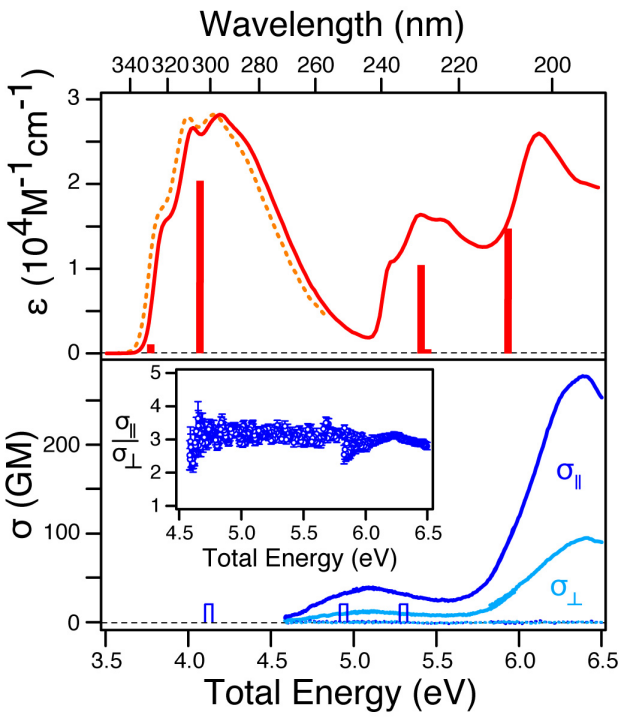

Figure 3.1 One- and two-photon absorption spectroscopy of *trans*-stilbene in solution. The top panel shows one-photon absorption spectra in cyclohexane (solid line) and in chloroform (dashed line). The bottom panel shows two-photon absorption spectra in chloroform, measured using both parallel (dark blue line) and perpendicular (light blue line) relative polarization of the pump and probe light. The inset shows the ratio of the two-photon cross sections for parallel and perpendicular polarization. The solid bars in the top panel are calculated one-photon transition energies and intensities, and the hollow bars in the lower panel are two-photon transition energies, both from Ref. 52.

The experimental 2PA cross sections at the maxima of the two absorption bands are 40±16 and 270±110 GM (1 GM = 10^{-50} $cm^4 \cdot s \cdot molecule^{-1} \cdot photon^{-1}$), respectively, for parallel polarization of the pump and probe light. The uncertainties in the absolute 2PA cross sections represent estimated 95% confidence intervals. As in all 2PA experiments, obtaining the absolute

cross section requires precise knowledge of the spatially dependent intensity profile,[53] therefore we measure the horizontal and vertical profiles of both beams at the sample position in order to determine the spatial overlap of the two beams. Small deviations from the ideal overlap conditions and subtle imperfections of the pump and probe beams are the primary sources of uncertainty in our measurement.

Table 3.1 One- and two-photon transition energies of *trans*-stilbene (in eV).

Excited State	Experimental	Calculated CASPT2 (major configuration)[a]	Calculated SDCI/P 200[b]
^1B_u	4.03	3.77 ($4a_u \rightarrow 5b_g$)[c]	4.31
		4.07 ($4a_u \rightarrow 4b_g$)[c]	4.67
^1A_g	5.12	4.13 ($3b_g \rightarrow 4b_g$)	4.67
		4.95 ($4a_u^2 \rightarrow 4b_g^2$)	5.23
		5.30 ($2b_g \rightarrow 4b_g$)	5.93
^1B_u	5.41	5.42 ($3a_u \rightarrow 4b_g$)	5.80
		5.42 ($4a_u \rightarrow 5b_g$)	6.27
		5.46 ($2a_u \rightarrow 4b_g$)	6.60
^1B_u	6.14	5.95 ($3a_u \rightarrow 5b_g$)	7.07
^1A_g	6.40		6.19
			7.05
			7.15

[a] Ref. 52. [b] Ref. 29. [c] See Ref. [54] for a discussion about the correct ordering of the two lowest states.

Our results for the lower energy band are in excellent agreement with degenerate 2PA cross sections in the range of 8-80 GM that were measured previously using various nonlinear techniques.[29-32,55-58] Although the cross section is not necessarily the same for degenerate and nondegenerate excitation at the same total energy, we expect only small deviations in this case, because both pump and probe photons are individually nonresonant, and therefore resonance-enhancement effects are negligible.

Importantly, these are the first 2PA spectra of stilbene to be measured on a continuous energy scale, rather than point by point. This is also the first *direct* measurement of the 2PA spectrum. Previous measurements used indirect methods, such as two-photon fluorescence or thermal lensing, to measure the "action" cross section on a point-by-point basis while tuning the excitation laser across the spectrum.[29-35] Even after applying a wavelength-dependent correction to obtain the two-photon absorption from the action cross section,[32] point-by-point measurements are susceptible to variation of the pump beam conditions at each wavelength. By simultaneously measuring a broad range of the 2PA spectrum with a broadband probe pulse, our measurement is less sensitive to variations across the spectrum, and therefore provides a more accurate representation of the energy-dependence of the 2PA cross section. Notably, we do not observe vibronic structure in the 2PA bands, as was previously reported.[29,33,35] By recording the absorption cross section directly, our measurement is also independent of the wavelength-varying fluorescence quantum yield.[29,31-35]

The polarization dependence of the 2PA spectrum in the inset of Figure 3.1 confirms that only A_g-symmetry states contribute to the 2PA spectrum below 6.5 eV. The polarization ratio $\sigma_{para}/\sigma_{perp}$ depends on the relative symmetry of the two transition dipole moments associated with a transition, and therefore reveals the overall symmetry of the transition.[59-61] For molecules in the C_{2h} point group, totally symmetric (A_g) transitions give a ratio $\geq 4/3$, and nontotally symmetric (B_g) transitions give a ratio $<4/3$.[59] The constant experimental polarization ratio of ~3 across the entire spectrum therefore indicates that only A_g-symmetry transitions are responsible for the 2PA bands below 6.5 eV. Our observation is consistent with the absence of calculated B_g-symmetry states within the range of our 2PA spectrum,[29,62] as well as the constant polarization ratio for degenerate excitation comparing circular and linearly polarized light, $\sigma_{circ}/\sigma_{para}$, across the lowest

2PA band.[29,31,33] Deviations from the planar equilibrium geometry play a negligible role in the spectrum of *trans*-stilbene in solution;[31] therefore, the polarization ratio provides a good measure of the electronic symmetries of the two-photon accessible excited states.

3.3.2 Excited-State Dynamics Following One- and Two-Photon Excitation

Figure 3.2A shows the evolution of the transient absorption spectrum of *trans*-stilbene following excitation with one-photon at 310 nm (total energy of 4.0 eV). Consistent with earlier studies,[9,13,16,19,63-65] the TA spectrum is dominated by an excited-state absorption (ESA) band centered near 585 nm and a weaker stimulated emission (SE) band near 365 nm. The asymmetry of the ESA band, including a weak shoulder near 550 nm, was previously assigned as a vibronic progression in the $S_n \leftarrow S_1$ transition.[13,66-70] Both the positive ESA band at 585 nm and the negative SE band at 365 nm decay to the baseline on a timescale that is consistent with the previously reported lifetime of 69±11 ps for *trans*-stilbene in cyclohexane.[11] We also observe very weak shifting and narrowing of the spectrum within the first 10-20 ps due to vibrational cooling in the excited state.[13]

On the basis of previous interpretations of the excited-state dynamics of *trans*-stilbene,[9,15,16,19,63,64] we model the ps-scale relaxation following one-photon excitation with a sequential, two-step kinetic scheme.

$$S_1^* \overset{k_1}{\rightarrow} S_1 \overset{k_2}{\rightarrow} S_0$$

The first species represents vibrationally excited stilbene in the first excited electronic state, S_1^*, which relaxes to the thermally populated S_1 state before returning to the ground electronic state. The TA signal is insensitive to the branching between *cis* and *trans* isomers

when returning to the ground state, because neither of the ground-state species absorb in the probe window.

A global fit to the broadband TA data using this simple kinetic model gives time constants of $(k_1)^{-1}$ = 8±2 ps and $(k_2)^{-1}$ = 78±6 ps (95% confidence) for the two steps in the sequential relaxation. Although the excitation at 310 nm deposits very little excess energy above the S_1 band origin,[71] we include the S_1^* state in the model in order to obtain the best possible fits to the data and for consistency with the analysis at higher excitation energies. Species-associated spectra (SAS) obtained from the best fit to the transient absorption data for one-photon excitation at 4.0 eV are shown in the top panel of Figure 3.3. The slight narrowing and shifting of the ESA band between the first and second species is characteristic of vibrational cooling in the excited state.[13,15,19]

The lower two panels of Figure 3.2 show the TA spectrum following two-photon excitation at 475 nm (total energy 5.2 eV) and 380 nm (total energy 6.5 eV), respectively. The TA signals are much weaker than for 1PE due to a substantially smaller cross section for two-photon excitation, that is only partially offset by the higher concentration and more intense pump pulses. Additionally, the two-photon process depends quadratically on the excitation intensity, which amplifies small fluctuations of the pump pulse intensity and further increases the noise level in the 2PE experiments. As expected from the relative 2PA cross sections, exciting the lower-energy band at 5.2 eV with two photons produces a weaker TA signal than does exciting the higher-energy band at 6.5 eV. To compensate for the lower signal-to-noise ratio in the lower-energy 2PE scan, we average three adjacent time points to obtain the TA spectrum in Figure 3.2B. Figure 3.7 in the Appendix compares the ps-scale time evolution of the ESA and SE bands for all three excitation pathways.

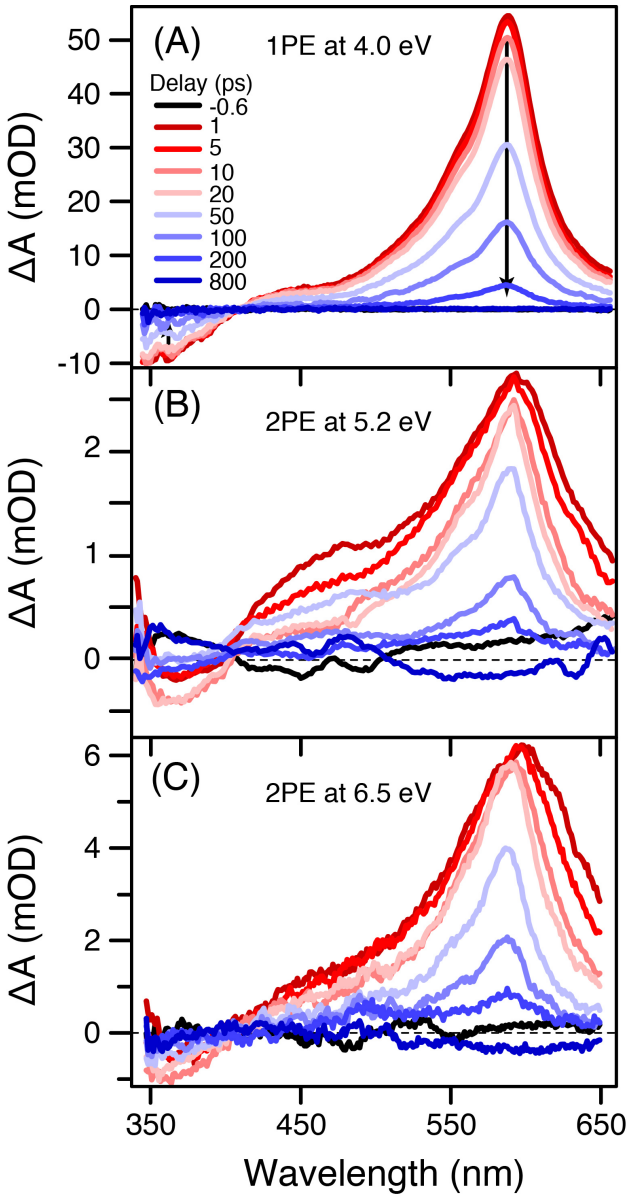

Figure 3.2 Transient absorption spectra of *trans*-stilbene following one-photon excitation at 310 nm (A), two-photon excitation at 475 nm (B), and two-photon excitation at 380 nm (C). The spectra in part B are averaged over three adjacent time points in order to improve the signal-to-noise ratio.

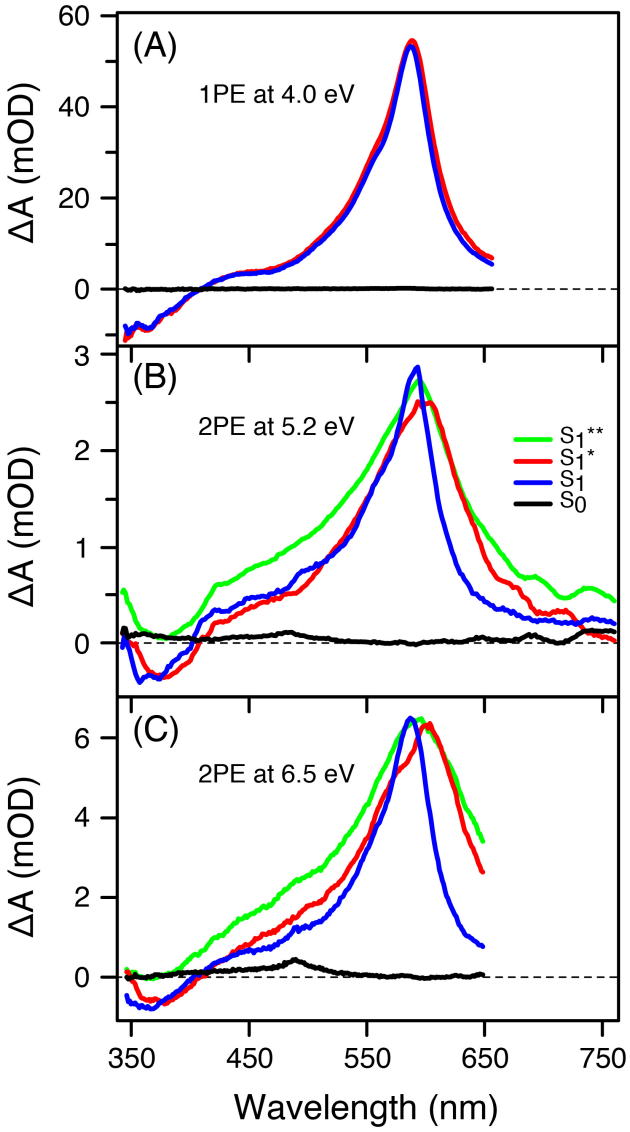

Figure 3.3 Species-associated spectra (SAS) from global fits to the transient absorption data using the sequential kinetics models described in the text. Excitation with one-photon of 310 nm (A), excitation with two photons of 475 nm (B), and excitation with two photons of 380 nm (C).

Despite the lower signal-to-noise ratio for the two-photon excitation experiments, we clearly observe additional spectral evolution on a timescale of 1-2 ps that is not observed following one-photon excitation into the lowest-energy absorption band. In order to model the

additional spectral evolution, we add an extra species to the sequential kinetic model to represent a precursor to S_1^*.

$$S_1^{**} \overset{k_1}{\rightarrow} S_1^* \overset{k_2}{\rightarrow} S_1 \overset{k_3}{\rightarrow} S_0$$

The lower two panels of Figure 3.3 show the SAS obtained from global fits to the ps-scale transient absorption data using this four-state model. The additional step in the relaxation reveals spectral narrowing (primarily on the high-energy side of the ESA band) with time constants of 1.9±1.2 ps and 1.5±0.3 ps following 2PE at 5.2 and 6.5 eV, respectively. In both cases, the initial relaxation is followed by two slower steps that occur on the same timescales as the relaxation following 1PE.

The similar spectra of all three species in the 2PE experiments (*i.e.* S_1^{**}, S_1^*, and S_1) suggest that S_1^{**} represents another vibrationally excited state of S_1. Therefore, we propose that S_1^{**} represents a highly nonstatistical distribution of vibrational energy in S_1 following rapid (sub-ps) internal conversion from the initially excited state, S_n. Intramolecular vibrational redistribution (IVR) produces a more statistical distribution of vibrational energy, represented by S_1^*, within the next 1-2 ps. The red-shift and broadening of the S_1^* spectrum is significantly more pronounced for excitation to the higher-lying states than it is following 1PE at 310 nm, because of the larger amount of excess energy deposited into the molecule. The ~8 ps relaxation time of S_1^* is consistent with vibrational cooling (VC) of the hot excited state.[9,19,63,64,71] Both the vibrational cooling time and the ~80 ps excited-state (ES) lifetime of S_1 are consistent with the 1PE result. Based on this picture, we re-label the time constants from the two kinetic models to reflect the underlying process in each step (*i.e.* τ_{IVR}, τ_{VC}, and τ_{ES}). Table 3.2 summarizes the time constants for all three excitation energies.

Table 3.2 Time constants for intramolecular vibrational relaxation (τ_{IVR}), vibrational cooling (τ_{VC}), and relaxation of the excited state (τ_{ES}) of *trans*-stilbene from global fits to the transient absorption spectra using sequential kinetic models.[a]

	τ_{IVR} / ps	τ_{VC} / ps	τ_{ES} / ps
1PE (4.0 eV)	–	7.6 (1.8)	78 (6)
2PE (5.2 eV)	1.9 (1.2)	6.2 (2.5)	83 (17)
2PE (6.5 eV)	1.5 (0.3)	9.3 (1.5)	82 (5)

[a] Values in parentheses are estimated uncertainties at 95% confidence. The wavelength-dependent amplitudes associated with each time constant are available as decay associated spectra (DAS) in Figure 3.8 of the Appendix.

We see evidence of the faster $S_n \rightarrow S_1$ electronic relaxation on a sub-ps timescale, as shown in Figure 3.4. The figure compares the evolution of the transient absorption spectrum within the first 600 fs following one- and two-photon excitation of *trans*-stilbene. The most obvious difference between the two transient spectra is a new, short-lived absorption band in the higher-energy region of the spectrum following 2PE. The short-lived absorption band precedes the formation of the 585-nm ESA band following two-photon excitation (Figure 3.4B), whereas the rise of the 585-nm ESA band is instrument-limited following one-photon excitation (Figure 3.4A). A delayed onset of the S_1 excited-state absorption and stimulated emission bands was also observed by Kovalenko et al.[13] following one-photon excitation into the second absorption band at 226 nm, therefore we interpret the delayed appearance of the 585-nm ESA band as relaxation from the initially excited electronic state S_n to the vibrationally hot S_1^{**}.

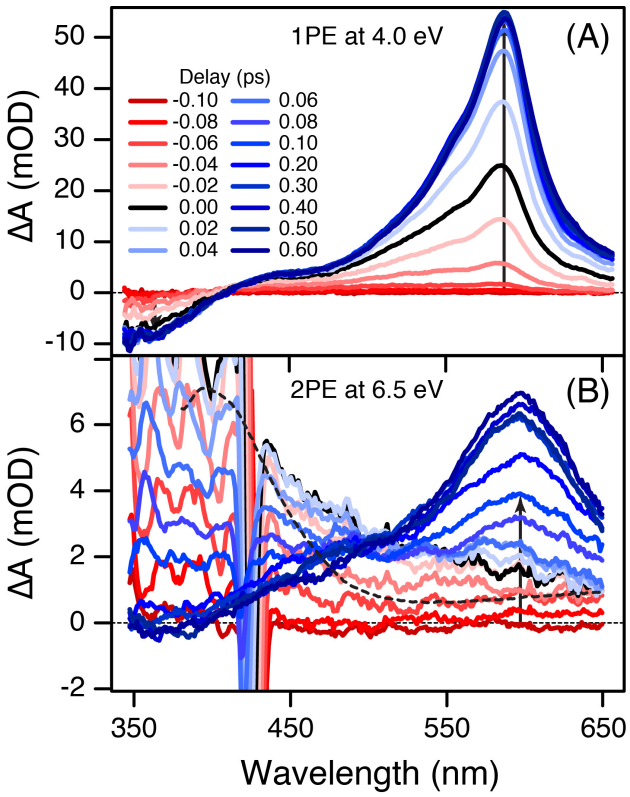

Figure 3.4 Transient absorption spectra of *trans*-stilbene at early time delays following excitation with one-photon at 310 nm (A) and two-photons at 380 nm (B). The black arrows show the rising excited-state absorption signal up to a delay of 100 fs. Note that the rise in the ESA band is complete with the instrument response time of ~75 fs in Part A, but the signal continues to rise for several hundred fs in Part B. The thin dashed line in part B is the scaled two-photon absorption spectrum, and therefore represents an upper limit for the 2PA contribution to the transient absorption signal at 0 ps delay (black line).

Figure 3.5 shows the temporal evolution of the sub-ps transient absorption signals at several probe wavelengths. Following two-photon excitation the short-lived TA signal at 400 nm decays within ~100 fs, with a weak tail extending to a few hundred fs. The fleeting transient absorption signal is at least partially due to ESA from an electronic state above S_1, as discussed

below. The initial decay of this band is comparable to the instrument response time of ~75 fs (FWHM), reflecting a very short lifetime for the higher-lying electronically excited state. The slower decaying tail at 400 nm, which matches the rise at 600 nm, could be either an intermediate electronic state, or a very nonstatistical distribution of vibrational energy in S_1 that precedes even S_1^{**}.

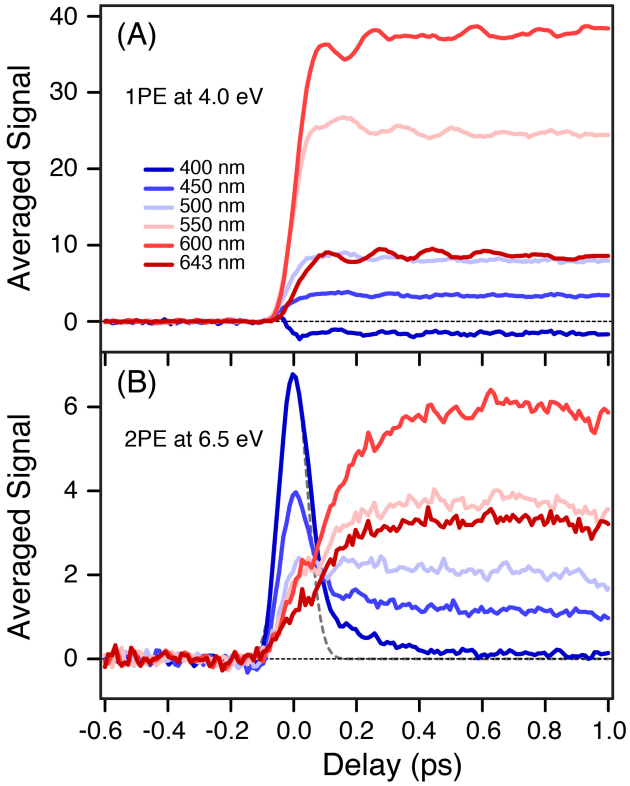

Figure 3.5 Evolution of the transient absorption of *trans*-stilbene at early time delays following excitation with one-photon at 310 nm (A) and two-photons at 380 nm (B). Each transient is averaged over an ~13 nm range of probe wavelengths (11 adjacent pixels) to improve the signal-to-noise. The dashed line in Part B is the instrument response function for the two-photon excitation experiment, based on the coherent Raman response of the solvent at 425 nm.

Nonresonant two-photon (pump + probe) absorption could also contribute to the short-lived TA signal within the instrument response time. However, the spectral shape of the TA feature in Figure 3.4B is inconsistent with the broadband 2PA spectrum in Figure 3.1. Most notably, the short-lived TA band decreases monotonically across the spectrum, with no evidence of the 2PA minimum at 5.6 eV. The 2PA minimum would be observed at a probe wavelength of 530 nm in the case of the 380-nm pump (*i.e.* 3.3 eV pump + 2.3 eV probe), as shown by the dashed line in Figure 3.4B. The 2PA signal cannot exceed the total TA signal at any single wavelength; therefore, the dashed line represents the *upper limit* of the signal due to nonresonant two-photon (pump + probe) absorption, and indicates that the ESA of an electronically excited state is responsible for at least a majority of the time-zero TA signal in the region 450-600 nm.[72] The isosbestic point near 500 nm further supports the picture of a sequential population decay from S_n to S_1^{**} following 2PE at 6.5 eV.

The situation is less clear following 2PE at 5.2 eV, due to the lower signal-to-noise ratio, and because the Raman response of the solvent induced by 475-nm pump light overlaps a broader region of the transient absorption spectrum. However, subtraction of the solvent signal (see the Appendix) indicates that there is probably a similar short-lived ESA band in that case, as well. Therefore, the sub-ps evolution of the TA spectrum reveals internal conversion from a higher-lying electronic state (or states) and the formation of the highly vibrationally excited S_1^{**} following 2PE at both excitation energies.

3.4 Discussion

One- and two-photon absorption spectroscopy reveals a great deal of information about the electronic structure of *trans*-stilbene. The one- and two-photon spectra are complementary,

because different transitions are allowed in the two cases based on parity selection rules and the C_{2h} symmetry of the planar molecule. The one-photon spectrum of *trans*-stilbene has been discussed widely,[29,34,51,52] therefore we describe primarily the 2PA spectrum. We observe two distinct, broad transitions near 5.1 and 6.4 eV, respectively. These two bands represent the two excited electronic states that we access in the transient absorption experiments.

As a first step toward identifying the two-photon-accessible excited states, the 2PA polarization ratio (Figure 3.1, inset) indicates that only A_g-symmetry states contribute to the two-photon spectrum below 6.5 eV. Calculations show that there are several two-photon accessible states with A_g symmetry in the region of our experiment.[21,22,29,52,62,73-75] Although we compare our experimental transition energies with the CASPT2 calculations by Molina et al.,[52] those authors did not report 2PA intensities; therefore, we look to lower-level configuration interaction calculations to help identify which states contribute to the 2PA spectrum (see Table 3.1). The latter calculations suggest that the lowest-lying A_g-symmetry state has a much smaller 2PA cross section than higher-lying states of the same symmetry.[29,76] The calculations are consistent with earlier observations of a very weak 2PA band near 4.1 eV that lies below the range of our 2PA spectrum.[29,35] In contrast, the second lowest-energy state with A_g-symmetry has a larger two-photon absorption cross section.[29] This transition has significant doubly excited character ($4a_u^2 \rightarrow 4b_g^2$),[52] and was previously attributed to the 2PA band near 5.1 eV. However, the identity of the higher-energy 2PA band near 6.4 eV is less clear. The calculations do not reveal a single electronic state that is responsible for this more intense, higher-lying two-photon transition, but rather several states that may contribute (see Table 3.1).[29] Given the high density of electronic states and significant configurational mixing, we expect strong coupling among these higher-lying electronic states.

The state diagram in Figure 3.6 provides a reference point for describing the excited-state dynamics in the context of the one- and two-photon absorption spectroscopy of *trans*-stilbene. The schematic energy-level diagram in the figure also incorporates information from electronic structure calculations,[25,27,77] as well as previous dynamics measurements.[9-13,15-19,63-65] The dynamics following excitation into the first absorption band have been discussed widely; however, the dynamics following excitation to the higher-lying states have received much less attention.[13,17,18,40]

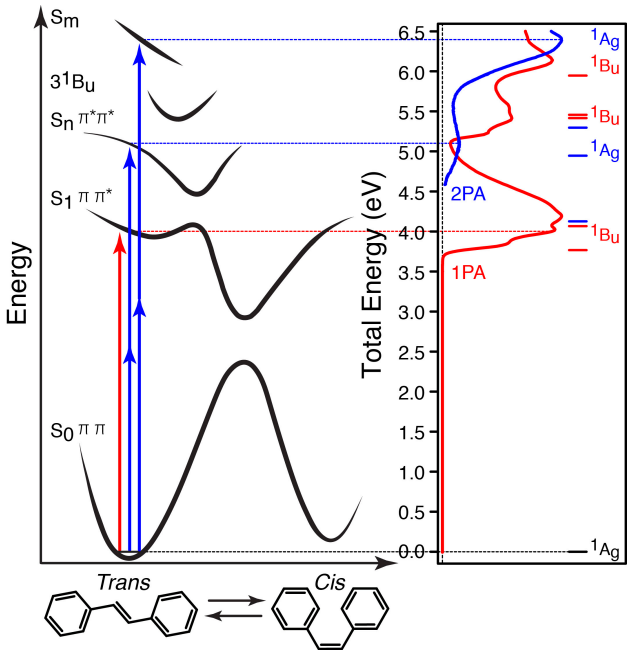

Figure 3.6 Schematic diagram comparing potential energies curves for several excited states of *trans*-stilbene with the one- and two-photon absorption spectra from the current work and with calculated transition energies from Ref. 52.

Two-photon excitation at 5.2 eV accesses a state with significant doubly excited ($\pi^*\pi^*$) character, and therefore correlates diabatically to the ground state of the *cis* isomer. Further

evidence to support the preferential correlation to the *cis* isomer are 2PE quantum yield measurements which revealed a 4:1 ratio of the *cis* and *trans* isomers following 2PE of *trans*-stilbene with 532 nm light.[37,38] Despite an electronic configuration that is diabatically similar to the ground state of the product, the ps-scale transient absorption spectroscopy and excited-state lifetimes following 2PE of this state are identical to the ps-scale results following 1PE of the lowest ($\pi^*\pi$) excited state at 4.0 eV. Similar ps-scale dynamics are also observed following two-photon excitation to a higher-lying state at 6.5 eV. The similar result for all three excitation energies indicates that the isomerization reaction follows an analogous path on the adiabatic S_1 state, regardless of the initial excitation level. In other words, rapid electronic relaxation from the higher-lying excited state puts the molecule on S_1 before crossing a barrier along the torsional coordinate that inhibits motion to the S_1–S_0 conical intersection. That is to say, the molecule probably does not reach a perpendicular geometry in the higher-excited state before relaxing onto S_1.

Fast electronic relaxation from the higher-lying states to the lowest excited state is predicted by Kasha's rule. Surprisingly, however, the excess vibrational energy following internal conversion to S_1 does not efficiently couple into the reaction coordinate. There are two explanations for this behavior. Either IVR is incomplete, and therefore the excess energy does not accelerate the barrier crossing before dissipating to the solvent, or else IVR is complete, but there is simply too little energy overall to accelerate the reaction substantially. Assuming equipartition, 2PE at 5.2 eV deposits only ~31 cm^{-1} of excess energy per mode and ~177 cm^{-1} for 2PE at 6.5 eV. Given the observation of rapid IVR in the first 1-2 ps following internal conversion to the S_1 state, the second situation seems more likely.

The 1-2 ps IVR process that we observe following two-photon excitation indicates an added degree of structural relaxation compared with one-photon excitation to S_1 directly. The highly nonstatistical distribution of vibrational energy in S_1^{**} is a result of the internal conversion from a higher-lying electronic state. Although that excess vibrational energy does not couple efficiently into the torsional motion of the molecule, the center wavelength of the ESA band temporarily shifts to lower energy in going from S_1^{**} to S_1^{*}, and then shifts back upon cooling to the S_1 equilibrium state (see the SAS in Figure 3.3). This behavior provides a sensitive probe of the energy disposal by probing the transient population of one or a few specific vibrational modes of the molecule that are responsible for changing the Franck-Condon overlap with the higher-lying state in the transition. For example, similar effects are responsible for coherent oscillations of the 585 nm ESA band within the first ps following 1PE (see Figure 3.5), which reveals an in-plane C=C–Ph bending motion on the S_1 excited state.[78] Bao and Weber observed coherent oscillations in a different mode that they assigned as torsional motion of the phenyl groups following excitation in the gas phase with one-photon at 5.93 eV.[17,18] In contrast, we do not observe any coherent oscillations following 2PE at 5.2 or 6.5 eV. Either the very short electronic lifetimes lead to rapid dephasing, or else electronic spectroscopy is simply not sensitive to the specific motions that are induced by excitation to these particular excited states. Electronic spectroscopy is a relatively insensitive measure of the vibrational dynamics, therefore transient Raman spectroscopy[65,71,79-85] could provide additional insight following excitation to the higher-lying states of *trans*-stilbene.

The transient absorption spectroscopy measurements also reveal a very short-lived excited state species following excitation to the higher-lying states. Unfortunately, we are not able to clearly resolve the ESA spectra in order to distinguish different states that may be

involved in the relaxation pathways following 2PE. Nevertheless, the TA spectra provide a direct probe of the timescales for electronic relaxation from the higher-lying states to S_1. Consistent with Kasha's rule, internal conversion to S_1 occurs very rapidly, even though the molecule starts in a state with different electronic symmetry. One possible pathway to explain the similar short-lived ESA spectra for the two excitation energies is that the molecule relaxes from the initially excited state to the lowest-lying A_g-symmetry state in <75 fs, and then relaxes to S_1^{**} on the ~100 fs timescale, in which case the ESA contribution that we observe in Figure 3.4B probes the population of the lowest-energy A_g state.

3.5 Conclusions

Complementary two-photon absorption spectroscopy and two-photon excitation measurements give new insight into the dynamics of the higher-lying excited states of *trans*-stilbene in solution. Spectroscopy is a fundamental tool for determining the excited-state energies and identifying the initial excited states that are populated by one- and two-photon transitions. For example, the absorption of a single photon at 310 nm excites the molecule slightly above the origin of the lowest excited state, depositing a small amount of excess vibrational energy that dissipates to the solvent in ~8 ps.[71] The molecule then returns to the ground electronic state in ~80 ps by passing through a conical intersection with roughly 1:1 branching between the *cis* and *trans* isomers.[4] Two additional relaxation processes are observed within the first few ps following excitation with two-photons to higher-lying excited-states. Internal conversion from the initially excited state, S_n, to a nonequilibrium S_1^{**} state occurs within ~100 fs, followed by rapid IVR (1–2 ps). The ensuing dynamics are exactly the same as the case of one-photon excitation.

Higher-lying excited states are a frontier in the field of chemical dynamics, because those states present significant challenges for both experiment and theory. We hope that our 2PA and TA measurements will stimulated renewed computational interest in the higher-lying states of *trans*-stilbene and other model systems by providing new spectroscopic benchmarks for high level calculations of the transition energies and intensities of two-photon allowed states, as well as experimental evidence of the electronic and nuclear relaxation dynamics. Additional experimental studies with better time resolution or more sensitive probes of the vibrational dynamics will provide further insight into the structural relaxation and isomerization dynamics of *trans*-stilbene following excitation to the higher-lying excited states.

3.6 Appendix

The additional figures include kinetic traces showing the evolution of the excited-state absorption (ESA) and stimulated emission (ES) bands for all three excitation energies, decay-associated spectra (DAS) from global fits to the data using a sum of exponentials, the time-dependent populations of the species-associated spectra (SAS) in Figure 3.3, the sub-ps evolution of the transient absorption (TA) spectrum following two-photon excitation (2PE) at 475 nm, and power dependence measurements for the 2PE experiments.

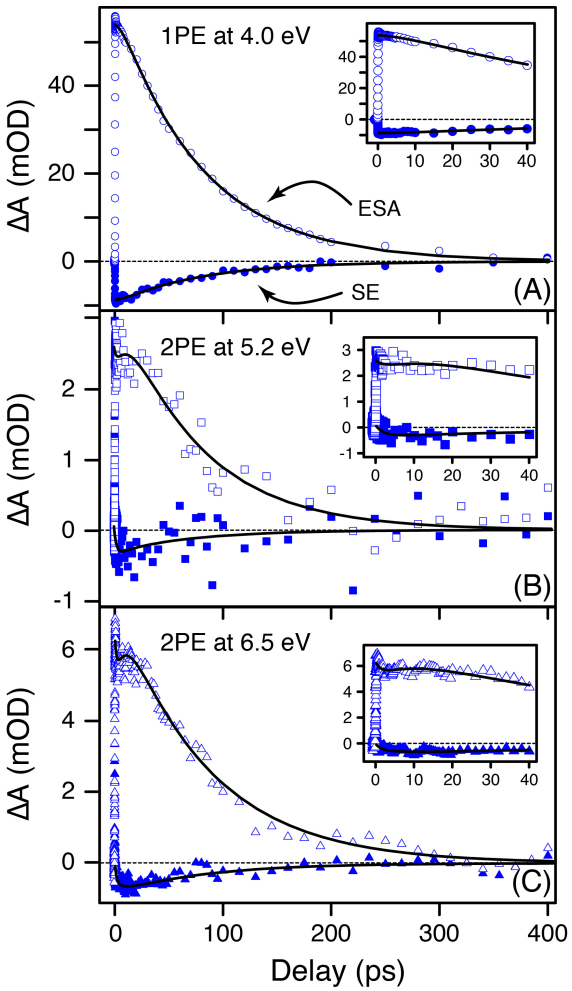

Figure 3.7 Evolution of the transient absorption of *trans*-stilbene in cyclohexane following one photon excitation at 310 nm (A), two photon excitation at 475 nm (B), and two photon excitation at 380 nm (C). The open markers follow the transient signal at 585 nm, the maximum of the S_1 excited-state absorption band. The closed markers follow the transient signal at 365 nm, the region of the S_1 stimulated emission band. The solid lines are from the global fits to the data using the kinetic models described in the main text. The fits begin at ~200 fs delay in this case to avoid complications from coherent contributions to the signal when the pump and probe overlap in time. We treat the sub-ps region in detail in the mail text (Figures 3.4 and 3.5). The insets show the transient absorption signals at shorter delay times.

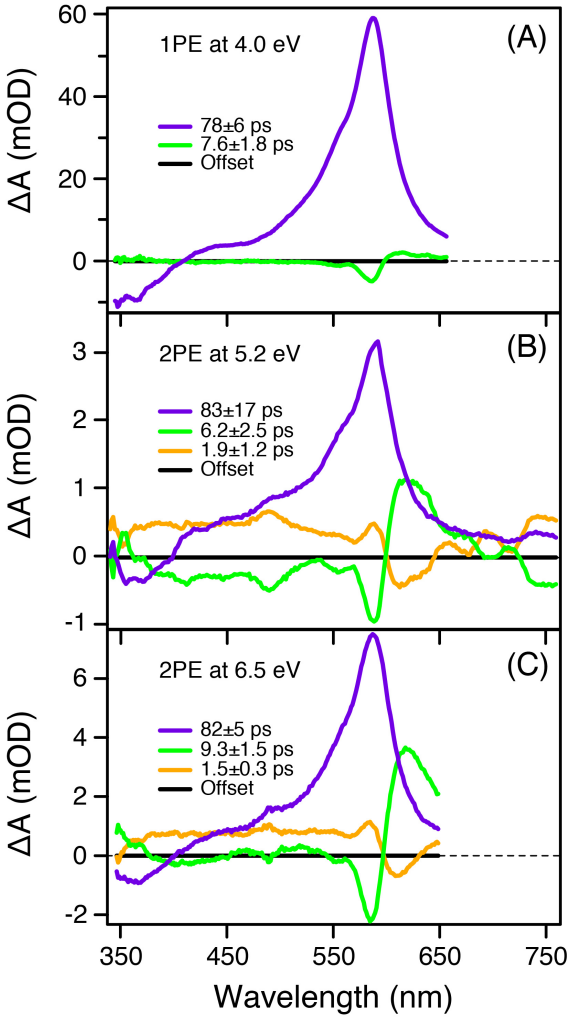

Figure 3.8 Decay-associated spectra (DAS) for *trans*-stilbene following excitation with one photon of 310 nm (A), two photons of 475 nm (B), and two photons of 380 nm (C). The DAS are extracted from best fits to the broadband transient absorption spectra in Figure 3.2 of the main text using a sum of exponentials. The exponentials are held constant across the spectrum, allowing only the amplitudes to vary. The DAS provide complementary information to the SAS, except that the latter applies to a specific kinetic model, whereas the DAS assume no connection between transient species.

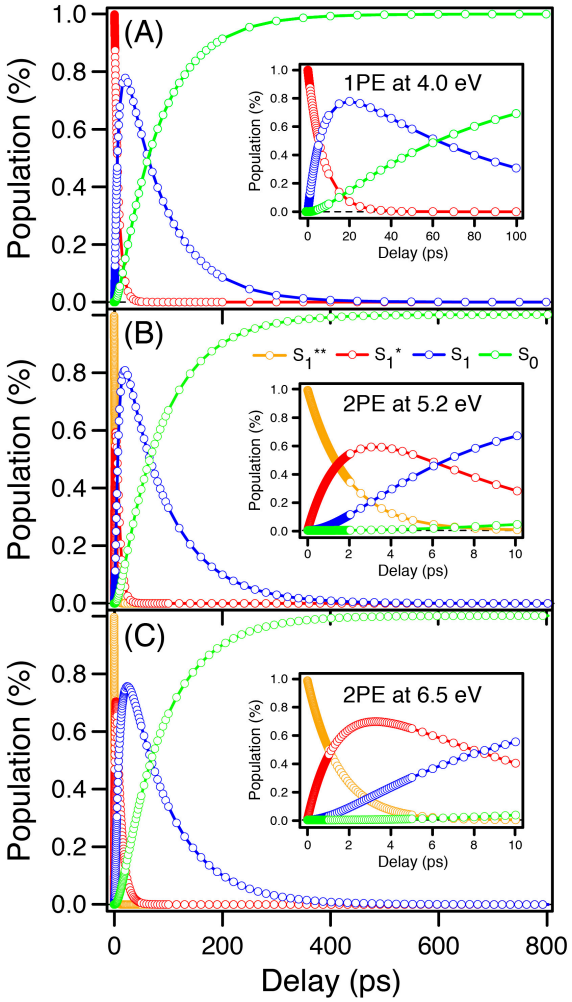

Figure 3.9 The populations of excited-state species of *trans*-stilbene from global fits to the kinetic models in the main text following excitation with one photon at 310 nm (A), two photons at 475 nm (B), and two photons at 380 nm (C). These populations follow the evolution of the SAS in Figure 3.3 of the text.

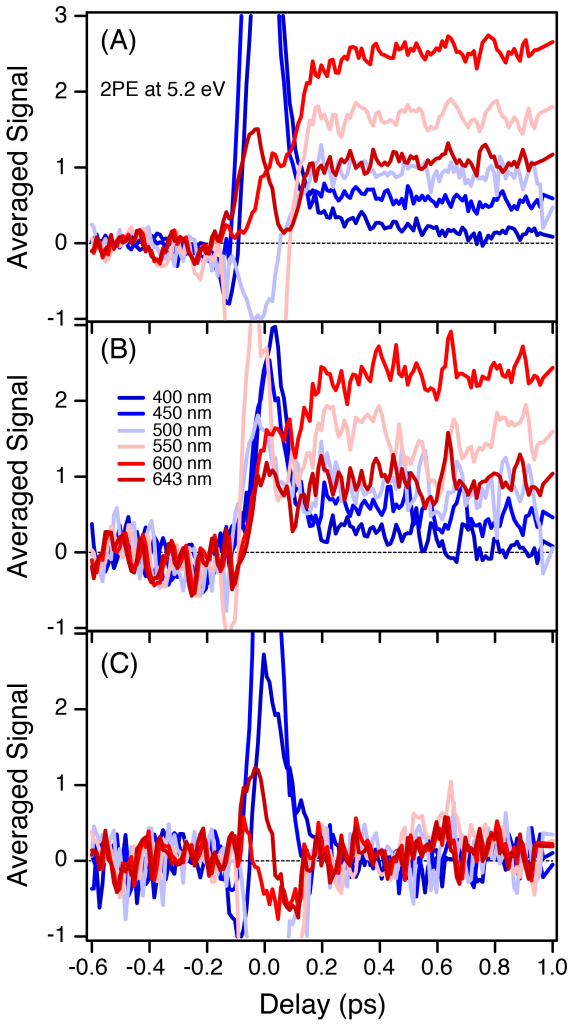

Figure 3.10 Evolution of the transient absorption at early time delays following two-photon excitation of *trans*-stilbene at 475 nm (A). Subtraction of the coherent Raman response of the solvent reveals the signal due to the solute alone (B). For comparison, the figure also shows the background solvent signal for cyclohexane irradiated under the same conditions (C). Each transient is averaged over a probe wavelength range of ~13 nm (11 adjacent pixels) in order to improve the signal-to-noise ratio. The early time dynamics have the same behavior as observed following excitation with two photons at 380 nm (see text, Figure 3.5).

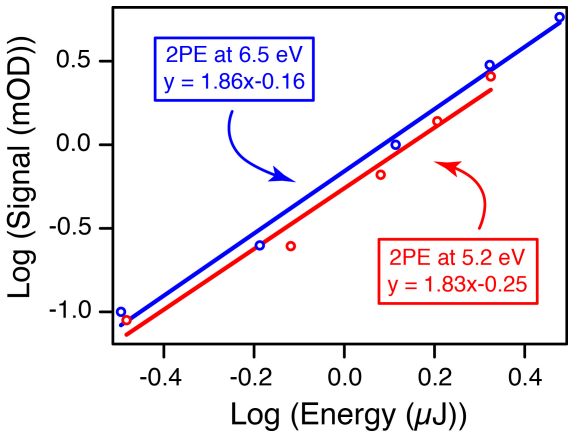

Figure 3.11 Dependence of the transient absorption signal on the energy of incident pump pulses for irradiation of *trans*-stilbene in cyclohexane. The solid lines are the linear fits to the log-log data. The slope is close to 2 for irradiation at wavelengths of 475 nm (red) and 380 nm (blue), indicating a two-photon-induced excitation in both cases.

3.7 References

(1) Houk, A. L.; Zheldakov, I. L.; Tommey, T. A.; Elles, C. G. Two-Photon Excitation of *trans*-Stilbene: Spectroscopy and Dynamics of Electronically Excited States Above S_1. *J. Phys. Chem. B* **2015,** *119*, 9335-9344.

(2) Thomas, J. K. Higher Excited States in Multiphoton Photochemical Reactions "Hint" Toward Rapid Chemistry. *J. Phys. Chem. Lett.* **2014,** *5*, 2586-2587.

(3) Kasha, M. Characterization of Electronic Transitions in Complex Molecules. *Discuss. Faraday Soc.* **1950,** *9*, 14-19.

(4) Waldeck, D. H. Photoisomerization Dynamics of Stilbenes. *Chem. Rev.* **1991,** *91*, 415-436.

(5) Meier, H. The Photochemistry of Stilbenoid Compounds and Their Role in Materials Technology. *Angew. Chem. Int. Ed. Engl.* **1992,** *31*, 1399-1420.

(6) Irie, M. Diarylethenes for Memories and Switches. *Chem. Rev.* **2000,** *100*, 1685-1716.

(7) Kay, E. R.; Leigh, D. A.; Zerbetto, F. Synthetic Molecular Motors and Mechanical Machines. *Angew. Chem. Int. Ed.* **2007,** *46*, 72-191.

(8) Budyka, M. F. Diarylethylene Photoisomerization and Photocyclization Mechanisms. *Russ. Chem. Rev.* **2012,** *81*, 477-493.

(9) Hochstrasser, R. M. Picosecond Processes in the Isomerism of Stilbenes. *Pure Appl. Chem.* **1980,** *52*, 2683-2691.

(10) Sension, R. J.; Repinec, S. T.; Hochstrasser, R. M. Femtosecond Laser Study of Energy Disposal in the Solution Phase Isomerization of Stilbene. *J. Chem. Phys.* **1990,** *93*, 9185-9188.

(11) Rice, J. K.; Baronavski, A. P. Ultrafast Studies of Solvent Effects in the Isomerization of *cis*-Stilbene. *J. Phys. Chem.* **1992,** *96*, 3359-3366.

(12) Baskin, J. S.; Bañares, L.; Pedersen, S.; Zewail, A. H. Femtosecond Real-Time Probing of Reactions. 20. Dynamics of Twisting, Alignment, and IVR in the *trans*-Stilbene Isomerization Reaction. *J. Phys. Chem.* **1996,** *100*, 11920-11933.

(13) Kovalenko, S. A.; Schanz, R.; Hennig, H.; Ernsting, N. P. Cooling Dynamics of an Optically Excited Molecular Probe in Solution from Femtosecond Broadband Transient Absorption Spectroscopy. *J. Chem. Phys.* **2001,** *115*, 3256-3273.

(14) Fuß, W.; Kosmidis, C.; Schmid, W. E.; Trushin, S. A. The Photochemical *cis-trans* Isomerization of Free Stilbene Molecules Follows a Hula-Twist Pathway. *Angew. Chem. Int. Ed.* **2004,** *43*, 4178-4182.

(15) Weigel, A.; Ernsting, N. P. Excited Stilbene: Intramolecular Vibrational Redistribution and Solvation Studied by Femtosecond Stimulated Raman Spectroscopy. *J. Phys. Chem. B* **2010,** *114*, 7879-7893.

(16) Kovalenko, S. A.; Dobryakov, A. L.; Ioffe, I.; Ernsting, N. P. Evidence for the Phantom State in Photoinduced *cis*-*trans* Isomerization of Stilbene. *Chem. Phys. Lett.* **2010,** *493*, 255-258.

(17) Bao, J.; Weber, P. M. Ultrafast Dynamics of Highly Excited *trans*-Stilbene: A Different Twist. *J. Phys. Chem. Lett.* **2010,** *1*, 224-227.

(18) Bao, J.; Weber, P. M. Electronic Effects on Photochemistry: The Diverse Reaction Dynamics of Highly Excited Stilbenes and Azobenzene. *J. Am. Chem. Soc.* **2011,** *133*, 4164-4167.

(19) Kovalenko, S. A.; Dobryakov, A. L. On the Excitation Wavelength Dependence and Arrhenius Behavior of Stilbene Isomerization Rates in Solution. *Chem. Phys. Lett.* **2013,** *570*, 56-60.

(20) Orlandi, G.; Siebrand, W. Model for Direct Photoisomerization of Stilbene. *Chem. Phys. Lett.* **1975,** *30*, 352-354.

(21) Orlandi, G.; Palmieri, P.; Poggi, G. An Ab Initio Study of the *Cis*-*Trans* Photoisomerization of Stilbene. *J. Am. Chem. Soc.* **1979,** *101*, 3492-3497.

(22) Bearpark, M. J.; Bernardi, F.; Clifford, S.; Olivucci, M.; Robb, M. A.; Vreven, T. Cooperating Rings in *cis*-Stilbene Lead to an S_0/S_1 Conical Intersection. *J. Phys. Chem. A* **1997,** *101*, 3841-3847.

(23) Orlandi, G.; Gagliardi, L.; Melandri, S.; Caminati, W. Torsional Potential Energy Surfaces and Vibrational Levels in *trans* Stilbene. *J. Mol. Struct.* **2002,** *612*, 383-391.

(24) Kwasniewski, S. P.; Claes, L.; François, J.-P.; Deleuze, M. S. High Level Theoretical Study of the Structure and Rotational Barriers of *trans*-Stilbene. *J. Chem. Phys.* **2003,** *118*, 7823-7836.

(25) Quenneville, J.; Martinez, T. J. Ab Initio Study of *Cis-Trans* Photoisomerization in Stilbene and Ethylene. *J. Phys. Chem. A* **2003,** *107*, 829-837.

(26) Improta, R.; Santoro, F. Excited-State Behavior of *trans* and *cis* Isomers of Stilbene and Stiff Stilbene: A TD-DFT Study. *J. Phys. Chem. A* **2005,** *109*, 10058-10067.

(27) Minezawa, N.; Gordon, M. S. Photoisomerization of Stilbene: A Spin-Flip Density Functional Theory Approach. *J. Phys. Chem. A* **2011,** *115*, 7901-7911.

(28) Ioffe, I. N.; Granovsky, A. A. Photoisomerization of Stilbene: The Detailed XMCQDPT2 Treatment. *J. Chem. Theory Comput.* **2013,** *9*, 4973-4990.

(29) Hohlneicher, G.; Dick, B. Experimental Determination of the Low-Lying Excited A States of *trans*-Stilbene. *J. Photochem.* **1984,** *27*, 215-231.

(30) Anderson, R. J. M.; Holtom, G. R.; McClain, W. M. Absolute Two-Photon Absorptivity of *trans*-Stilbene Near the Two-Photon Absorption Maximum via Three Wave Mixing. *J. Chem. Phys.* **1977,** *66*, 3832-3833.

(31) Stachelek, T. M.; Pazoha, T. A.; McClain, W. M.; Drucker, R. P. Detection and Assignment of the "Phantom" Photochemical Singlet of *trans*-Stilbene by Two-Photon Excitation. *J. Chem. Phys.* **1977,** *66*, 4540-4543.

(32) Fuke, K.; Sakamoto, S.; Ueda, M.; Itoh, M. Two-Photon Absorption Spectrum of *trans*-Stilbene: *trans-cis* Photoisomerization via Upper ^1A_g State. *Chem. Phys. Lett.* **1980,** *74*, 546-548.

(33) Dick, B.; Gonska, H.; Hohlneicher, G. Two Photon Spectroscopy of Dipole Forbidden Transitions III. Experimental Determination of Two Photon Absorption Spectra Including Polarization Control. *Ber. Bunsenges. Phys. Chem.* **1981,** *85*, 746-754.

(34) Gudipati, M. S.; Maus, M.; Daverkausen, J.; Hohlneicher, G. Higher Excited States of Aromatic Hydrocarbons. III. Assigning the in-Plane Polarized Transitions of Low-Symmetry Molecules: Chrysene and E-Stilbene. *Chem. Phys.* **1995,** *192*, 37-47.

(35) Hohlneicher, G.; Wrzal, R.; Lenoir, D.; Frank, R. Two-Photon Spectra of Stiff Stilbenes: A Contribution to the Assignment of the Low Lying Electronically Excited States of the Stilbene System. *J. Phys. Chem. A* **1999,** *103*, 8969-8975.

(36) Heflin, J. R.; Wong, K. Y.; Zamani-Khamiri, O.; Garito, A. F. Nonlinear Optical Properties of Linear Chains and Electron-Correlation Effects. *Phys. Rev. B* **1988,** *38*, 1573-1576.

(37) Miyazawa, T.; Koshihara, S. Y.; Segawa, Y.; Kira, M. Selective Isomerization of *cis*-Stilbene by Non-Resonant Two-Photon Excitation. *Chem. Lett.* **1995,** *24*, 217-218.

(38) Miyazawa, T.; Liu, Z.; Liu, C.; Koshihara, S.-y.; Kira, M. Action Spectra of Non-Resonant Two-Photon (NRTP) Isomerization of *α,ω*-Diphenylpolyenes. *Chem. Lett.* **1996,** *25*, 1023-1024.

(39) Miyazawa, T.; Liu, C.; Koshihara, S.-y.; Kira, M. Remarkable Suppression of [2+2] Cycloaddition during Nonresonant Two-photon Photoreaction of *trans*-Stilbene in the Presence of Tetramethylethylene. *Photochem. Photobiol.* **1997,** *66*, 566-568.

(40) Bao, J.; Minitti, M. P.; Weber, P. M. Ring-Closing and Dehydrogenation Reactions of Highly Excited *cis*-Stilbene: Ultrafast Spectroscopy and Structural Dynamics. *J. Phys. Chem. A* **2011,** *115*, 1508-1515.

(41) Elles, C. G.; Rivera, C. A.; Zhang, Y.; Pieniazek, P. A.; Bradforth, S. E. Electronic Structure of Liquid Water from Polarization-Dependent Two-Photon Absorption Spectroscopy. *J. Chem. Phys.* **2009,** *130*, 084501.

(42) Negres, R. A.; Hales, J. M.; Kobyakov, A.; Hagan, D. J.; Van Stryland, E. W. Two-Photon Spectroscopy and Analysis with a White-Light Continuum Probe. *Opt. Lett.* **2002,** *27*, 270-272.

(43) Negres, R. A.; Hales, J. M.; Hagan, D. J.; Van Stryland, E. W. Experiment and Analysis of Two-Photon Absorption Spectroscopy Using a White-Light Continuum Probe. *IEEE J. Quantum Elect.* **2002,** *38*, 1205-1216.

(44) Yamaguchi, S.; Tahara, T. Two-Photon Absorption Spectrum of all-*trans* Retinal. *Chem. Phys. Lett.* **2003,** *376*, 237-243.

(45) Yamaguchi, S.; Tahara, T. Observation of an Optically Forbidden State of C_{60} by Nondegenerate Two-Photon Absorption Spectroscopy. *Chem. Phys. Lett.* **2004,** *390*, 136-139.

(46) Ward, C. L.; Elles, C. G. Controlling the Excited-State Reaction Dynamics of a Photochromic Molecular Switch with Sequential Two-Photon Excitation. *J. Phys. Chem. Lett.* **2012,** *3*, 2995-3000.

(47) Zheldakov, I. L.; Wasylenko, J. M.; Elles, C. G. Excited-State Dynamics and Efficient Triplet Formation in Phenylthiophene Compounds. *Phys. Chem. Chem. Phys.* **2012,** *14*, 6211-6218.

(48) Nagura, C.; Suda, A.; Kawano, H.; Obara, M.; Midorikawa, K. Generation and Characterization of Ultrafast White-Light Continuum in Condensed Media. *Appl. Opt.* **2002,** *41*, 3735-3742.

(49) Buchvarov, I.; Trifonov, A.; Fiebig, T. Toward an Understanding of White-Light Generation in Cubic Media-Polarization Properties Across the Entire Spectral Range. *Opt. Lett.* **2007,** *32*, 1539-1541.

(50) Kovalenko, S. A.; Dobryakov, A. L.; Ruthmann, J.; Ernsting, N. P. Femtosecond Spectroscopy of Condensed Phases with Chirped Supercontinuum Probing. *Phys. Rev. A* **1999,** *59*, 2369-2384.

(51) Suzuki, H. Relations Between Electronic Absorption Spectra and Spatial Configurations of Conjugated Systems. V. Stilbene. *Bull. Chem. Soc. Jpn.* **1960,** *33*, 379-388.

(52) Molina, V.; Merchán, M.; Roos, B. O. Theoretical Study of the Electronic Spectrum of *trans*-Stilbene. *J. Phys. Chem. A* **1997,** *101*, 3478-3487.

(53) Xu, C.; Webb, W. W. Measurement of Two-Photon Excitation Cross Sections of Molecular Fluorophores with Data from 690 to 1050 nm. *J. Opt. Soc. Am. B* **1996,** *13*, 481-491.

(54) Angeli, C.; Improta, R.; Santoro, F. On the Controversial Nature of the 1^1B_u and 2^1B_u States of *trans*-Stilbene: The *n*-Electron Valence State Perturbation Theory Approach. *J. Chem. Phys.* **2009,** *130*, 174307.

(55) Kleinschmidt, J.; Rentsch, S.; Tottleben, W.; Wilhelmi, B. Measurement of Strong Nonlinear Absorption in Stilbene-Chloroform Solutions, Explained by Superposition of Two-Photon Absorption and One-Photon Absorption from the Excited-State. *Chem. Phys. Lett.* **1974,** *24*, 133-135.

(56) Anderson, R. J. M.; Holtom, G. R.; McClain, W. M. Two-Photon Absorptivities of the all-*trans* α, ω-Diphenylpolyenes From Stilbene to Diphenyloctatetraene via Three Wave Mixing. *J. Chem. Phys.* **1979,** *70*, 4310-4315.

(57) Chen, C. H.; McCann, M. P. Measurements of Two-Photon Absorption Cross Sections of Common Blue Dyes. *Opt. Commun.* **1987,** *63*, 335-338.

(58) Svetlichnyi, V. A.; Meshalkin, Y. P. Two-Photon Absorption and Laser Photolysis of *trans*-Stilbene Substitutes. *Opt. Commun.* **2007,** *280*, 379-386.

(59) Monson, P. R.; McClain, W. M. Polarization Dependence of the Two-Photon Absorption of Tumbling Molecules with Application to Liquid 1-Chloronaphthalene and Benzene. *J. Chem. Phys.* **1970,** *53*, 29-37.

(60) McClain, W. M. Excited State Symmetry Assignment Through Polarized Two-Photon Absorption Studies of Fluids. *J. Chem. Phys.* **1971,** *55*, 2789-2796.

(61) Monson, P. R.; McClain, W. M. Complete Polarization Study of the Two-Photon Absorption of Liquid 1-Chloronaphthalene. *J. Chem. Phys.* **1972,** *56*, 4817-4825.

(62) Kwasniewski, S. P.; Deleuze, M. S.; François, J. P. Optical Properties of *trans*-Stilbene Using Semiempirical and Time-Dependent Density Functional Theory: A Comparative Study. *Int. J. Quantum Chem.* **2000,** *80*, 672-680.

(63) Greene, B. I.; Hochstrasser, R. M.; Weisman, R. B. Spectroscopic Study of the Picosecond Photoisomerization of Stilbene. *Chem. Phys. Lett.* **1979,** *62*, 427-430.

(64) Doany, F. E.; Greene, B. I.; Hochstrasser, R. M. Excitation Energy Effects in the Photophysics of *trans*-Stilbene in Solution. *Chem. Phys. Lett.* **1980,** *75*, 206-208.

(65) Quick, M.; Berndt, F.; Dobryakov, A. L.; Ioffe, I. N.; Granovsky, A. A.; Knie, C.; Mahrwald, R.; Lenoir, D.; Ernsting, N. P.; Kovalenko, S. A. Photoisomerization Dynamics of Stiff-Stilbene in Solution. *J. Phys. Chem. B* **2014,** *118*, 1389-1402.

(66) Weaver, W. L.; Huston, L. A.; Iwata, K.; Gustafson, T. L. Solvent/Solute Interactions Probed by Picosecond Transient Raman Spectroscopy: Mode-Specific Vibrational Dynamics in S_1 *trans*-Stilbene. *J. Phys. Chem.* **1992,** *96*, 8956-8961.

(67) Qian, J.; Schultz, S. L.; Bradburn, G. R.; Jean, J. M. Picosecond Resonance Raman Studies of Vibrational Cooling of Electronically Excited *trans*-Stilbene in Alcohols and Alkanes. *J. Phys. Chem.* **1993,** *97*, 10638-10644.

(68) Qian, J.; Schultz, S. L.; Jean, J. M. Observation of Intramolecular Vibrational Redistribution and Vibrational Cooling in S_1 *trans*-Stilbene and 2-Phenylindene in Solution. *Chem. Phys. Lett.* **1995,** *233*, 9-15.

(69) Nakabayashi, T.; Okamoto, H.; Tasumi, M. Probe-Wavelength Dependency of Picosecond Anti-Stokes Raman Spectra of *trans*-Stilbene in the S_1 State. *J. Phys. Chem. A* **1997,** *101*, 7189-7193.

(70) Nakabayashi, T.; Okamoto, H.; Tasumi, M. Vibrational Relaxation Dynamics of *trans*-Stilbene in the Lowest Excited Singlet State. Pump and Probe Wavelength Dependencies of the Picosecond Time-Resolved Anti-Stokes Raman Spectrum. *J. Phys. Chem. A* **1998,** *102*, 9686-9695.

(71) Kovalenko, S. A.; Dobryakov, A. L.; Pollak, E.; Ernsting, N. P. Communication: Optical Cooling of *trans*-Stilbene. *J. Chem. Phys.* **2013,** *139*, 011101.

(72) In principle, the linear versus quadratic intensity dependence of the two signals can be used to separate the relative 2PA and ESA contributions.

(73) Soos, Z. G.; Ramasesha, S.; Galvão, D. S.; Etemad, S. Excitation and Relaxation Energies of *trans*-Stilbene: Confined Singlet, Triplet, and Charged Bipolarons. *Phys. Rev. B* **1993,** *47*, 1742-1753.

(74) Castleton, C. W. M.; Barford, W. Screening and the Quantitative π-Model Description of the Optical Spectra and Polarizations of Phenyl Based Oligomers. *J. Chem. Phys.* **2002,** *117*, 3570-3582.

(75) Chen, P. C.; Chieh, Y. C. Azobenzene and Stilbene: A Computational Study. *J. Mol. Struc.-THEOCHEM* **2003,** *624*, 191-200.

(76) Stålring, J.; Gagliardi, L.; Malmqvist, P.-Å.; Lindh, R. A Theoretical Study of the $2^1A_g \leftarrow 1^1A_g$ Two-Photon Transition and Its Vibronic Band in *trans*-Stilbene. *Mol. Phys.* **2002,** *100*, 1791-1796.

(77) Lei, Y.; Yu, L.; Zhou, B.; Zhu, C.; Wen, Z.; Lin, S. H. Landscapes of Four-Enantiomer Conical Intersections for Photoisomerization of Stilbene: CASSCF Calculation. *J. Phys. Chem. A* **2014**, DOI: 10.1021/jp5020109.

(78) Takeuchi, S.; Ruhman, S.; Tsuneda, T.; Chiba, M.; Taketsugu, T.; Tahara, T. Spectroscopic Tracking of Structural Evolution in Ultrafast Stilbene Photoisomerization. *Science* **2008,** *322*, 1073-1077.

(79) Kovalenko, S. A.; Dobryakov, A. L.; Ernsting, N. P. An Efficient Setup for Femtosecond Stimulated Raman Spectroscopy. *Rev. Sci. Instrum.* **2011,** *82*, 063102.

(80) Dobryakov, A. L.; Ioffe, I.; Granovsky, A. A.; Ernsting, N. P.; Kovalenko, S. A. Femtosecond Raman Spectra of *cis*-Stilbene and *trans*-Stilbene with Isotopomers in Solution. *J. Chem. Phys.* **2012,** *137*, 244505.

(81) Kukura, P.; McCamant, D. W.; Yoon, S.; Wandschneider, D. B.; Mathies, R. A. Structural Observation of the Primary Isomerization in Vision with Femtosecond-Stimulated Raman. *Science* **2005,** *310*, 1006-1009.

(82) Shim, S.; Dasgupta, J.; Mathies, R. A. Femtosecond Time-Resolved Stimulated Raman Reveals the Birth of Bacteriorhodopsin's J and K Intermediates. *J. Am. Chem. Soc.* **2009,** *131*, 7592-7597.

(83) Hoffman, D. P.; Mathies, R. A. Photoexcited Structural Dynamics of an Azobenzene Analog 4-nitro-4'-dimethylamino-azobenzene from Femtosecond Stimulated Raman. *Phys. Chem. Chem. Phys.* **2012,** *14*, 6298-6306.

(84) Hoffman, D. P.; Ellis, S. R.; Mathies, R. A. Characterization of a Conical Intersection in a Charge-Transfer Dimer with Two-Dimensional Time-Resolved Stimulated Raman Spectroscopy. *J. Phys. Chem. A* **2014,** *118*, 4955-4965.

(85) Pontecorvo, E.; Ferrante, C.; Elles, C. G.; Scopigno, T. Structural Rearrangement Accompanying the Ultrafast Electrocyclization Reaction of a Photochromic Molecular Switch. *J. Phys. Chem. B* **2014,** *118*, 6915-6921.

4. Two-Photon Absorption Spectroscopy of *trans*-Stilbene, *cis*-Stilbene, and Phenanthrene

4.1 Introduction

Stilbene has been extensively studied experimentally and computationally; making this compound a prototypical system for studying electronic excited states.[1-5] Stilbene is a simple photochromic molecule that undergoes reversible photoisomerization and photocyclization reactions.[2,3,5,6] *Trans*-stilbene photoisomerizes to *cis*-stilbene and following further irradiation cyclizes to 4a,4b-dihydrophenanthrene, which can easily oxidize irreversibly to phenanthrene.

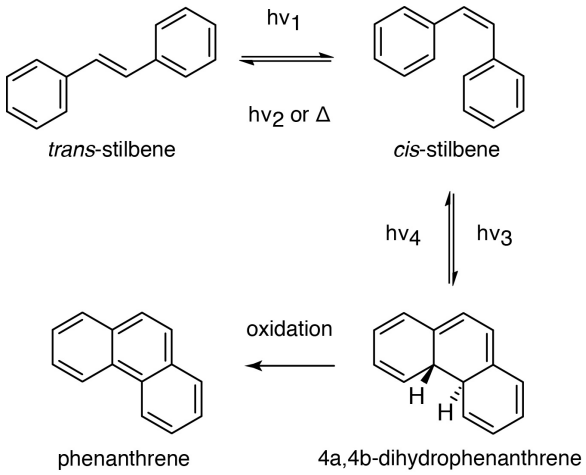

Figure 4.1 Stilbene photoisomerization and photocyclization reactions.

These stilbene compounds are a convenient series of structurally related compounds to compare experimental and computational excited-state energies, absolute two-photon absorption (2PA) cross sections, and polarization ratios. This series of compounds is structurally similar, but each molecule belongs to a different symmetry point group. Specifically, *trans*-stilbene belongs to the C_{2h} point group, *cis*-stilbene to C_2, and phenanthrene to C_{2v}. The structural symmetry of these molecules determines the electronic symmetry of the one- and two-photon accessible

excited states, whereas the absolute 2PA cross section is a measure of the strength of two-photon accessible transitions. Previous experimental and computational measurements of the absolute 2PA cross sections of the stilbene series are inconsistent with each other, which highlights the need for new experimental and computational measurements of the excited-state energies, absolute 2PA cross sections, and polarization ratios.

In this chapter we present the one-photon absorption and broadband two-photon absorption spectroscopy of *trans*-stilbene, *cis*-stilbene, and phenanthrene. We also report the absolute 2PA cross sections of these molecules. Measuring the broadband 2PA spectra back-to-back for this series of structurally similar molecules reduces uncertainties of the experimental parameters between measurements. We compare our experimentally measured excited-state energies and 2PA cross sections with calculations found in the literature. A series of new calculations are in progress by one of our collaborators using EOM-EE-CCSD (equation-of-motion for excitation energies CC with single and double substitutions)[7] in the Q-Chem electronic structure program.[8,9] Our collaborators are calculating the two-photon absorption cross sections, polarization ratios, and transition energies for this series of molecules to compare with our experimental measurements.[7] Our experimental two-photon absorption spectroscopy for this series of molecules serve as a benchmark for high-level calculations of the excited-state energies, polarization ratios, and 2PA cross sections.

4.2 Experimental Methods

We use a broadband pump-probe technique to measure the two-photon absorption (2PA) spectroscopy of *trans*-stilbene, *cis*-stilbene, and phenanthrene in solution. The details of the broadband 2PA measurement have been discussed previously,[10-15] and are only briefly described

here. The 2PA spectrum is measured by spatially and temporally overlapping a nonresonant pump pulse with a broadband probe pulse within the sample and then measuring the wavelength-dependent attenuation of the broadband probe pulse. The pump and probe pulses are generated from an ultrafast Ti:Sapphire laser. An optical parametric amplifier generates tunable pump pulses in the visible-UV. The broadband probe pulse is generated by focusing fundamental 800 nm into a 1 cm quartz cuvette of water producing a white light continuum ranging from 750–350 nm.[16,17] We control the relative orientation of the linearly polarized pump and probe beams with a λ/2 waveplate in the pump beam. After the sample the transmitted probe beam is dispersed through a transmission grating onto a 256-element photodiode array for shot-to-shot detection. An optical chopper wheel blocks every other pump pulse before the sample for active background subtraction.

Two-photon absorption occurs when the total energy of one pump and one probe photon is resonant with a two-photon allowed transition. Importantly, neither photon is absorbed alone by the solute. The pump and probe diameters are typically ~200 and ~70 μm, respectively. The average pump energy is usually ~100 nJ/pulse. The 2PA measurements have a resolution of ~0.14 eV, limited by the convolution of the bandwidth of the pump pulse and the resolution of the spectrograph. The samples for the 2PA measurements are 0.5 M solutions of *trans*-stilbene, *cis*-stilbene, or phenanthrene (all from Sigma-Aldrich, >96%) in chloroform (Sigma-Aldrich, ≥99%) contained in a 1 mm quartz cuvette.

4.3 Results and Discussion

Figure 4.2 compares the one- and two-photon absorption spectra of *trans*-stilbene, *cis*-stilbene, and phenanthrene. The one- and two-photon absorption spectra show distinctly different

absorption bands when exciting with one versus two photons. The linear absorption spectrum of *trans*-stilbene has three absorption bands near 4.1, 5.4, and 6.1 eV, while the two-photon absorption (2PA) spectrum has two bands near 4.2 and 5.1 eV. For *cis*-stilbene the linear absorption spectrum has bands near 4.4 and 5.5 eV, while the 2PA spectrum has bands near 4.5 and 5.2 eV. The linear absorption spectrum for phenanthrene has two strong bands with significant vibronic structure near 4.9 and 5.8 eV, while the 2PA spectrum has two strong bands near 4.8 and 5.5 eV.

Phenanthrene has the most clearly resolved vibronic structure of the three molecules. The observed vibronic structure in the linear absorption spectrum is expected since phenanthrene is a rigid, planar molecule.[18] Despite the vibrational structure of the one-photon absorption (1PA) spectrum, no vibronic bands are resolved in the 2PA spectrum of phenanthrene (Figure 4.2F). The 2PA measurements have a resolution of ~0.14 eV, which is sufficient to resolve vibronic structure similar to that observed in the linear absorption spectrum, although with some broadening. The 1PA spectrum has a resolution of ~0.03 eV. Our experimental transition energies and absolute 2PA cross sections are summarized in Table 4.1.

Table 4.1 Summary of experimental 2PA transition energies and cross sections.[a,b]

Trans-Stilbene		*Cis*-Stilbene		Phenanthrene	
Energy (eV)	σ_{2PA} (GM)	Energy (eV)	σ_{2PA} (GM)	Energy (eV)	σ_{2PA} (GM)
4.3	4.3 ± 1.8	4.4	1.3 ± 0.6	3.8	0.4 ± 0.2
5.1	32 ± 13	5.2	10 ± 4	4.0	0.2 ± 0.1
	40 ± 16[c]			4.8	4.7 ± 1.9
6.4	270 ±110[c]			5.5	10 ± 4

[a] Uncertainties are estimated 95% confidence limits. [b] Two-photon absorption cross sections are measured in GM (1 GM = 10^{-50} $cm^4 \cdot s \cdot molecule^{-1} \cdot photon^{-1}$). [c] From Ref. 10.

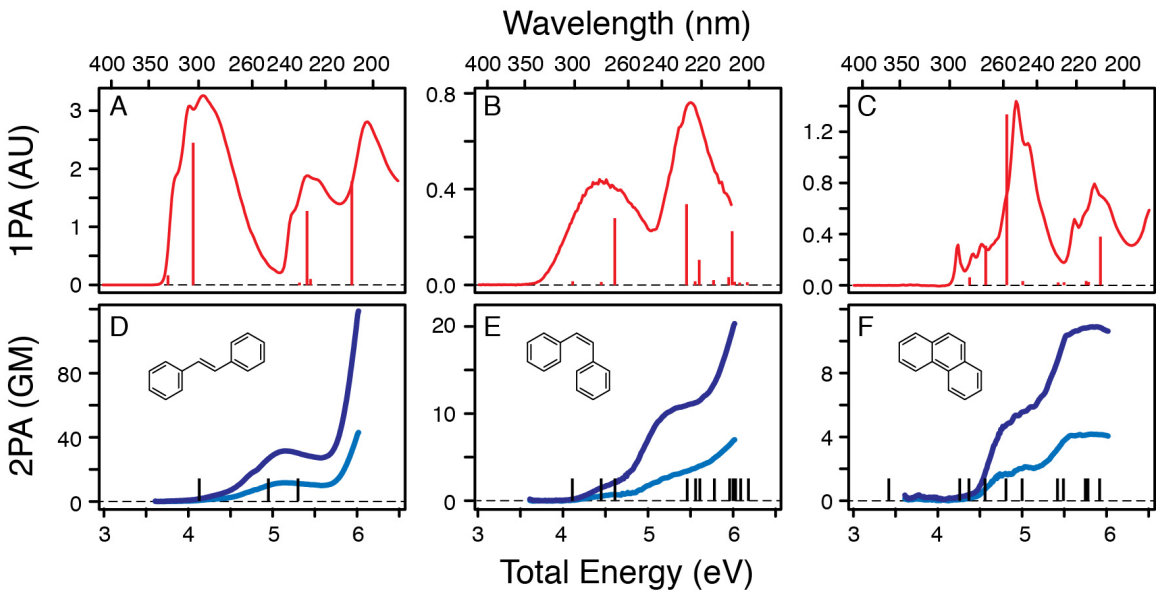

Figure 4.2 One-photon absorption (1PA) spectra of (A) *trans*-stilbene, (B) *cis*-stilbene, and (C) phenanthrene in cyclohexane. Two-photon absorption (2PA) spectra of (D) *trans*-stilbene, (E) *cis*-stilbene, and (F) phenanthrene in chloroform. The 2PA spectra are measured with parallel (dark blue line) and perpendicular (light blue line) relative polarization of the pump and probe beams. The red sticks in the top panels represent the CASPT2 calculated one-photon excited state transition energies and oscillator strengths. The black sticks in the bottom panels represent the CASPT2 calculated two-photon excited state transition energies but the heights are all the same because the two-photon intensities were not reported.[19-21]

The two-photon absorption cross section of a molecule depends on the relative polarization of the two photons being absorbed, therefore we obtained the 2PA spectra for both parallel (σ_{2PA}^{para}) and perpendicular (σ_{2PA}^{perp}) relative polarization of the pump and probe beams (Figure 4.2D–F). The polarization dependence of a given 2PA band depends on the symmetry of the transition, with totally symmetric transitions giving a ratio $\sigma_{2PA}^{para}/\sigma_{2PA}^{perp} \geq 4/3$ and nontotally symmetric transitions giving a ratio $\sigma_{2PA}^{para}/\sigma_{2PA}^{perp} < 4/3$. Figure 4.3 shows that the

polarization ratios are 2–3 across the entire 2PA spectrum for each molecule, indicating that the two-photon transitions in this energy range primarily access totally symmetric excited states. *Trans*-stilbene belongs to the C_{2h} point group, *cis*-stilbene to C_2, and phenanthrene to C_{2v}, so the totally symmetric transitions access states of A_g-symmetry, A-symmetry, and A_1-symmetry, respectively. Slight variations of the polarization ratios across each spectrum are consistent with weaker, underlying contributions to the 2PA spectra near 4.2 eV for *trans*-stilbene, and 4.5 eV for both *cis*-stilbene and phenanthrene, as highlighted in Figure 4.3. In other words, the decrease in the polarization ratio at lower energies may be due to the two-photon allowed state having a different symmetry than the 2PA states at higher energies. Calculations of the excited-state energies, the two-photon absorption cross sections, and the character of those states are in progress to determine which states contribute to the decrease in the polarization ratio.[7]

Figure 4.4 shows the one- and two-photon absorption spectra on an expanded scale, where the weaker 2PA bands are more evident. The onset of the 2PA spectra for *trans*- and *cis*-stilbene is at about 4.0 eV and for linear excitation the first absorption band starts near 3.6 eV. The relative intensities of the lowest one- and two-photon accessible states are different for these molecules, indicating different states are accessed following one- and two-photon excitation. In contrast, phenanthrene has a weak 2PA contribution ranging from 3.6–4.0 eV, while the lowest-lying linear absorption band is weak and extends from 3.5–3.8 eV[22]. The lowest energy one- and two-photon absorption bands measured for phenanthrene may be associated with the same transition because this compound is noncentrosymmetric, so the molecule has no strict parity selection rules or vibronic symmetry selection rules. The previously calculated oscillator strength of the lowest-lying singlet transition is <0.001, indicating this state has a very weak electronic transition.[21]

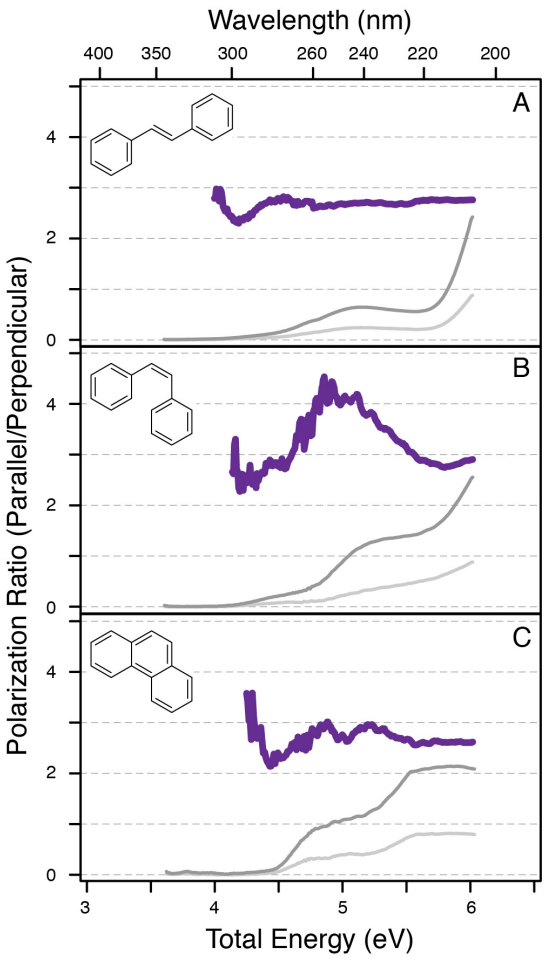

Figure 4.3 Two-photon absorption (2PA) polarization ratios ($\sigma_{2PA}^{para}/\sigma_{2PA}^{perp}$) with the respective broadband 2PA spectra measured at parallel and perpendicular polarization for (A) *trans*-stilbene, (B) *cis*-stilbene, and (C) phenanthrene.

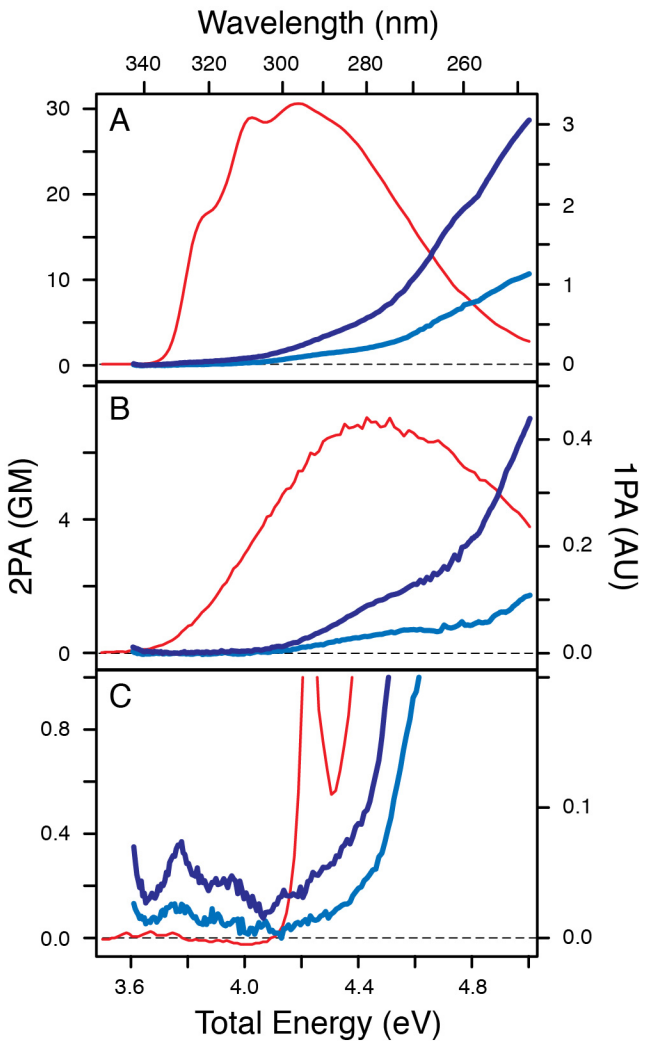

Figure 4.4 Expanded view of the absorption spectra showing the onset of one- and two-photon absorption for (A) *trans*-stilbene, (B) *cis*-stilbene, and (C) phenanthrene. These are the same spectra shown in Figure 4.2.

Calculated transition energies have been reported previously for *trans*-stilbene,[19,23-38] *cis*-stilbene,[20,27-29,31-37,39] and phenanthrene[18,21,40] using various levels of theory. Merchan and coworkers reported some of the most comprehensive computational work on the full series of molecules using CASPT2 and CASSCF.[19-21] The character of the excited states, transition energies, and oscillator strengths of the entire molecular series are reported in Table 4.2.[19-21] The

one-photon allowed transition energies and oscillator strengths calculated with CASPT2 are plotted in Figure 4.2A–C as red sticks.[19-21] In Figure 4.2D–F the black sticks are the calculated two-photon allowed transition energies using CASPT2, but the heights of the sticks are not representative of two-photon transition strengths because the two-photon intensities were not calculated for these measurements.[19-21] The calculated excited-state energies of one- and two-photon accessible transitions are in good agreement with our experimental spectroscopic measurements, as well as the oscillator strengths of one-photon transitions (Figure 4.2).

For *trans*-stilbene the two-photon accessible states have A_g-symmetry because *trans*-stilbene is centrosymmetric. Only a two-photon absorption can access excited states with *gerade* symmetry, while one-photon absorption accesses excited states with *ungerade* symmetry. The calculated lowest-lying A_g-symmetry state for *trans*-stilbene is at 4.13 eV,[19] which closely matches our experimental 2PA band near 4.2 eV.

Cis-stilbene is noncentrosymmetric, therefore the excited electronic states are accessible with one or two photons. The calculated lowest energy A-symmetry state of *cis*-stilbene is at 4.45 eV,[20] which corresponds well with the lowest-lying 2PA band we observe near 4.5 eV.

Phenanthrene is also a noncentrosymmetric molecule, so the excited state transitions are one and two photon accessible. The two lowest A_1-symmetry states calculated for phenanthrene are at 3.42 and 4.56 eV.[21] The lowest energy transition is outside of the range of our measurement but the second transition matches our experiment. However, the 2PA band that we measure ranging from 3.5–3.8 eV does not correspond to any calculated two-photon electronic transition. The measured 2PA transition may be forbidden by electronic symmetry but may be weakly allowed via vibronic coupling.

Table 4.2 Calculated vertical excitation energies and oscillator strengths from literature.[19-21]

Trans-Stilbene[a]				*Cis*-Stilbene[b]				Phenanthrene[c]			
State	CASSCF (eV)	CASPT2 (eV)	Osc. Str.	State	CASSCF (eV)	CASPT2 (eV)	Osc. Str.	State	CASSCF (eV)	CASPT2 (eV)	Osc. Str.
1^1B_u	5.42	3.77	0.038	1^1B	5.79	4.11	0.007	$2^1A_1(^1L_b)$	4.25	3.42	0.000
2^1B_u	6.05	4.07	0.723	2^1A	5.64	4.45	0.004	1^1B_2	5.68	4.26	0.000
2^1A_g	5.41	4.13		2^1B	6.57	4.61	0.334	$2^1B_2(^1L_a)$	6.14	4.37	0.038
3^1A_g	5.92	4.95		3^1B	8.14	5.46	0.406	3^1A_1	6.36	4.56	0.268
4^1A_g	7.41	5.30		3^1A	6.79	5.56	0.007	$3^1B_2(^1B_a)$	6.94	4.81	1.218
$1^1A_u(3s)$	5.54	5.33	0.001	4^1A	7.61	5.61	0.118	$4^1A_1(^1B_b)$	6.57	5.00	0.011
3^1B_u	7.96	5.42	0.371	$4^1B(3s)$	6.11	5.78	0.013	$1^1B_1(3s)$	5.23	5.42	0.002
4^1B_u	7.76	5.42	0.117	5^1B	7.89	5.96	0.029	4^1B_2	7.22	5.49	0.003
5^1B_u	7.18	5.46	0.019	6^1B	8.32	6.00	0.057	5^1A_1	6.81	5.75	0.000
$1^1B_g(3p_x,3p_y)$	5.73	5.53		7^1B	8.37	6.00	0.266	6^1A_1	7.14	5.75	0.012
$2^1B_g(3p_x,3p_y)$	5.94	5.69		$8^1B(3p_z)$	6.22	6.03	0.005	5^1B_2	7.56	5.78	0.005
6^1B_u	8.36	5.95	0.524	$5^1A(3p_x,3p_y)$	6.25	6.09	0.001	6^1B_2	8.18	5.92	0.333
1^3B_u	3.02	2.56		$6^1A(3p_x,3p_y)$	6.35	6.18	0.002				
				1^3B	3.61	3.16					

[a] From Ref. 19. [b] From Ref. 20. [c] From Ref. 21.

CASPT2 gives accurate one- and two-photon transition energies of the stilbene series and agrees well with our experimentally measured spectra.[19-21] However, the two-photon absorption transition strengths, namely the absolute 2PA cross sections were not reported using CASPT2 and only a limited number of absolute 2PA cross sections have been calculated using different levels of theory for *trans*-stilbene,[38,41-50] *cis*-stilbene,[39] and phenanthrene[18,51]. Even worse, the calculated absolute 2PA cross sections for these molecules vary by orders of magnitude between different levels of theory, and the polarization ratios were not reported for any of the calculated results. Consistent computational results are needed for comparison with our experimental 2PA cross sections and polarization ratios. Such calculations are in progress by our collaborator,[7] and will provide consistent calculations of the excited-state energies, absolute 2PA cross sections, and polarization ratios. Conversely, our broadband 2PA spectroscopy measurements of *trans*-stilbene, *cis*-stilbene, and phenanthrene provide a consistent set of benchmarks for comparing the calculated two-photon accessible excited-state energies, polarization ratios, and the 2PA cross sections.[7,52]

4.4 Conclusions

The broadband 2PA spectroscopy and the measured 2PA cross sections provide information about the two-photon accessible excited states of *trans*-stilbene, *cis*-stilbene, and phenanthrene. The spectroscopy of this series of molecules shows that different excited electronic states are accessed following one- and two-photon absorption for molecules with various symmetry point groups. The measured excited-state energies are in good agreement with the calculated energies using CASPT2.[19-21] Unfortunately, the most complete set of calculations to date did not include 2PA intensities for comparison. Other calculations are inconsistent because the excited-state energies and the absolute 2PA cross sections vary by orders of magnitude depending on the computational method. The limited absolute 2PA cross sections available are inconsistent with our experimental measurements, highlighting the need for a consistent series of calculations to compare with our experimental results. The advantage of our consistent 2PA measurements is that these molecules are measured back-to-back, which reduces uncertainties of the experimental parameters between measurements. These 2PA spectroscopy measurements of this series of stilbene molecules provide a new consistent benchmark for further computational studies of two-photon accessible excited states, which includes excited-state energies, polarization ratios, and 2PA cross sections.

4.5 References

(1) Waldeck, D. H. Photoisomerization Dynamics of Stilbenes. *Chem. Rev.* **1991,** *91*, 415-436.

(2) Meier, H. The Photochemistry of Stilbenoid Compounds and Their Role in Materials Technology. *Angew. Chem. Int. Ed. Engl.* **1992,** *31*, 1399-1420.

(3) Irie, M. Diarylethenes for Memories and Switches. *Chem. Rev.* **2000,** *100*, 1685-1716.

(4) Kay, E. R.; Leigh, D. A.; Zerbetto, F. Synthetic Molecular Motors and Mechanical Machines. *Angew. Chem. Int. Ed.* **2007,** *46*, 72-191.

(5) Budyka, M. F. Diarylethylene Photoisomerization and Photocyclization Mechanisms. *Russ. Chem. Rev.* **2012,** *81*, 477-493.

(6) Irie, M.; Fukaminato, T.; Matsuda, K.; Kobatake, S. Photochromism of Diarylethene Molecules and Crystals: Memories, Switches, and Actuators. *Chem. Rev.* **2014,** *114*, 12174-12277.

(7) Nanda, K. D.; Krylov, A. I. Two-Photon Absorption Cross Sections Within Equation-of-Motion Coupled-Cluster Formalism Using Resolution-of-the-Identity and Cholesky Decomposition Representations: Theory, Implementation, and Benchmarks. *J. Chem. Phys.* **2015,** *142*, 064118.

(8) Krylov, A. I.; Gill, P. M. W. Q-Chem: An Engine for Innovation. *WIREs Comput. Mol. Sci.* **2013,** *3*, 317-326.

(9) Shao, Y.; Gan, Z.; Epifanovsky, E.; Gilbert, A. T. B.; Wormit, M.; Kussmann, J.; Lange, A. W.; Behn, A.; Deng, J.; Feng, X.; Ghosh, D.; Goldey, M.; Horn, P. R.; Jacobson, L. D.; Kaliman, I.; Khaliullin, R. Z.; Kuś, T.; Landau, A.; Liu, J.; Proynov, E. I.; Rhee, Y. M.; Richard, R. M.; Rohrdanz, M. A.; Steele, R. P.; Sundstrom, E. J.; Woodcock, H. L.; Zimmerman, P. M.; Zuev, D.; Albrecht, B.; Alguire, E.; Austin, B.; Beran, G. J. O.; Bernard, Y. A.; Berquist, E.; Brandhorst, K.; Bravaya, K. B.; Brown, S. T.; Casanova, D.; Chang, C.-M.; Chen, Y.; Chien, S. H.; Closser, K. D.; Crittenden, D. L.; Diedenhofen, M.; DiStasio, R. A.; Do, H.; Dutoi, A. D.; Edgar, R. G.; Fatehi, S.; Fusti-Molnar, L.; Ghysels, A.; Golubeva-Zadorozhnaya, A.; Gomes, J.; Hanson-Heine, M. W. D.; Harbach, P. H. P.; Hauser, A. W.; Hohenstein, E. G.; Holden, Z. C.;

Jagau, T.-C.; Ji, H.; Kaduk, B.; Khistyaev, K.; Kim, J.; Kim, J.; King, R. A.; Klunzinger, P.; Kosenkov, D.; Kowalczyk, T.; Krauter, C. M.; Lao, K. U.; Laurent, A. D.; Lawler, K. V.; Levchenko, S. V.; Lin, C. Y.; Liu, F.; Livshits, E.; Lochan, R. C.; Luenser, A.; Manohar, P.; Manzer, S. F.; Mao, S.-P.; Mardirossian, N.; Marenich, A. V.; Maurer, S. A.; Mayhall, N. J.; Neuscamman, E.; Oana, C. M.; Olivares-Amaya, R.; O'Neill, D. P.; Parkhill, J. A.; Perrine, T. M.; Peverati, R.; Prociuk, A.; Rehn, D. R.; Rosta, E.; Russ, N. J.; Sharada, S. M.; Sharma, S.; Small, D. W.; Sodt, A.; Stein, T.; Stück, D.; Su, Y.-C.; Thom, A. J. W.; Tsuchimochi, T.; Vanovschi, V.; Vogt, L.; Vydrov, O.; Wang, T.; Watson, M. A.; Wenzel, J.; White, A.; Williams, C. F.; Yang, J.; Yeganeh, S.; Yost, S. R.; You, Z.-Q.; Zhang, I. Y.; Zhang, X.; Zhao, Y.; Brooks, B. R.; Chan, G. K. L.; Chipman, D. M.; Cramer, C. J.; Goddard, W. A.; Gordon, M. S.; Hehre, W. J.; Klamt, A.; Schaefer, H. F.; Schmidt, M. W.; Sherrill, C. D.; Truhlar, D. G.; Warshel, A.; Xu, X.; Aspuru-Guzik, A.; Baer, R.; Bell, A. T.; Besley, N. A.; Chai, J.-D.; Dreuw, A.; Dunietz, B. D.; Furlani, T. R.; Gwaltney, S. R.; Hsu, C.-P.; Jung, Y.; Kong, J.; Lambrecht, D. S.; Liang, W.; Ochsenfeld, C.; Rassolov, V. A.; Slipchenko, L. V.; Subotnik, J. E.; Van Voorhis, T.; Herbert, J. M.; Krylov, A. I.; Gill, P. M. W.; Head-Gordon, M. Advances in Molecular Quantum Chemistry Contained in the Q-Chem 4 Program Package. *Mol. Phys.* **2014,** *113*, 184-215.

(10) Houk, A. L.; Zheldakov, I. L.; Tommey, T. A.; Elles, C. G. Two-Photon Excitation of *trans*-Stilbene: Spectroscopy and Dynamics of Electronically Excited States Above S_1. *J. Phys. Chem. B* **2015,** *119*, 9335-9344.

(11) Elles, C. G.; Rivera, C. A.; Zhang, Y.; Pieniazek, P. A.; Bradforth, S. E. Electronic Structure of Liquid Water from Polarization-Dependent Two-Photon Absorption Spectroscopy. *J. Chem. Phys.* **2009,** *130*, 084501.

(12) Negres, R. A.; Hales, J. M.; Kobyakov, A.; Hagan, D. J.; Van Stryland, E. W. Two-Photon Spectroscopy and Analysis with a White-Light Continuum Probe. *Opt. Lett.* **2002,** *27*, 270-272.

(13) Negres, R. A.; Hales, J. M.; Hagan, D. J.; Van Stryland, E. W. Experiment and Analysis of Two-Photon Absorption Spectroscopy Using a White-Light Continuum Probe. *IEEE J. Quantum Elect.* **2002,** *38*, 1205-1216.

(14) Yamaguchi, S.; Tahara, T. Two-Photon Absorption Spectrum of all-*trans* Retinal. *Chem. Phys. Lett.* **2003,** *376*, 237-243.

(15) Yamaguchi, S.; Tahara, T. Observation of an Optically Forbidden State of C_{60} by Nondegenerate Two-Photon Absorption Spectroscopy. *Chem. Phys. Lett.* **2004,** *390*, 136-139.

(16) Nagura, C.; Suda, A.; Kawano, H.; Obara, M.; Midorikawa, K. Generation and Characterization of Ultrafast White-Light Continuum in Condensed Media. *Appl. Opt.* **2002,** *41*, 3735-3742.

(17) Buchvarov, I.; Trifonov, A.; Fiebig, T. Toward an Understanding of White-Light Generation in Cubic Media-Polarization Properties Across the Entire Spectral Range. *Opt. Lett.* **2007,** *32*, 1539-1541.

(18) Dick, B.; Hohlneicher, G. Two-Photon Excitation Spectroscopy of Phenanthrene Singlet States Below 50000 cm-1. *Chem. Phys. Lett.* **1983,** *97*, 324-330.

(19) Molina, V.; Merchán, M.; Roos, B. O. Theoretical Study of the Electronic Spectrum of *trans*-Stilbene. *J. Phys. Chem. A* **1997,** *101*, 3478-3487.

(20) Molina, V.; Merchán, M.; Roos, B. O. A Theoretical Study of the Electronic Spectrum of *cis*-Stilbene. *Spectrochim. Acta. A* **1999,** *55*, 433-446.

(21) González-Luque, R.; Serrano-Andrés, L.; Merchán, M.; Fülscher, M. P. Theoretical Characterization of the Absorption Spectra of Phenanthrene and Its Radical Cation. *Theor. Chem. Acc.* **2003,** *110*, 224-232.

(22) Dick, B.; Hohlneicher, G. Two-Photon Spectroscopy of the Low-Lying Singlet States of Naphthalene and Acenaphthene. *Chem. Phys. Lett.* **1981,** *84*, 471-478.

(23) Soos, Z. G.; Ramasesha, S.; Galvão, D. S.; Etemad, S. Excitation and Relaxation Energies of *trans*-Stilbene: Confined Singlet, Triplet, and Charged Bipolarons. *Phys. Rev. B* **1993,** *47*, 1742-1753.

(24) Bearpark, M. J.; Bernardi, F.; Clifford, S.; Olivucci, M.; Robb, M. A.; Vreven, T. Cooperating Rings in *cis*-Stilbene Lead to an S_0/S_1 Conical Intersection. *J. Phys. Chem. A* **1997,** *101*, 3841-3847.

(25) Kwasniewski, S. P.; Deleuze, M. S.; François, J. P. Optical Properties of *trans*-Stilbene Using Semiempirical and Time-Dependent Density Functional Theory: A Comparative Study. *Int. J. Quantum Chem.* **2000,** *80*, 672-680.

(26) Castleton, C. W. M.; Barford, W. Screening and the Quantitative π-Model Description of the Optical Spectra and Polarizations of Phenyl Based Oligomers. *J. Chem. Phys.* **2002,** *117*, 3570-3582.

(27) Chen, P. C.; Chieh, Y. C. Azobenzene and Stilbene: A Computational Study. *J. Mol. Struc.-THEOCHEM* **2003,** *624*, 191-200.

(28) Quenneville, J.; Martinez, T. J. Ab Initio Study of *Cis-Trans* Photoisomerization in Stilbene and Ethylene. *J. Phys. Chem. A* **2003,** *107*, 829-837.

(29) Improta, R.; Santoro, F. Excited-State Behavior of *trans* and *cis* Isomers of Stilbene and Stiff Stilbene: A TD-DFT Study. *J. Phys. Chem. A* **2005,** *109*, 10058-10067.

(30) Angeli, C.; Improta, R.; Santoro, F. On the Controversial Nature of the 1^1B_u and 2^1B_u States of *trans*-Stilbene: The *n*-Electron Valence State Perturbation Theory Approach. *J. Chem. Phys.* **2009,** *130*, 174307.

(31) Minezawa, N.; Gordon, M. S. Photoisomerization of Stilbene: A Spin-Flip Density Functional Theory Approach. *J. Phys. Chem. A* **2011,** *115*, 7901-7911.

(32) Chaudhuri, R. K.; Freed, K. F.; Chattopadhyay, S.; Mahapatra, U. S. Theoretical Studies of the Ground and Excited State Structures of Stilbene. *J. Phys. Chem. A* **2013,** *117*, 9424-9434.

(33) Ioffe, I. N.; Granovsky, A. A. Photoisomerization of Stilbene: The Detailed XMCQDPT2 Treatment. *J. Chem. Theory Comput.* **2013,** *9*, 4973-4990.

(34) Pal, A. K.; Hansda, S.; Datta, S. N.; Illas, F. Theoretical Investigation of Stilbene as Photochromic Spin Coupler. *J. Phys. Chem. A* **2013,** *117*, 1773-1783.

(35) Tomasello, G.; Garavelli, M.; Orlandi, G. Tracking the Stilbene Photoisomerization in the S_1 State Using RASSCF. *Phys. Chem. Chem. Phys.* **2013,** *15*, 19763-19773.

(36) Harabuchi, Y.; Keipert, K.; Zahariev, F.; Taketsugu, T.; Gordon, M. S. Dynamics Simulations with Spin-Flip Time-Dependent Density Functional Theory: Photoisomerization and Photocyclization Mechanisms of cis-Stilbene in ππ* States. *J. Phys. Chem. A* **2014,** *118*, 11987-11998.

(37) Lei, Y.; Yu, L.; Zhou, B.; Zhu, C.; Wen, Z.; Lin, S. H. Landscapes of Four-Enantiomer Conical Intersections for Photoisomerization of Stilbene: CASSCF Calculation. *J. Phys. Chem. A* **2014**, DOI: 10.1021/jp5020109.

(38) Hohlneicher, G.; Dick, B. Experimental Determination of the Low-Lying Excited A States of *trans*-Stilbene. *J. Photochem.* **1984,** *27*, 215-231.

(39) Clark, A. E. Time-Dependent Density Functional Theory Studies of the Photoswitching of the Two-Photon Absorption Spectra in Stilbene, Metacyclophenadiene, and Diarylethene Chromophores. *J. Phys. Chem. A* **2006,** *110*, 3790-3796.

(40) Chakrabarti, A.; Ramasesha, S. Properties of the Low-Lying

Electronic States of Phenanthrene:

Exact PPP Results*. *Int. J. Quantum Chem.* **1996,** *60*, 381-391.

(41) Albota, M.; Beljonne, D.; Brédas, J.-L.; Ehrlich, J. E.; Fu, J.-Y.; Heikal, A. A.; Hess, S. E.; Kogej, T.; Levin, M. D.; Marder, S. R.; McCord-Maughon, D.; Perry, J. W.; Röckel, H.; Rumi, M.; Subramaniam, G.; Webb, W. W.; Wu, X.-L.; Xu, C. Design of Organic Molecules with Large Two-Photon Absorption Cross Sections. *Science* **1998,** *281*, 1653-1656.

(42) Norman, P.; Luo, Y.; Ågren, H. Structure-to-Property Relations for Two-Photon Absorption of Hydrocarbon Oligomers. *Chem. Phys. Lett.* **1998,** *296*, 8-18.

(43) Morel, Y.; Stephan, O.; Andraud, C.; Baldeck, P. L. Enhanced Two-Photon Absorption with Dimers of π-Conjugated Molecules. *Synthetic Met.* **2001,** *124*, 237-239.

(44) Cronstrand, P.; Luo, Y.; Ågren, H. Generalized Few-State models for Two-Photon Absorption of Conjugated Molecules. *Chem. Phys. Lett.* **2002,** *352*, 262-269.

(45) Das, G. P.; Yeates, A. T.; Dudis, D. S. An AM1 Study of the Two-Photon Absorption in bis(styryl)benzene Derivatives. *Chem. Phys. Lett.* **2002,** *361*, 71-78.

(46) Nakano, M.; Fujita, H.; Takahata, M.; Yamaguchi, K. Density Analysis of Imaginary Part of γ Related to Two-Photon Absorption. *Chem. Phys. Lett.* **2002,** *356*, 462-468.

(47) Stålring, J.; Bernhardsson, A.; Malmqvist, P.-Å. A Linear Response Approach to Second-Order Electronic Transition Intensities for Multiconfigurational Self-Consistent Field Wave Functions. *J. Chem. Phys.* **2002,** *117*, 1010-1016.

(48) Jha, P. C.; Das, M.; Ramasesha, S. Two-Photon Absorption Cross Sections of trans-Stilbene, and 7,8-Disubstituted Stilbenes in Different Molecular Conformations: A Model Exact Study. *J. Phys. Chem. A* **2004,** *108*, 6279-6285.

(49) Frediani, L.; Rinkevicius, Z.; Ågren, H. Two-Photon Absorption in Solution by Means of Time-Dependent Density-Functional Theory and the Polarizable Continuum Model. *J. Chem. Phys.* **2005,** *122*, 244104.

(50) Yang, G.; Qin, C.; Su, Z.; Dong, S. Calculations of Two-Photon Absorption Cross-Sections of Stibene and bis(styryl)benzene Derivatives by Means of TDDFT-SOS Method. *J. Mol. Struc.-THEOCHEM* **2005,** *726*, 61-65.

(51) Marchese, F. T.; Seliskar, C. J.; Jaffé, H. H. The Use of CNDO in Spectroscopy. XV. Two Photon Absorption. *J. Chem. Phys.* **1980,** *72*, 4194-4203.

(52) Beerepoot, M. T. P.; Friese, D. H.; List, N. H.; Kongsted, J.; Ruud, K. Benchmarking Two-Photon Absorption Cross Sections: Performance of CC2 and CAM-B3LYP. *Phys. Chem. Chem. Phys.* **2015,** *17*, 19306-19314.

5. One- and Two-Photon Absorption Spectroscopy and Quantum Yields of the Cycloreversion Reaction of a Photochromic Molecular Switch

5.1 Introduction

Photochromic molecular switches, in particular, diarylethenes convert between open- and closed-ring isomers and the different isomers exhibit drastically different optical and electronic properties.[1,2] Diarylethene derivatives are a widely studied group of photochromic molecules that are thermally stable and fatigue resistant.[1,2] The properties of diarylethene derivatives make them ideal model systems to study higher-lying excited-state properties and dynamics. The electrocyclization reaction induced with UV light efficiently produces the closed-ring isomer in high yield, while visible light induces the cycloreversion reaction that has a much lower quantum.[3,4]

Diarylethene derivatives are used in molecular applications, which range from molecular electronics to biological imaging to optical memories.[1,2,5-7] In terms of optical memories or data storage applications, UV light is used to "write" data because of the efficient electrocyclization reaction that converts transparent molecules to their colored form and visible light nondestructively "reads-out" the data since the cycloreversion yield is low. To make these devices "erasable" the cycloreversion reaction yield needs to be selectively increased. Previous studies have observed a measureable increase in the cycloreversion reaction quantum yield by exciting the diarylethene molecules through a sequential two-photon excitation mechanism.[1,2,8-13] Diarylethene molecules have also been shown to undergo cycloreversion by a direct simultaneous two-photon excitation that may enhance the cycloreversion quantum yield.[14-16]

This chapter examines the spectroscopy and cycloreversion quantum yields following one- and two-photon absorption of 1,2-bis(2,4-dimethyl-5-phenyl-3-thienyl)perfluorocyclo-

pentene (DMPT-PFCP). The broadband two-photon absorption (2PA) spectroscopy measurements reveal two-photon accessible states of the open- and closed-isomers. The 2PA cross sections of the closed-isomer are determined using broadband 2PA spectroscopy, as well as degenerate single-wavelength 2PA measurements. Separate measurements of the cycloreversion quantum yield (Φ) are measured following one- and two-photon absorption processes. We discuss the difference between the one- and two-photon absorption quantum yields and comment on possible mechanisms to explain the discrepancy.

5.2 Experimental Methods

5.2.1 One- and Two-Photon Absorption Spectroscopy

We implement an ultrafast pump-probe technique to measure the two-photon absorption (2PA) spectroscopy of DMPT-PFCP in solution. The 2PA spectroscopy technique is discussed elsewhere,[17-22] and therefore is described here only briefly. A regeneratively amplified Ti:Sapphire laser (Legend Elite HE, Coherent) produces nonresonant pump and broadband probe pulses. The pump and probe pulses are overlapped temporally and spatially in the sample, and we measure the attenuation of the probe pulse, which is wavelength depend. Tunable pump pulses in the infrared-UV range are generated with an optical parametric amplifier and a white light continuum probe ranging from 1000–700 nm or 750–450 nm is generated in a 1 cm quartz cuvette of water.[23,24] A λ/2 waveplate in the pump beam controls the relative orientation of linearly polarized pump and probe beams. After the probe beam passes through the sample the beam is dispersed onto a 256-element photodiode array for shot-to-shot detection and a chopper wheel blocks every other pump pulse for active background subtraction.

A two-photon allowed transition is accessed when the simultaneous absorption of one pump and one probe photon has a total energy resonant with the transition, while neither photon is independently resonant. The average energy of the pump light is 2–8 μJ/pulse and the diameters of the pump and probe beams are typically ~250 μm and ~80 μm, respectively. The samples for the 2PA measurements are in a 1 mm quartz cuvette filled with a 0.1 M solution of DMPT-PFCP (TCI America, >98.0%) in chloroform (Sigma-Aldrich, ≥99%).

The absolute 2PA cross section at a single wavelength is measured with the simultaneous absorption of two photons within the pump beam. For the single-wavelength measurements a small portion of the pump beam is used as a reference to determine the pump intensities at the sample and the other portion of the beam is transmitted through the sample. We record the intensity of every pump pulse to measure the reference and transmitted intensities simultaneously and to monitor laser fluctuations. A variable neutral density filter is used prior to splitting the pump beam to control the intensity at the sample. The transmittance through the sample as a function of the incident intensity is proportional to the two-photon coefficient, β. The absolute 2PA cross section is then proportional to β as a function of sample concentration.

The samples for the single-wavelength measurements consist of a 1 cm quartz cuvette filled with 1 mL of a 0.1 M solution of DMPT-PFCP in chloroform and stirred continuously with a magnetic stir bar. The sample is irradiated on the order of several minutes to measure the change in transmitted light while varying the intensity, but not long enough to induce a measureable change in concentration. The pump beam, which is collimated, has a diameter of ~300 μm (FWHM) across the entire 1 cm path length of the sample. The beam is collimated to prevent self-focusing and continuum generation[23-25] at the maximum pulse energy of ~15 μJ.

5.2.2 One- and Two-Photon Cycloreversion Quantum Yields

The quantum yield (Φ) of the cycloreversion reaction of DMPT-PFCP is determined following both one- and two-photon excitation by measuring the change in concentration as a function of irradiation time under the appropriate conditions. The quantum yields following excitation with one and two photons are measured with a similar experimental setup as the single-wavelength measurement of the absolute 2PA cross section above. In these measurements the light is held at a constant intensity while the sample is irradiated up to several hours to allow for a measureable concentration change. The main difference between measuring the quantum yields following excitation with one or two photons is the peak intensity, which is inversely proportional to the square of the peak diameter. The one-photon excitation quantum yield measurements uses a peak intensity of ~4 GW·cm^{-2} with a beam diameter of ~600 μm (FWHM) and peak intensity increases to ~18 GW·cm^{-2} for the two-photon excitation measurement with a beam diameter of ~300 μm (FWHM), when using the same maximum pulse energy of ~15 μJ.

The samples for the one-photon excitation quantum yield measurements use a 1 mL aliquot of 2.3×10^{-5} M DMPT-PFCP in cyclohexane (Sigma-Aldrich, >99%) held within a 1 cm quartz cuvette that is constantly stirring. For the two-photon excitation quantum yield measurements the samples are continuously stirring in a 1 cm quartz cuvette filled with 1 mL of 0.1 M solution of DMPT-PFCP in chloroform.

5.3 Results and Discussion

5.3.1 One- and Two-Photon Absorption Spectroscopy

Figure 5.1 shows the one-photon absorption (1PA) spectrum of the closed-ring isomer of DMPT-PFCP as a solid red line and red circles represent the broadband two-photon absorption

(2PA) spectrum. The 1PA spectrum has four distinct absorption bands that peak near 565, 375, 290, and 200 nm.[1,3,12,13] The broadband 2PA spectrum is measured over a narrower range than the 1PA spectrum and the range for the 2PA spectrum consists of 550–375 nm (total energy of 2.2–3.3 eV). The 2PA spectrum has a strong two-photon allowed transition above ~3 eV, with the strongest transition at 3.3 eV, equivalent to a two-photon excitation at 750 nm.

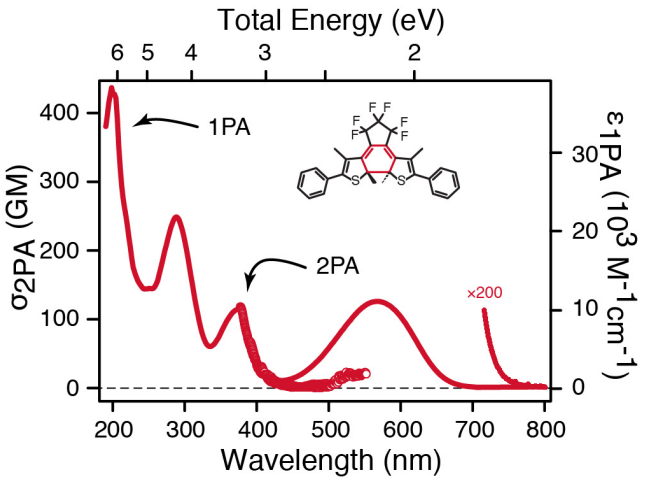

Figure 5.1 One- and two-photon absorption spectra of the closed-ring isomer of DMPT-PFCP.

Five nonresonant pump wavelengths (1250, 1080, 980, 880, and 800 nm) with 1000–700 nm probe light are used to generate the 2PA broadband spectrum of the closed-ring isomer of DMPT-PFCP. The broadband 2PA cross sections (σ_{2PA}) are measured for the parallel and perpendicular polarizations of the pump and probe beams relative to each other. The polarization dependence for DMPT-PFCP, which belongs to the C_2 point group, is consistent with totally symmetric two-photon allowed (A) transitions across the entire probing region.[26-28] Table 5.1 includes measured 2PA cross sections with the relative parallel polarization of the pump and probe beams across the broadband range and 2PA cross sections are reported in GM (1 GM =

10^{-50} cm^4·s·molecule^{-1}·photon^{-1}).

Table 5.1 Two-photon cross sections and quantum yields.[a]

		σ_{2PA} (GM)	
λ_{2PA} (nm)	Energy (eV)	Broadband	β, Single λ_{2PA}
750	3.3	107 (20)	37 (2)
1000	2.5	9 (4)	17 (4)
1160	2.1	20 (8)	29 (4)

[a] The parentheses are the error, at 95% confidence.

Figure 5.2 shows the 1PA and 2PA spectroscopy for the open-ring isomer of DMPT-PFCP, which undergoes cyclization to produce the closed-ring isomer. The 1PA spectrum shows two absorption bands peaking near 270 and 200 nm.[1,3,12,13] The 2PA broadband spectrum from 4.0–5.8 eV of the open-ring isomer is measured with three pump wavelengths (520, 430, and 410 nm) and 750–450 nm probe light. The broadband 2PA spectrum has an absorption band peak between the 1PA bands at 240 nm (total energy of 5.1 eV) and again has a polarization dependence consistent with accessing totally symmetric two-photon allowed (A) transitions. The remainder of this chapter focuses on the closed-ring isomer, which undergoes a cycloreversion reaction.

The absolute 2PA cross section of the closed-ring isomer of DMPT-PFCP are measured following degenerate two-photon absorption at 1160, 1000, and 750 nm by measuring the two-photon absorption coefficient, β, as a function of concentration. The β values are experimentally determined by fitting the transmittance data as a function of incident intensity (W·cm^{-2}) with,

$$\text{transmittance} = \frac{I}{I_0} = \frac{1}{1+\beta \ell I_0} \quad (1)$$

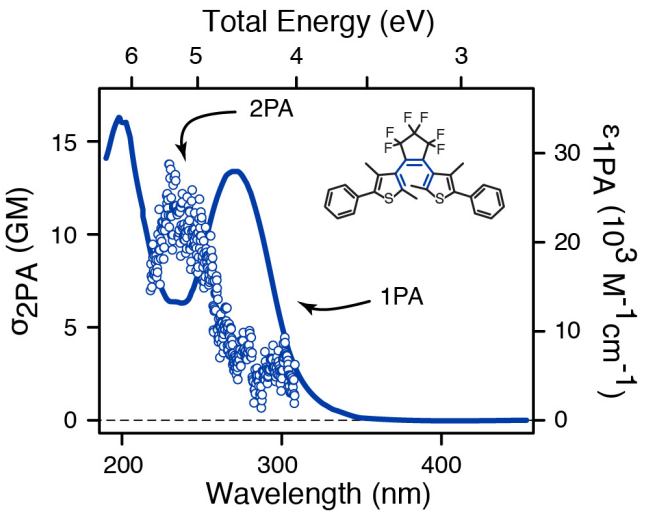

Figure 5.2 One- and two-photon absorption spectra of the open-ring isomer of DMPT-PFCP.

Here the incident intensity is I, the transmitted intensity is I_0, and the path length is ℓ. Exciting the closed-ring isomer of DMPT-PFCP with 750 nm is resonant with both one- and two-photon transitions, so the additional one-photon absorption component needs to be accounted for when determining β. Including the one-photon absorption component Equation 1 becomes,[29-33]

$$\text{transmittance} = \frac{I}{I_0} = \frac{e^{-\alpha\ell}}{1+\beta I_0\left(\frac{1-e^{-\alpha\ell}}{\alpha}\right)} \tag{2}$$

Here the one-photon absorption coefficient is α, *i.e.* $\alpha = \ln(10)\cdot\varepsilon\cdot c$.

From the variation of the measured β values versus concentration, we obtain the absolute 2PA cross section at a single wavelength when including all intensity losses from α, β, and the solvent (see the Appendix). Table 5.1 compares the measured absolute 2PA cross sections at three different excitation energies with values from the broadband 2PA measurement. The absolute 2PA cross sections from both measurements are in agreement with one another by factor of <3 difference between the two methods.

5.3.2 One- and Two-Photon Cycloreversion Quantum Yields

The 1PA and 2PA spectroscopy reveal the energies of one- and two-photon accessible electronic excited states. The quantum yield (Φ) for the cycloreversion reaction of DMPT-PFCP is a measure of the number of molecules converted per number of photons absorbed.

$$\Phi = \frac{\text{molecules converted}}{\text{photons absorbed}} \quad (3)$$

The quantum yield following one-photon excitation (Φ_{1PA}) is determined following a one-photon absorption (1PA) within the two lowest energy absorption bands. The wavelengths used to induce the 1PA conversion to determine the 1PA quantum yield include 750, 690, 600, 580, 550, 500, 470, and 375 nm. A representative 1PA quantum yield measurement that depicts the reference and transmitted light through the DMPT-PFCP sample is shown in the Appendix. The summation of the difference between the reference and transmitted energies is proportional to the number of photons absorbed by the sample, which is inversely proportional to the 1PA quantum yield. Table 5.2 and Figure 5.3 give the measured 1PA quantum yield across the two lowest energy absorption bands using this method. Figure 5.3 shows that the 1PA quantum yield is essentially constant at ~1.5% across the two lowest energy absorption bands, which is the same behavior observed by Irie and coworkers across the lowest energy absorption band.[4]

Table 5.2 One-photon extinction coefficients and quantum yields.[a]

λ_{1PA} (nm)	Energy (eV)	ε_{1PA} (10^3 $M^{-1}cm^{-1}$)	Φ_{1PA} (%)
375	3.3	10.3	1.7 (0.4)
470	2.6	2.4	1.9 (0.3)
500	2.5	5.0	1.9 (0.2)
550	2.3	10.4	1.6 (0.5)
580	2.1	10.4	1.7 (0.6)
600	2.1	9.1	1.4 (0.2)
690	1.8	0.4	1.2 (0.2)
750	1.6	0.0	3.8 (2.2)

[a] The parentheses are the error, at 95% confidence.

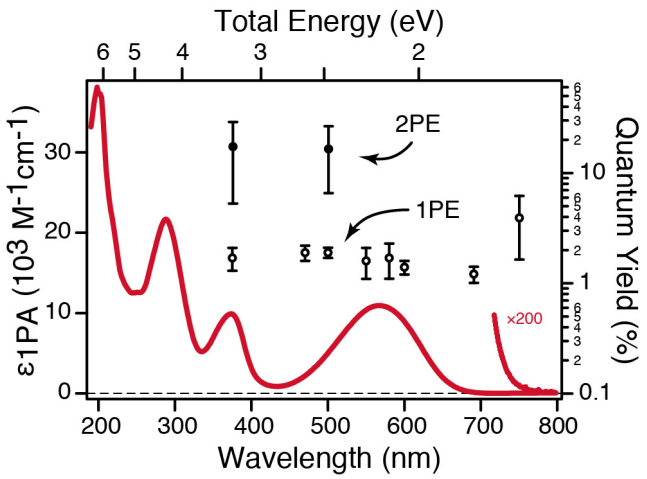

Figure 5.3 One- and two-photon excitation quantum yields (open and closed markers, respectively), measured in molecules converted per absorption event and the error bars represent 95% confidence, compared with the one-photon absorption spectrum (solid red line).

The quantum yield following two-photon excitation (Φ_{2PA}) is determined following a degenerate two-photon absorption within the two lowest energy absorption bands, using 1000 and 750 nm. A similar technique to measure the 1PA quantum yield is used to obtain the 2PA quantum yield by measuring the reference and transmitted intensity through the sample. In the case of the 1PA quantum yield measurement the transmitted energy reaches an asymptotic limit that matches the reference energy, indicating complete conversion of the DMPT-PFCP sample to the open-ring isomer, while the 2PA quantum yield measurement does not show the same complete conversion; therefore, we use the initial conversion rate to determine the 2PA quantum yield.

The initial conversion rate is proportional to the two-photon action cross section ($\sigma_{2PA}\Phi_{2PA}$). We define the two-photon action cross section as the product of the absolute 2PA cross section and the 2PA quantum yield, so to determine the 2PA quantum yield the absolute 2PA cross section needs to be known with some certainty. Table 5.3 reports the two-photon

action cross section as ~8 GM within the two lowest absorption bands. Since the absolute 2PA cross section was determined separately the 2PA quantum yield can be disentangled from the 2PA action cross section. Table 5.3 also includes the measured 2PA quantum yield, which are ~16% for the two lowest absorption bands. The 2PA quantum yields are plotted in Figure 5.3 as a comparison to the 1PA quantum yields, showing the 2PA quantum yields are about an order of magnitude larger than the 1PA quantum yields.

Table 5.3 Two-photon quantum yields.[a,b]

λ_{2PA} (nm)	Energy (eV)	$\sigma_{2PA}\Phi_{2PA}$ (GM)	Φ_{2PA} (%)[c]
750	3.3	8.2 (2.4)	16.1 (11.0)[d]
1000	2.5	7.9 (6.7)	16.3 (9.8)

[a] Quantum yields are reported in molecules converted per absorption event.

[b] The parentheses are the error, at 95% confidence.

[c] Quantum yield determined assuming only a two-photon induced cycloreversion.

[d] Quantum yield determined assuming a one- and two-photon induced cycloreversion, with the one-photon contribution subtracted from the reported value.

The above determination of the 2PA quantum yield includes any additional resonant one-photon absorption contribution from 750 nm since the low energy tail of the 1PA spectrum of DMPT-PFCP is excited at that wavelength. In other words, exciting with 750 nm light induces a cycloreversion reaction through a one- and two-photon excitation process. The additional 1PA contribution is included in the derivation of the quantum yield and gives the 2PA quantum yield as ~16%, as reported above.

Importantly, two-photon excitation may not be the highest-order excitation process initiating the cycloreversion reaction. The optical limiting response of DMPT-PFCP, which is the

transmitted energy as a function of the incident energy shows a nonlinear deviation from a purely linear response (see the Appendix). The divergence from linearity is due to DMPT-PFCP absorbing two or more photons per simultaneous absorption event to induce the cycloreversion reaction.

Exciting with focused, high intensity nonlinear light gives a quantum yield that is greater than the 1PA quantum yield by about an order of magnitude. Since the 1PA and 2PA spectroscopy both have strong transitions above ~3 eV along with DMPT-PFCP being a low symmetry molecule, one may argue that the same states are accessed with one or two photons. If the same state is accessed following a 1PA or 2PA, then the reaction quantum yields should be similar because the conversion mechanism is expected to be the same. However, we observe about an order of magnitude difference between the measured quantum yields following one- and two-photon excitation, suggesting different excitation mechanisms and pathways.

One explanation for the difference in quantum yields between the 1PA and 2PA processes may be that different excited electronic states are initially excited leading to different cycloreversion mechanisms and pathways. As stated above, the similarities between the 1PA and 2PA spectroscopy and the low symmetry of DMPT-PFCP we likely access the same states with both a one- and two-photon excitation process. Another possible explanation for the increased quantum yields may be due to the formation of a triplet state in the excited state that may preferentially lead to the open-ring isomer following relaxation to the ground state.[34] An additional explanation for the different quantum yields may be due to opening up an additional pathway through a higher-order excitation process, such as resonance-enhanced multi-photon ionization.[35-42] The resonance-enhanced multi-photon ionization may occur through a 2+1, 2+2, or 2+*n* ionization process. The ionization mechanism would account for the quantum yields

increasing by about an order of magnitude following irradiation with focused, intense light that induces a multi-photon absorption. Transient absorption pump-probe spectroscopy following one- and two-photon excitation may be used to measure the excited-state dynamics. The pump-probe spectroscopy may provide insight into the mechanism and increased quantum yields of the cycloreversion reaction after exciting DMPT-PFCP with a focused, intense beam, which will be discussed in **Chapter 6**.

5.4 Conclusions

The two methods used to measure the absolute 2PA cross sections of the closed-ring isomer agree in both instances. The spectroscopy provides information about the symmetry of the excited electronic states along with the energies of those transitions following absorption with either one or two photons. The 1PA quantum yields are effectively constant at ~1.5% across the two lowest absorption bands of the closed-ring isomer, while the 2PA quantum yields are increased by about an order of magnitude to ~16%. The 2PA quantum yields are likely much larger than the 1PA quantum yields because the high intensity light used to induce the two-photon excitation may open an additional pathway that leads to more molecules undergoing cycloreversion to the open-ring isomer. Meaning the reported 2PA quantum yields are likely not purely from a two-photon excitation process, but includes contributions from an additional higher-order process. An ionization mechanism may explain the differences in the quantum yields because the excited molecules may lead more favorably to the open-ring isomer. Further reaction dynamics experiments are required to elucidate the mechanism that increases the cycloreversion quantum yield of DMPT-PFCP following intense nonlinear irradiation.

5.5 Appendix

The additional figures include the measured two-photon absorption coefficient as a function of number density following degenerate two-photon excitation that the slope of the linear fit to the data is proportional to the absolute 2PA cross section, representative quantum yield measurements following one- and two-photon excitation, and a representative optical limiting response of DMPT-PFCP indicating a nonlinear excitation.

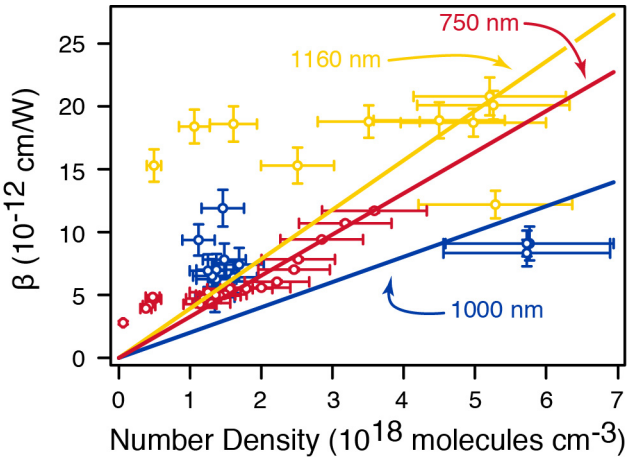

Figure 5.4 Two-photon absorption coefficient, β, (circles) is proportional to the degenerate two-photon absorption cross section of the closed-ring isomer of DMPT-PFCP. The degenerate two-photon absorption cross section is determined from the slope of the fit to the data (solid lines).

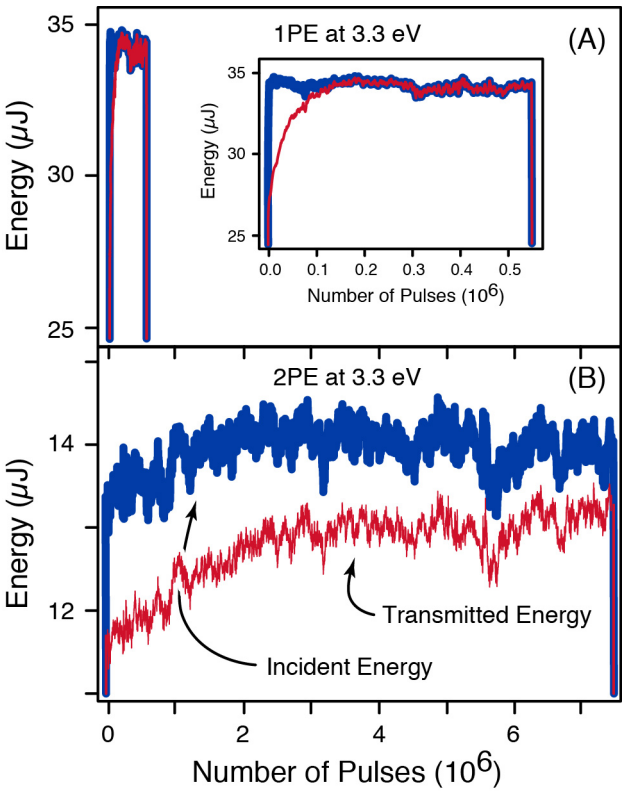

Figure 5.5 Representative (A) one-photon absorption quantum yield measurement and (B) two-photon absorption quantum yield measurement. The integrated area between the incident and transmitted energy measurements and the initial conversion rate of cycloreversion reaction of DMPT-PFCP are measured, respectively, to determine the quantum yield following either a one- or two-photon excitation process.

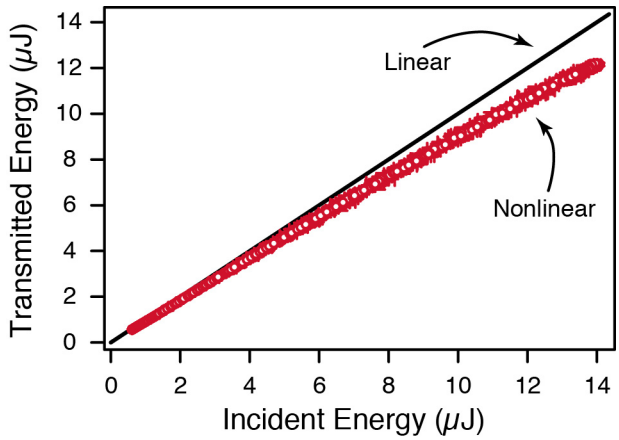

Figure 5.6 Representative optical limiting response of DMPT-PFCP in chloroform, which shows a nonlinear (red circles) deviation from linearity (black line).

5.6 References

(1) Irie, M. Diarylethenes for Memories and Switches. *Chem. Rev.* **2000,** *100*, 1685-1716.

(2) Irie, M.; Fukaminato, T.; Matsuda, K.; Kobatake, S. Photochromism of Diarylethene Molecules and Crystals: Memories, Switches, and Actuators. *Chem. Rev.* **2014,** *114*, 12174-12277.

(3) Irie, M.; Sakemura, K.; Okinaka, M.; Uchida, K. Photochromism of Dithienylethenes with Electron-Donating Substituents. *J. Org. Chem.* **1995,** *60*, 8305-8309.

(4) Sumi, T.; Takagi, Y.; Yagi, A.; Morimoto, M.; Irie, M. Photoirradiation Wavelength Dependence of Cycloreversion Quantum Yields of Diarylethenes. *Chem. Comm.* **2014,** *50*, 3928-3930.

(5) Piao, X.; Zou, Y.; Wu, J.; Li, C.; Yi, T. Multiresponsive Switchable Diarylethene and Its Application in Bioimaging. *Org. Lett.* **2009,** *11*, 3818-3821.

(6) Yun, C.; You, J.; Kim, J.; Huh, J.; Kim, E. Photochromic Fluorescence Switching From Diarylethenes and Its Applications. *J. Photochem. Photobiol. C* **2009,** *10*, 111-129.

(7) Liu, H.; Chen, Y.; Yao, B. Two-Photon Absorption of Photochromic Diarylethene and Its Application to Rewritable Holographic Recording. *Front. Chem. China* **2010,** *5*, 221-225.

(8) Miyasaka, H.; Murakami, M.; Itaya, A.; Guillaumont, D.; Nakamura, S.; Irie, M. Multiphoton Gated Photochromic Reaction in a Diarylethene Derivative. *J. Am. Chem. Soc.* **2001,** *123*, 753-754.

(9) Miyasaka, H.; Murakami, M.; Okada, T.; Nagata, Y.; Itaya, A.; Kobatake, S.; Irie, M. Picosecond and Femtosecond Laser Photolysis Studies of a Photochromic Diarylethene Derivative: Multiphoton Gated Reaction. *Chem. Phys. Lett.* **2003,** *371*, 40-48.

(10) Murakami, M.; Miyasaka, H.; Okada, T.; Kobatake, S.; Irie, M. Dynamics and Mechanisms of the Multiphoton Gated Photochromic Reaction of Diarylethene Derivatives. *J. Am. Chem. Soc.* **2004,** *126*, 14764-14772.

(11) Ishibashi, Y.; Tani, K.; Miyasaka, H.; Kobatake, S.; Irie, M. Picosecond Laser Photolysis Study of Cycloreversion Reaction of a Diarylethene Derivative in Polycrystals: Multiphoton-Gated Reaction. *Chem. Phys. Lett.* **2007,** *437*, 243-247.

(12) Ishibashi, Y.; Okuno, K.; Ota, C.; Umesato, T.; Katayama, T.; Murakami, M.; Kobatake, S.; Irie, M.; Miyasaka, H. Multiphoton-Gated Cycloreversion Reactions of Photochromic Diarylethene Derivatives with Low Reaction Yields Upon One-Photon Visible Excitation. *Photochem. Photobiol. Sci.* **2010,** *9*, 172-180.

(13) Ward, C. L.; Elles, C. G. Cycloreversion Dynamics of a Photochromic Molecular Switch via One-Photon and Sequential Two-Photon Excitation. *J. Phys. Chem. A* **2014,** *118*, 10011-10019.

(14) Ryo, S.; Ishibashi, Y.; Murakami, M.; Miyasaka, H.; Kobatake, S.; Irie, M. Multiphoton-Gated Photochromic Reaction of Diarylethene Derivatives in PMMA Solid Film. *J. Phys. Org. Chem.* **2007,** *20*, 953-959.

(15) Mori, K.; Ishibashi, Y.; Matsuda, H.; Ito, S.; Nagasawa, Y.; Nakagawa, H.; Uchida, K.; Yokojima, S.; Nakamura, S.; Irie, M.; Miyasaka, H. One-Color Reversible Control of Photochromic Reactions in a Diarylethene Derivative: Three-Photon Cyclization and Two-Photon Cycloreversion by a Near-Infrared Femtosecond Laser Pulse at 1.28 μm. *J. Am. Chem. Soc.* **2011,** *133*, 2621-2625.

(16) Corredor, C. C.; Belfield, K. D.; Bondar, M. V.; Przhonska, O. V.; Hernandez, F. E.; Kachkovsky, O. D. One- and Two-Photon Photochromism of 3,4-bis-(2,4,5-trimethyl-thiophen-3-yl)furan-2,5-dione. *J. Photochem. Photobiol. A* **2006,** *184*, 177-183.

(17) Negres, R. A.; Hales, J. M.; Kobyakov, A.; Hagan, D. J.; Van Stryland, E. W. Two-Photon Spectroscopy and Analysis with a White-Light Continuum Probe. *Opt. Lett.* **2002,** *27*, 270-272.

(18) Negres, R. A.; Hales, J. M.; Hagan, D. J.; Van Stryland, E. W. Experiment and Analysis of Two-Photon Absorption Spectroscopy Using a White-Light Continuum Probe. *IEEE J. Quantum Elect.* **2002,** *38*, 1205-1216.

(19) Yamaguchi, S.; Tahara, T. Two-Photon Absorption Spectrum of all-*trans* Retinal. *Chem. Phys. Lett.* **2003,** *376*, 237-243.

(20) Yamaguchi, S.; Tahara, T. Observation of an Optically Forbidden State of C_{60} by Nondegenerate Two-Photon Absorption Spectroscopy. *Chem. Phys. Lett.* **2004,** *390*, 136-139.

(21) Elles, C. G.; Rivera, C. A.; Zhang, Y.; Pieniazek, P. A.; Bradforth, S. E. Electronic Structure of Liquid Water from Polarization-Dependent Two-Photon Absorption Spectroscopy. *J. Chem. Phys.* **2009,** *130*, 084501.

(22) Houk, A. L.; Zheldakov, I. L.; Tommey, T. A.; Elles, C. G. Two-Photon Excitation of *trans*-Stilbene: Spectroscopy and Dynamics of Electronically Excited States Above S_1. *J. Phys. Chem. B* **2015,** *119*, 9335-9344.

(23) Nagura, C.; Suda, A.; Kawano, H.; Obara, M.; Midorikawa, K. Generation and Characterization of Ultrafast White-Light Continuum in Condensed Media. *Appl. Opt.* **2002,** *41*, 3735-3742.

(24) Buchvarov, I.; Trifonov, A.; Fiebig, T. Toward an Understanding of White-Light Generation in Cubic Media-Polarization Properties Across the Entire Spectral Range. *Opt. Lett.* **2007,** *32*, 1539-1541.

(25) Brodeur, A.; Chin, S. L. Ultrafast White-Light Continuum Generation and Self-Focusing in Transparent Condensed Media. *J. Opt. Soc. Am. B* **1999,** *16*, 637-650.

(26) Monson, P. R.; McClain, W. M. Polarization Dependence of the Two-Photon Absorption of Tumbling Molecules with Application to Liquid 1-Chloronaphthalene and Benzene. *J. Chem. Phys.* **1970,** *53*, 29-37.

(27) McClain, W. M. Excited State Symmetry Assignment Through Polarized Two-Photon Absorption Studies of Fluids. *J. Chem. Phys.* **1971,** *55*, 2789-2796.

(28) Monson, P. R.; McClain, W. M. Complete Polarization Study of the Two-Photon Absorption of Liquid 1-Chloronaphthalene. *J. Chem. Phys.* **1972,** *56*, 4817-4825.

(29) Bechtel, J. H.; Smith, W. L. Two-Photon Absorption in Semiconductors with Picosecond Laser Pulses. *Phys. Rev. B* **1976,** *13*, 3515-3522.

(30) Liu, P.; Smith, W. L.; Lotem, H.; Bechtel, J. H.; Bloembergen, N.; Adhav, R. S. Absolute Two-Photon Absorption Coefficients at 355 and 266 nm. *Phys. Rev. B* **1978,** *17*, 4620-4632.

(31) Dragonmir, A.; McInerney, J. G.; Nikogosyan, D. N. Femtosecond Measurements of Two-Photon Absorption Coefficients at λ = 264 nm in Glasses, Crystals, and Liquids. *Appl. Opt.* **2002,** *41*, 4365-4376.

(32) Dragomir, A.; McInerney, J. G.; Nikogosyan, D. N.; Ruth, A. A. Two-Photon Absorption Coefficients of Several Liquids at 264 nm. *IEEE J. Quantum Electron.* **2002,** *38*, 31-36.

(33) Dragomir, A.; McInerney, J. G.; Nikogosyan, D. N.; Kazansky, P. G. Two-Photon Absorption Properties of Commercial Fused Silica and Germanosilicate Glass at 264 nm. *Appl. Phys. Lett.* **2002,** *80*, 1114-1116.

(34) Buckup, T.; Weigel, A.; Hauer, J.; Motzkus, M. Ultrafast Multiphoton Transient Absorption of β-Carotene. *Chem. Phys.* **2010,** *373*, 38-44.

(35) Takeshita, M.; Irie, M. Enhancement of the Photocyclization Quantum Yield of 2,2'-dimethyl-3,3'-(perfluorocyclopentene-1,2-diyl)bis(benzo[*b*]-thiophene-6-sulfonate) by Inclusion in a Cyclodextrin Cavity. *Chem. Comm.* **1997**, 10.1039/A705677J, 2265-2266.

(36) Hara, M.; Miwa, M.; Takeshita, T.; Watanabe, S. Resonance Two-Photon Ionization of Diarylethene in the Presence of Cyclodextrin. *Int. J. Photoenergy* **2013,** *2013*, 6.

(37) Takeshita, T.; Hara, M. Resonance Photoionization of a Diarylethene Derivative in the Presence of Cyclodextrins Using Multi-Color Multi-Laser Irradiation. *J. Photochem. Photobiol. A* **2015,** *310*, 180-188.

(38) Hara, M.; Samori, S.; Cai, X.; Fujitsuka, M.; Majima, T. Importance of Properties of the Lowest and Higher Singlet Excited States on the Resonant Two-Photon Ionization of Stilbene

and Substituted Stilbenes Using Two-Color Two-Lasers. *J. Phys. Chem. A* **2005,** *109*, 9831-9835.

(39) Samori, S.; Hara, M.; Tojo, S.; Fujitsuka, M.; Majima, T. Important Factors for the Formation of Radical Cation of Stilbene and Substituted Stilbenes During Resonant Two-Photon Ionization with a 266- or 355-nm Laser. *J. Photochem. Photobiol. A* **2006,** *179*, 115-124.

(40) Miki, H.; Yoshida, K.; Kawate, C.; Shimada, R.; Takaya, T.; Iwata, K.; Hamaguchi, H.-o. Two-Step Photoionization of *trans*-Stilbene in Acetonitrile via an Ion-Pair Precursor Studied with Picosecond Time-Resolved Absorption and Raman Spectroscopies. *Chem. Phys. Lett.* **2012,** *527*, 27-30.

(41) Moreno, J.; Dobryakov, A. L.; Ioffe, I. N.; Granovsky, A. A.; Hecht, S.; Kovalenko, S. A. Broadband Transient Absorption Spectroscopy with 1- and 2-Photon Excitations: Relaxation Paths and Cross Sections of a Triphenylamine Dye in Solution. *J. Chem. Phys.* **2015,** *143*, 024311.

(42) Moreno, J.; Gerecke, M.; Dobryakov, A. L.; Ioffe, I. N.; Granovsky, A. A.; Bléger, D.; Hecht, S.; Kovalenko, S. A. Two-Photon-Induced versus One-Photon-Induced Isomerization Dynamics of a Bistable Azobenzene Derivative in Solution. *J. Phys. Chem. B* **2015,** *119*, 12281-12288.

6. Multi-Photon Excitation and Photoionization of a Photochromic Molecular Switch: A New Mechanism for Increasing the Cycloreversion Yield

6.1 Introduction

Nonlinear excitation provides a means of populating highly excited states of a molecule that are not necessarily accessible via single-photon (linear) excitation due to symmetry selection rules and other constraints.[1-4] Accessing the higher-lying states potentially opens new reaction channels, and therefore raises the possibility of selectively controlling the reactivity of a molecule by tuning the excitation conditions.[4-8] However, the reaction dynamics of higher-lying excited states are difficult to probe, both experimental and theoretically, due to strong coupling and the high density of states above the lowest excited state, S_1. Lifetimes of these states are typically on the order of a few hundred fs or less, even for molecules containing only a few atoms.[3,9-15] Nevertheless, the prospect of controlling the reactivity of a molecule through nonlinear excitation provides strong motivation for studying the dynamics of higher-lying states.[16-20]

Photochromic molecular switches are excellent model systems for studying excited-state dynamics because these compounds often have distinctly different optical and electronic properties depending on the structure (or state) of the molecule, which simplifies the analysis of transient absorption spectra, and therefore provides a valuable window on the reaction dynamics.[8,21,22] Diarylethene derivatives that reversibly photoisomerize between open- and closed-ring isomers comprise a particularly popular group of photochromic switches due to their excellent fatigue resistance, thermal stability, and rapid conversion rates.[8,22] Many of these compounds have a low cycloreversion quantum yield following one-photon excitation,[21,22] but have been shown to isomerize more efficiently following nonlinear excitation.[4] For example,

sequential two-photon excitation[6,8,22-29] increases the cycloreversion quantum yield for many of these compounds by re-exciting the molecule from a relatively unreactive initially excited state to a higher-lying state that increases the efficiency of the ring-opening reaction.[6,8,22-29]

We previously compared the dynamics following direct one-photon excitation at 375 nm with the behavior following sequential two-photon excitation at similar total excitation energies, from which we determined the molecule must evolve out of the Franck-Condon region of S_1 *prior to* re-excitation in order for the reaction yield to increase.[1,2] That observation is consistent with the ground-breaking work of Miyasaka and co-workers, who inferred that the cycloreversion yield does not increase under immediate re-excitation from the initially excited state, but rather requires some delay between absorption of the first and second photons. In contrast, we found more recently that the efficiency of the cycloreversion reaction increases by at least an order of magnitude (from ~1.7% to more than ~16%) due to *nonresonant* multi-photon excitation under intense irradiation at 750 nm.[4] Similar examples of direct (nonresonant) two-photon excitation were also reported by Belefield and coworkers for other molecular switches.[30-32]

The spectra in Figure 6.1 show that both one- and two-photon transitions access the second absorption band of DMPT-PFCP at ~3.3 eV (*i.e.* one-photon excitation at 375 nm or two-photon excitation at 750 nm), where the 2PA cross section of 37±2 GM is more than an order of magnitude larger than for excitation of the lowest absorption band (total energy of ~2.5 eV).[4]

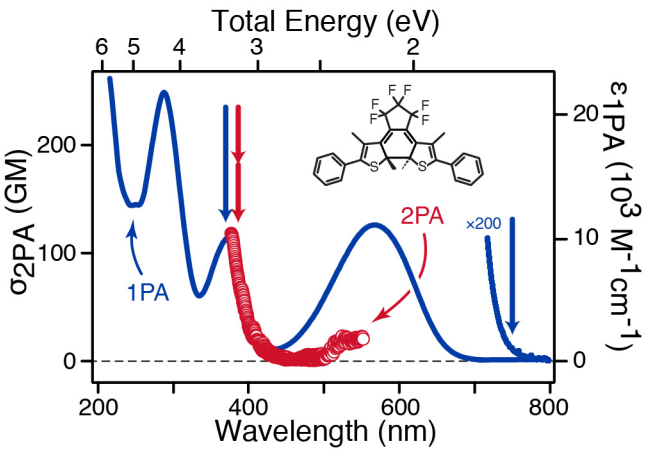

Figure 6.1 One- and two-photon absorption spectra of the closed-ring isomer of DMPT-PFCP.

In this chapter, we monitor the transient absorption (TA) spectroscopy of DMPT-PFCP following both linear excitation at 375 nm and nonlinear excitation at 750 nm. We present evidence of a new cycloreversion pathway following nonlinear excitation that is different from the known dynamics induced by either linear or sequential two-photon excitation. This new reaction pathway is a result of a nonlinear process that is highly dependent on the intensity of pump light, and probably involves resonance-enhanced multi-photon ionization of the molecule. We discuss this proposed mechanism in the context of the observed order of magnitude increase of the cycloreversion quantum yield under nonresonant, high-intensity irradiation.[4]

6.2 Experimental Methods

We use ultrafast pump-probe spectroscopy to monitor the reaction dynamics of DMPT-PFCP in solution following linear excitation at 375 nm and nonlinear excitation at 750 nm.[1-3,33] Both one-photon excitation at 375 nm and two-photon excitation at 750 nm are resonant with the second absorption band of DMPT-PFCP at a total energy of 3.3 eV (see Figure 6.1). The pump and probe pulses are derived from a regeneratively amplified Ti:Sapphire laser (Lesgend Elite,

Coherent) that produces <35 fs pulses of 800 nm fundamental light at 1 kHz. Nonlinear frequency conversion of the fundamental laser light in an optical parametric amplifier (TOPAS-C) produces the pump pulses, and white-light continuum generation in a 2 mm CaF_2 crystal provides broadband probe pulses spanning the range 750–350 nm.[34,35]

We measure the dynamics following one-photon excitation at 375 nm by weakly focusing a beam of 2.0 μJ pump pulses to a diameter of ~210 μm at the sample. Multi-photon excitation at 750 nm requires higher-intensity pump pulses, which we obtain with a beam diameter of ~70 μm and pulse energies as high as ~32 μJ. For both linear and nonlinear excitation experiments, the pump beam intersects the probe at the sample, where the latter has a beam diameter of ~60 μm. The relative orientation of the linearly polarized pump and probe light is set to the magic angle (54.7°) to eliminate anisotropic contributions,[9,36] and a synchronized chopper blocks every other pump pulse before the sample for active background subtraction.

The sample consists of a windowless liquid jet with a path length of 300 μm. Sample solutions were prepared by dissolving DMPT-PFCP (TCI America) in cyclohexane (Sigma-Aldrich, ≥99%), methanol (Sigma-Aldrich, ≥99%), or cyclohexanone (Acros Organics, ≥99.8%). The concentration was 0.2 mM for the one-photon excitation measurements at 375 nm and 0.5 mM for the nonlinear excitation measurements at 750 nm. In some experiments, we use N_2O to quench solvated electrons by bubbling the gas through the sample solution prior to the TA measurement.

6.3 Results

6.3.1 Transient Absorption Spectroscopy Following Linear and Nonlinear Excitation

Figure 6.2 shows the evolution of the transient absorption (TA) spectrum following excitation of the closed-ring isomer of DMPT-PFCP under several different conditions. As a reference for the nonlinear excitation experiments, the top panels (Figure 6.2A–B) show the TA spectra following one-photon excitation into the second absorption band at 375 nm.[2,4,21,22] An excited-state absorption (ESA) band near 590 nm appears within the instrument response time, and then decays on the same timescale that two new bands appear near 410 and 700 nm.[2] The ESA band near 590 nm was previously assigned as a transition from the initially excited state S_n, which relaxes to S_1 in about 90 fs.[2] Following the initial relaxation, the TA spectrum at 600 fs contains contributions from the two S_1 ESA bands, as well as the ground-state bleach (GSB), which is responsible for the negative signal near 565 nm.[2] The ESA bands evolve on a 1 ps timescale due to vibrational cooling of S_1, followed by 3 ps spectral evolution associated with an activated barrier crossing on S_1, before finally decaying to the baseline in about 10 ps due to relaxation back to the ground electronic state.[2] A small fraction of the GSB, matching the inverse of the linear absorption spectrum of the closed-ring isomer, lasts for the duration of our measurement due to excited molecules that undergo cycloreversion to the transparent open-ring isomer (Figure 6.3). The magnitude of the GSB in the long-time limit is consistent with the previously reported cycloreversion yield of 1.7±0.4% following UV excitation of DMPT-PFCP.[4] This low quantum yield for excitation into the second absorption band is similar to the quantum yield of ~2% across the entire first absorption band,[4,21,37] and is consistent with the picture of rapid $S_n \rightarrow S_1$ relaxation.[2]

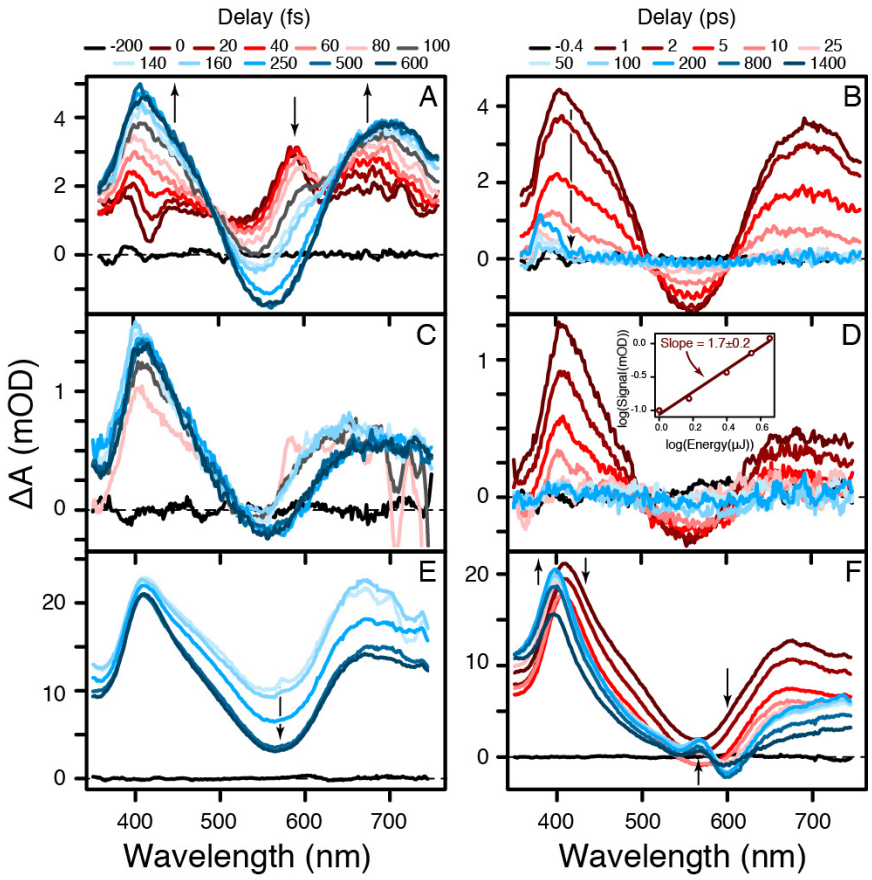

Figure 6.2 Sub-picosecond (left column) and picosecond (right column) transient absorption of the closed-ring isomer of DMPT-PFCP in cyclohexane with (top panels, A–B) 375 nm linear excitation, (middle panels, C–D) 750 nm nonlinear excitation, in the low intensity regime, and (bottom panels, E–F) 750 nonlinear excitation, in the high intensity regime. Oscillations from cross-phase modulation obscure the TA prior to ~100 fs delay for the nonlinear excitation with 750 nm. The inset in panel D is the log-log power dependence of the transient absorption measured at 1 ps delay following nonlinear excitation with 750 nm measured with 410 nm probe light and the slope is 1.7, indicating a two-photon excitation process.

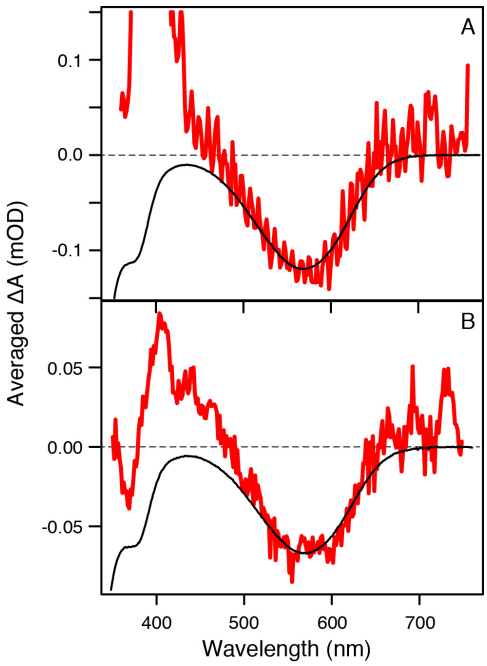

Figure 6.3 Long time limit of TA signal for (A) linear and (B) nonlinear excitation, compared with the linear one-photon spectrum.

The middle panels of Figure 6.2C–D show the sub-picosecond and picosecond TA spectra following nonlinear excitation at 750 nm using moderate intensities. We observe only subtle differences compared with linear excitation. Although cross-phase modulation partially obscures the TA signal at very short delay times, there is a rapidly decaying ESA band near 590 nm that precedes the appearance of two new ESA bands centered near 410 and 700 nm. Global fits emphasize the similar behavior for linear and nonlinear excitation under these conditions, including the predominant short-lived ESA band near 590 nm (see Figure 6.9 in the Appendix). The two ESA bands near 410 and 700 nm decay to the baseline and the GSB mostly recovers within ~10 ps, leaving only a small negative signal from the residual GSB. Figure 6.3 compares the GSB at 200 ps for linear and nonlinear excitation with the inverted ground state absorption spectrum of the closed-ring isomer of DMPT-PFCP. In general, the only noticeable differences

between TA signals for the two excitation conditions in Figure 6.2A–D are the slightly narrower ESA band near 410 nm and the different relative intensities of the 410 and 700 nm ESA bands.

At higher excitation intensities, on the other hand, there are more significant differences in the transient spectrum, as shown in the lower panels of Figure 6.2E–F. Most notably, higher intensity excitation generates a transient signal that persists well beyond the ~10 ps excited-state lifetime of DMPT-PFCP. We highlight the different kinetics for high-intensity excitation in Figure 6.4, which shows the evolution of the TA signal at 400 nm for all three excitation conditions. Following linear excitation at 375 nm and nonlinear excitation using moderate intensities of 750 nm light, the TA signals return to the baseline with a time constant of about 10 ps. In stark contrast, the TA following high-intensity nonlinear excitation remains positive for the duration of the experiment (1400 ps). The long-lived TA signal observed under high-intensity irradiation at 750 nm decays slightly on a timescale of ~800 ps or longer. Concentration-dependent measurements confirm that the long-lived TA signal is entirely due to excitation of the closed-ring isomer, rather than residual open-ring isomer or the solvent (see the Appendix).

The transient absorption signal at the earliest time delays following high-intenisty excitation also deviates from the other two cases (Figure 6.3). Specifically, high-intensity excitation gives a broad TA signal that decays on a longer timescale (~250 fs) than the narrower 590 nm ESA band in the other two cases. Figure 6.5 emphasizes the differences by comparing the TA spectra at 600 fs. Unlike linear and low-intensity nonlinear excitation, the transient signal is positive across the entire spectrum, including the region of the GSB. We return to this point below, after first discussing the intensity dependence of the transient absorption signals.

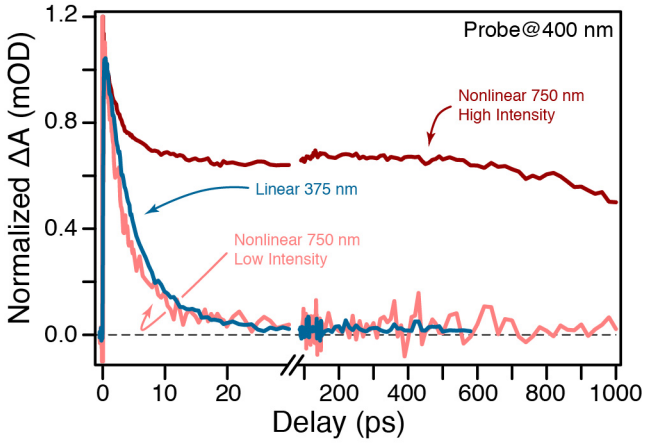

Figure 6.4 Kinetics of the transient absorption of the closed-ring isomer of DMPT-PFCP in cyclohexane following excitation with one photon of 375 nm (blue line), multiple photons of 750 nm, in the low intensity regime (pink line), and multiple photons of 750 nm, in the high intensity regime (dark red line). The transient absorption signal was integrated in a 20 nm range (13 pixels), with 400 nm as the center wavelength.

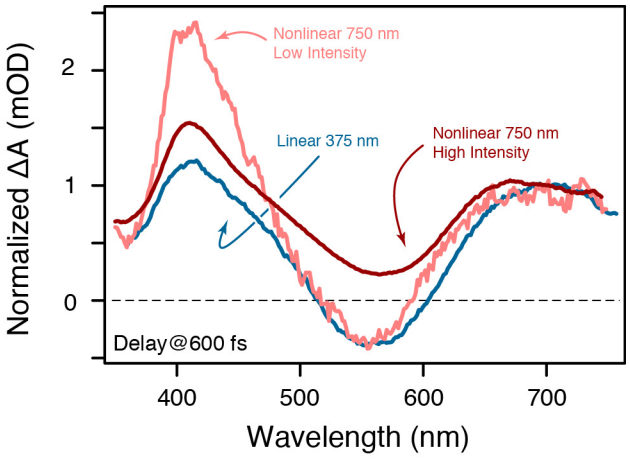

Figure 6.5 Transient absorption spectra of DMPT-PFCP at 600 fs delay normalized at 700 nm probe light, following one-photon excitation with 375 nm (blue line), multi-photon excitation with 750 nm, in the low intensity regime (pink line), and multi-photon excitation with 750 nm, in the high intensity regime (dark red line).

6.3.2 Intensity Dependence of Transient Absorption Signals

The intensity dependence of the transient absorption signals provides valuable insight on the competition between various linear and nonlinear excitation processes under 750 nm irradiation. The linear (one-photon) extinction coefficient of the closed-ring isomer at 750 nm is 4.5 M^{-1} cm^{-1}, giving an optical density of only $\sim 3\times10^{-5}$ under the current experimental conditions, therefore we expect very little contribution from linear excitation at this wavelength. In contrast, the absolute two-photon absorption (2PA) cross section at this wavelength is 37±2 GM, which corresponds to a relatively strong transition into the second absorption band of the closed-ring isomer (Figure 6.1).[4] The inset of Figure 6.2D shows the intensity dependence of the 410 nm TA signal measured at 1 ps delay under relatively low excitation intensities (1–5 μJ/pulse). Even for low-intensity irradiation, the excitation process is nearly quadratic, as indicated by the slope of ~1.7 in the log-log plot. Therefore, the TA signal is predominantly from two-photon excitation, with only a negligible contribution from one-photon excitation under these conditions.

Figure 6.6 shows the log-log power dependence of the TA signal at 400 nm for higher intensity excitation (up to ~32 μJ/pulse), and at two different delay times. Below ~10 μJ, the signal at 1 ps delay has the same nearly quadratic power dependence as in the inset of Figure 6.2D, but the TA signal at 200 ps has a higher-order power dependence that gives a slope of ~4 in the log-log plot. The steeper slope at 200 ps delay indicates a higher-order process than the two-photon excitation process responsible for the TA signal at 1 ps. In other words, the two different delay times probe different signals. At a delay of 200 ps we selectively probe only the higher-order process that gives rise to the long-lived signal, whereas the 1 ps delay has contributions from both two-photon excitation and the higher-order process. Only the signal

resulting from higher-order nonlinear excitation contributes at long delay times, because the excited-state population decays completely on a timescale of ~10 ps following two-photon excitation at 750 nm. The power dependence of the ESA band centered near 700 nm is essentially the same as the dependence of the 400 nm ESA band for both delay times.

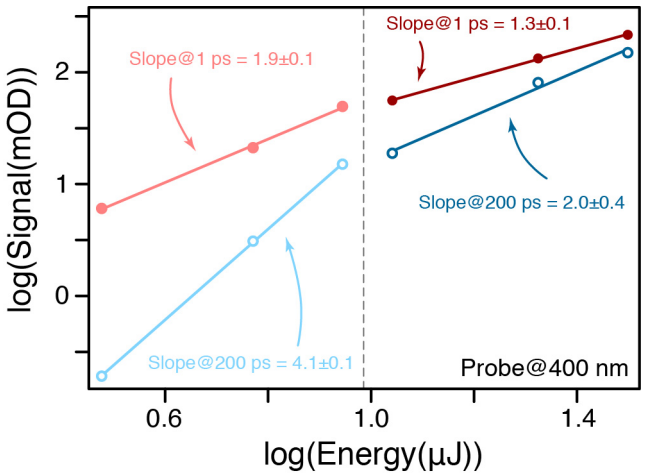

Figure 6.6 Log-log power dependence of the transient absorption measured following excitation with multiple photons of 750 nm at delays of 1 and 200 ps and measured with 400 nm probe light, the gray dotted line indicates the saturation energy. The transient absorption signal was integrated in a 20 nm range (13 pixels), with 400 nm as the center wavelength.

At both delay times, we find that the slope of the log-log plot changes with increasing excitation intensity due to saturation effects above ~10 μJ pulse energy. Saturation occurs when nonlinear excitation sufficiently depletes the pump beam such that the effective intensity is lower than the incident intensity, giving a smaller than expected increase of the TA signal with increasing intensity of the laser pulses. The onset of saturation occurs at an intensity that is inversely proportional to the square root of the 2PA cross section and the pulse duration.[38-40] Based on our independently measured 2PA cross section (37 GM) and the excitation conditions

of the current experiment, the calculated saturation intensity of 2.7×10^{12} W/cm^2 (pulse energy of 9.7 μJ), is in excellent agreement with the data in Figure 6.6.

The higher-order power dependence suggests that the long-lived TA signal is the result of a resonance-enhanced 2+*n* multi-photon excitation above the two-photon resonance at 3.3 eV. The slope of 4 in the log-log plot indicates that the secondary excitation (the "+*n*" process) is also nonlinear, $n \geq 2$, which explains why we are able to observe the two-photon process at intermediate intensities. If the secondary excitation was linear, then almost every molecule that reaches the intermediate state via two-photon excitation would be efficiently re-excited with an additional photon from the same laser pulse. Instead, the nonlinear secondary excitation requires sufficient population in the excited state before a significant fraction of the population can be re-excited. The fact that the TA signals saturate at the same intensity for both 1 and 200 ps delay times suggests that the same saturation effect is responsible for the turnover in each case. In other words, the saturation of the 2+*n* process is probably due to depletion of the pump pulse intensity, rather than depletion of the intermediate excited-state population.

The situation for 750 nm excitation is somewhat unique, because the one-photon absorption cross section is sufficiently small to avoid linear excitation, but the two-photon absorption cross section is sufficiently large to allow efficient nonlinear excitation (Figure 6.1). The one-photon absorption cross section increases rapidly for shorter excitation wavelengths, leading to a dominant one-photon excitation process. For example, the TA signal following excitation with 700 nm is dominated by one-photon excitation due to the larger excitation coefficient at this wavelength (170 M^{-1} cm^{-1}). On the other hand, the two-photon cross section decreases rapidly below ~3 eV, making the two-photon process increasingly unlikely for longer excitation wavelengths.[4] More importantly, the higher-order 2+*n* process that leads to the long-

lived TA signal is only observed at relatively high intensities because even the secondary excitation is nonlinear. In other words, both the initial two-photon excitation and a 2+1 process would have similar (quadratic) intensity dependence, therefore the 2+1 process would be difficult to distinguish from two- (and only two) photon excitation.

6.3.3 Evidence of Multi-Photon Ionization

Figure 6.7 shows the evolution of the TA spectrum following high-intensity nonlinear excitation of DMPT-PFCP in cyclohexanone and in methanol. Similar to the results for cyclohexane in Figures 6.2E–F, the TA spectra have strong absorption bands near 400 and 700 nm. However, the TA spectrum in methanol (Figure 6.6D) includes an additional, broad absorption band centered near 620 nm that appears on a timescale of about 60 ps. This new feature near 620 nm is the characteristic absorption of solvated electrons in methanol.[41-43] The absorption spectrum of solvated electrons in methanol has been measured previously using pulse radiolysis and the spectrum has a broad absorption peak near 620 nm.[41-43] The absorption spectra of solvated electrons in cyclohexane and cyclohexanone are broad and featureless in this region of the spectrum.[44,45]

In contrast with the negative TA signal in the region of the GSB following linear excitation at 375 nm (Figure 6.2A), we emphasize that the TA signal is positive across the entire spectrum for high-intensity irradiation, even in the region of the GSB. Adding N_2O reduces the TA signal across the entire probe wavelength range, confirming the presence of solvated electrons (see the Appendix). These observations are consistent with the formation of solvated electrons in all three solvents. The solvated electrons are generated from the solute, because no TA signal is observed after exciting the pure solvent under the same conditions. Importantly, the

kinetics are not affected by the addition of N_2O when the solvated electron is removed from solution; therefore, the solvated electron is not responsible for the slow ~800 ps reaction.

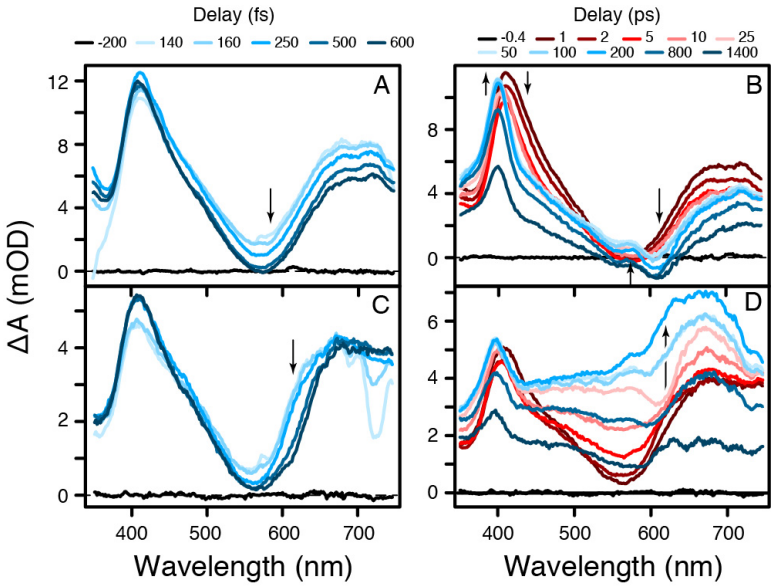

Figure 6.7 Sub-picosecond (left column) and picosecond (right column) transient absorption of the closed-ring isomer of DMPT-PFCP following excitation with multi-photons of 750 nm in the high intensity regime in (top panels) cyclohexanone and (bottom panels) methanol.

Finally, we point to the development of two relatively narrow contributions to the TA spectrum at 400 and 565 nm following high-intensity irradiation. Together, these observations provide clear evidence for ionization of DMPT-PFCP under intense nonresonant irradiation at 750 nm. Therefore, the long-lived TA signal probably includes contributions from both the solvated electron and the molecular cation, DMPT-PFCP$^+$, generated via 2+*n* multi-photon ionization. This resonance-enhanced ionization process involves nonlinear electron ejection from the two-photon excited state of the neutral molecule, the dynamics of which are observed under

lower-intensity irradiation at 750 nm. Importantly, the MPI process becomes dominant only at higher intensities, because of the secondary (ionization) step is also nonlinear.

6.4 Discussion

The evolution of the TA spectrum for linear and nonlinear excitation in the low intensity regime gives similar results despite the different excitation pathways (linear vs quadratic). However, Figure 6.5 shows the TA spectra for the nonlinear excitation has an additional absorption within the band near 410 nm. The additional absorption probably represents a new species following excitation with two or more photons, such as the cation that was proposed by Hara and coworkers.[46] A small quantity of the additional species is formed under moderate intensity irradiation at 750 nm, which may be responsible for the different TA spectra. If the additional species is a cation, it must recombine quickly with a free electron in solution, thus eliminating the TA signal within about 10 ps. Also, we observe no sign of an increased cycloreversion reaction quantum yield under nonlinear excitation with moderate intensity (Figure 6.3), which is consistent with a previous sequential two-photon excitation measurement that shows the one- and two-photon quantum yields are the same when the two excitation photons are overlapped in time.[2]

However, we observe an additional signal generated via a higher-order nonlinear process under high-intensity irradiation. Evidence of increasing solvated electrons under these excitation conditions suggests that multi-photon ionization contributes to the TA signal, thus the ionization process produces cations of DMPT-PFCP and ejects an electron into solution. The evolution of the long-lived TA signals following high-intensity nonlinear excitation at 750 nm shows the appearance of two narrow absorption bands near 400 and 565 nm on a timescale of about 20 ps.

The absorption bands near 400 and 565 nm for DMPT-PFCP in cyclohexanone and methanol exhibit more pronounced narrowing than in cyclohexane. The narrowed bands are likely attributed to the formation of cation species of DMPT-PFCP in solution, specifically the 2+ cation.[47,48]

Electrochemistry measurements of a similar fluorinated diarylethene molecule indicate cycloreversion occurs for the 2+ cation of the closed-ring isomer following two-electron oxidation at 1.0 V.[47,48] The 1+ cation could not be isolated for the fluorinated compound because the two one-electron oxidation states are not well separated from each other.[47,48] However, a similar hydrogenated molecule has well separated one-electron oxidation states and the spectroelectrochemistry of the 1+ and 2+ cations were measured for the hydrogenated diarylethene.[47,48] The spectroelectrochemistry shows the +1 cation has absorption bands shifted to either side of the first absorption band of the closed-ring isomer, but the 2+ cation has two narrower bands peaked at about the maximum of the first absorption band of the neutral molecule and another band to the blue of the first absorption band.[47,48] Comparing the spectroelectrochemistry result of the hydrogenated compound with the TA spectra of DMPT-PFCP the narrow absorption band at 565 nm is likely attributed to the 2+ cation because the 2+ cation absorption band peaks at about the same energy as the first absorption band of the neutral form and the 1+ cation does not absorb in the range of the first absorption band.[47,48]

The absorption spectrum of the possible cation species may be extracted from the TA signal by subtracting TA spectra at two different time delays. Figure 6.8 is the difference spectrum of the TA spectra at delays of 15 and 200 ps. The 15 ps delay corresponds to the timescale of the formation of the 2+ cation and the two-photon excitation dynamics are complete by 15 ps, while the 200 ps component is the maximum absorption signal for the 2+ cation. The

subtracted TA spectra give a reasonable absorption spectrum of the ionization products and are then compared to the linear absorption spectrum.

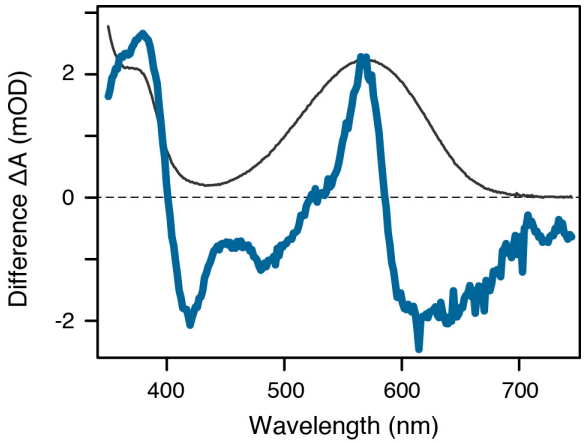

Figure 6.8 Transient absorption measurement of DMPT-PFCP following excitation with nonlinear, multi-photons of 750 nm with high intensity light produces difference spectra by subtracting the 200 ps delay spectrum and the 15 ps delay spectrum. The difference spectrum gives a reasonable spectrum of what the absorption spectrum of the ionization product looks like and is compared to the one-photon absorption spectrum of the closed-ring isomer.

This additional multi-photon ionization pathway might explain the increase of the quantum yield from ~1.7% to ~16% for high-intensity nonlinear excitation.[4] Previous work on a closely related fluorinated diarylethene compound is shown to undergo cycloreversion while in a 2+ oxidative state. Assuming DMPT-PFCP also undergoes cycloreversion as a 2+ cation then the closed-form isomer likely switches to the open-ring isomer through the 2+ oxidation state before relaxing to the ground state in >1400 ps.[47,48]

6.5 Conclusions

Following direct nonlinear excitation the cycloreversion reaction quantum yield increases to ~16% from ~1.7% for linear excitation, about an order of magnitude increase for nonlinear excitation.[4] An increase for the cycloreversion reaction quantum yield was also previously observed following sequential two-photon excitation,[6,8,22-29] which means the quantum yield can be increased by exciting to higher-lying excited states that couple efficiently to the cycloreversion reaction coordinate. However, the ionization pathway provides a different route to producing additional open-ring isomers through the cycloreversion reaction while the molecules are in a 2+ cation state. Previous work on determining the cycloreversion reaction quantum yield of DMPT-PFCP in the presence of cyclodextrins following ionization with two photons of 266 nm showed a relatively small increase in the quantum yield, which is still on the order of 1–2%.[46] The low cycloreversion quantum yield following two-photon excitation of DMPT-PFCP in the presence of cyclodextrins may be due to only producing DMPT-PFCP^{+}.[46] A similar fluorinated diarylethene molecule does not undergo cycloreversion from the 1+ oxidation state[47,48] so, recombination of the cation and electron may only be observed. Consequently, the quantum yield does not change significantly from the linear excitation result.

Sequential two-photon excitation measurements would be helpful in elucidating the mechanism of ionization by controlling the pulse duration. Choosing shorter pulses than the ~100 fs pulses used in this study could be used to control the 2+n process to determine the ionization mechanism, *i.e.* a one-step simultaneous excitation or a sequential two-step excitation. Additional experiments are needed to elucidate the ns timescale dynamics, as well as the spectroelectrochemistry of DMPT-PFCP to determine the absorption spectra of the cation species. Probing the dynamics of molecules in their higher-lying excited states are pushing the

boundaries of our understanding of chemical reaction dynamics and the above findings of the studied molecular systems using two-photon excitation provide benchmarks for further experimental and computational studies of the higher-lying excited states.

6.6 Appendix

The additional figures include decay-associated spectra (DAS) from global fits to the data using a sum of exponentials, table of the time constants from the global fits, transient absorption (TA) and kinetics traces following linear excitation with 800, 750, and 700 nm, TA and kinetics traces following multi-photon excitation of 750 nm with varying concentrations of the closed-ring isomer of DMPT-PFCP in solution, TA following ionization of cyclohexane, cyclohexanone, and methanol, and TA and kinetics traces of the closed-ring isomer DMPT-PFCP in cyclohexane saturated with N_2O following multi-photon ionization with 750 nm.

Table 6.1 Time constants for relaxation of DMPT-PFCP following excitation with 3.3 eV from global fits to the transient absorption spectra using sequential kinetic models.

	τ_1 (ps)	τ_2 (ps)	τ_3 (ps)	τ_4 (ps)
1PE	0.09	1.0	3.9	10.4
2PE	0.09	1.0	2.8	12.4

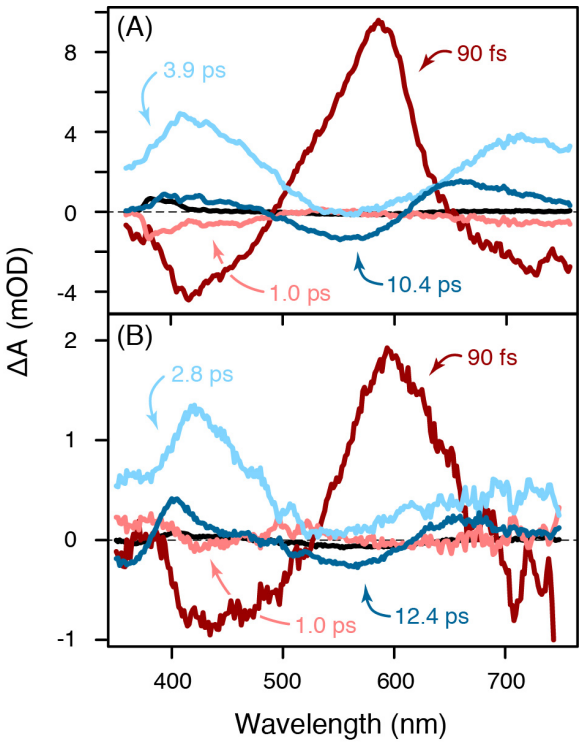

Figure 6.9 Decay associated spectra (DAS) of DMPT-PFCP following (A) one-photon excitation with 375 nm and (B) two-photon excitation with 750 nm, low intensity regime.

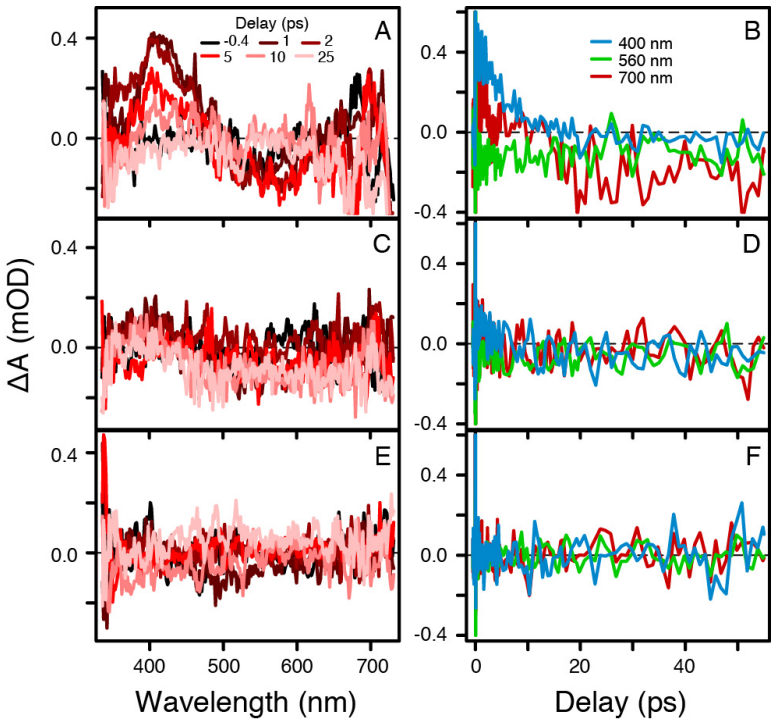

Figure 6.10 Transient absorption (left column) and kinetics (right column) of the closed-ring isomer of DMPT-PFCP following one-photon excitation with (A) 700 nm, (B) 750 nm, and (C) 800 nm.

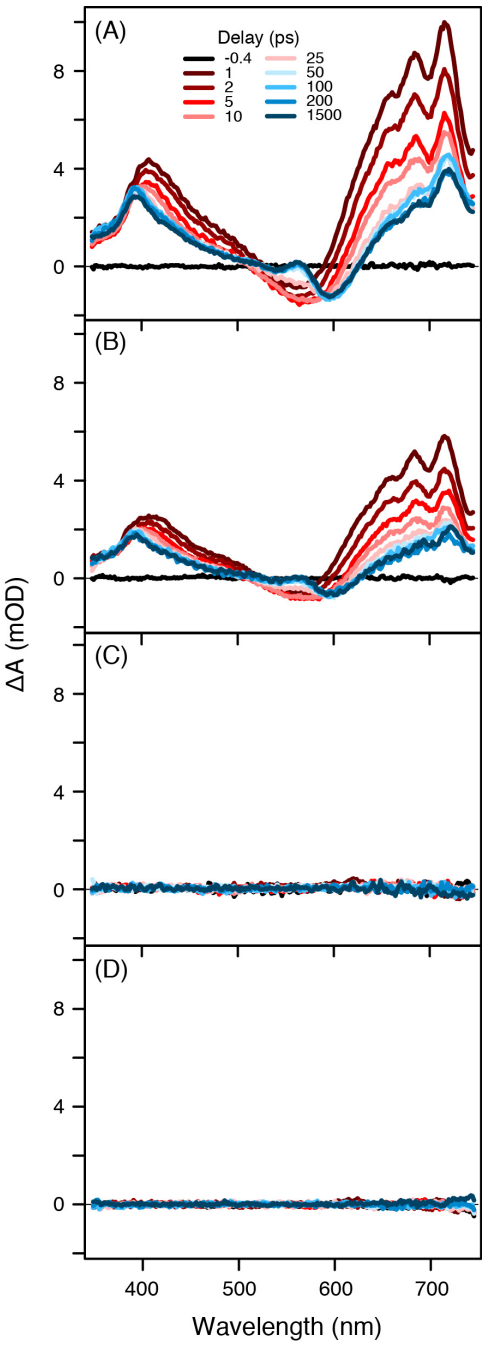

Figure 6.11 Transient absorption of DMPT-PFCP following excitation with multiple photons of 750 nm light with varying concentrations of closed-ring isomer in solution, but with the same overall concentration of DMPT-PFCP in solution. (A) Closed-ring isomer near photostationary state, (B) closed-ring isomer at half the photostationary state, (C) open-ring isomer, and (D) cyclohexane.

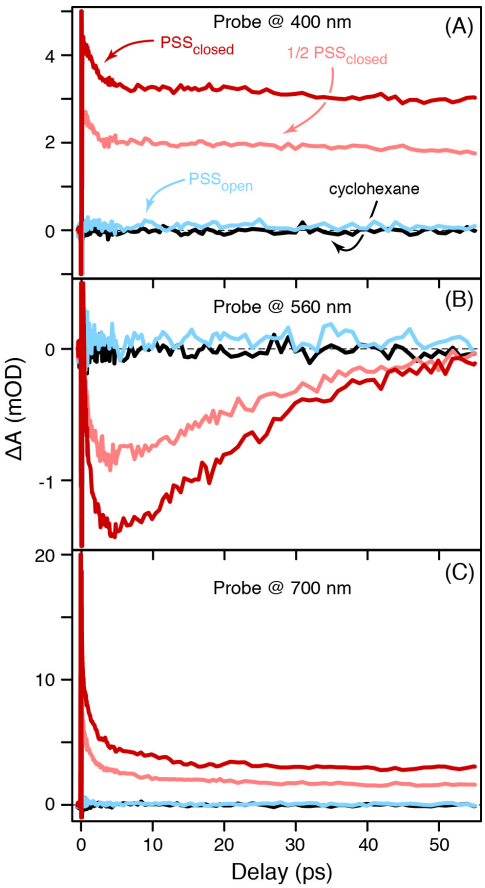

Figure 6.12 Kinetics of DMPT-PFCP following excitation with two photons of 750 nm light with varying concentrations of closed-ring isomer in solution, but with the same overall concentration of DMPT-PFCP in solution. Probe wavelengths for monitoring the kinetics are (A) 400 nm, (B) 560 nm, and (C) 700 nm, and the left column of figures are long time dynamics and the right column depicts earlier time dynamics. The closed-ring isomer near photostationary state is represented by the dark red line, the closed-ring isomer at half the photostationary state is the pink line, the open-ring isomer is the light blue line, and cyclohexane is the black line.

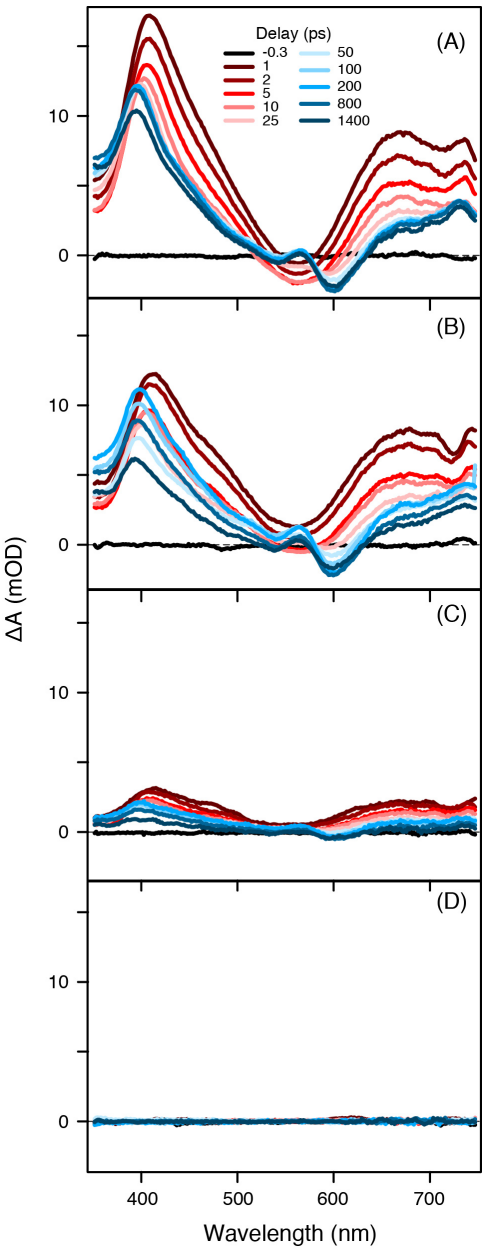

Figure 6.13 Transient absorption of DMPT-PFCP following excitation with two photons of 750 nm light with varying concentrations of closed-ring isomer in solution. (A) High concentration of closed-ring isomer, (B) half of the high concentration of closed-ring isomer, (C) low concentration of closed-ring isomer, and (D) cyclohexane.

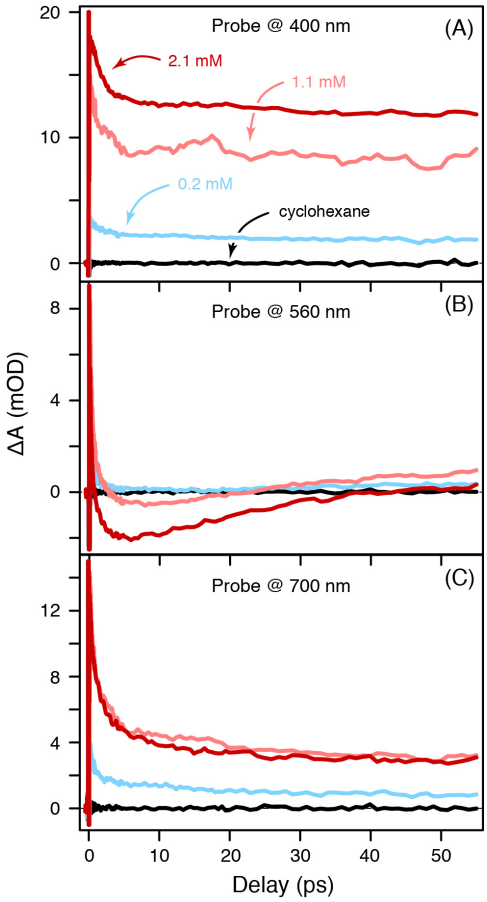

Figure 6.14 Kinetics of DMPT-PFCP following excitation with two photons of 750 nm light with varying concentrations of closed-ring isomer in solution. Probe wavelengths for monitoring the kinetics are (A) 400 nm, (B) 560 nm, and (C) 700 nm, and the left column of figures are long time dynamics and the right column depicts earlier time dynamics. The high concentration of closed-ring isomer is represented by the dark red line, the closed-ring isomer at half the concentration is the pink line, the low concentration of closed-ring isomer is the light blue line, and cyclohexane is the black line.

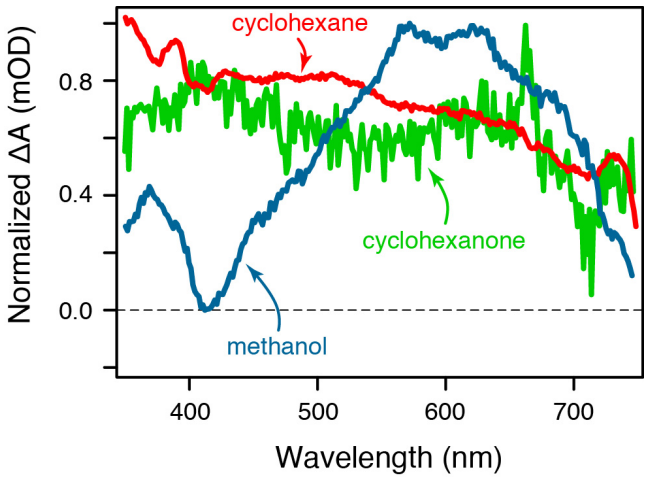

Figure 6.15 Ionization of pure solvents following high-intensity excitation, cyclohexane (red), cyclohexanone (green), and methanol (blue).

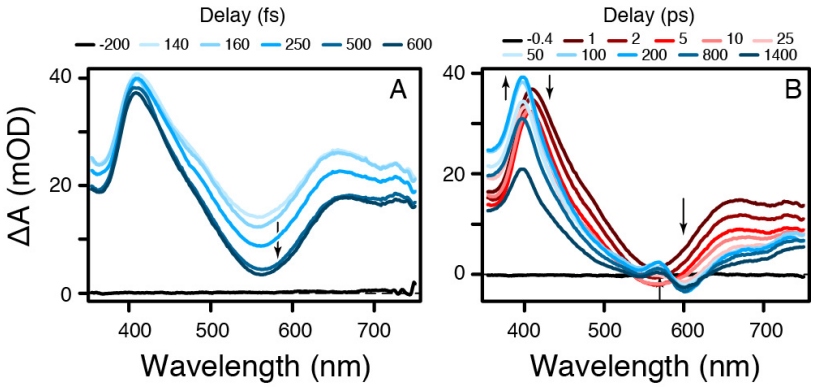

Figure 6.16 Sub-picosecond (A) and picosecond (B) transient absorption of the closed-ring isomer of DMPT-PFCP in cyclohexane, saturated with N_2O, following excitation with multi-photons of 750 nm in the high intensity regime.

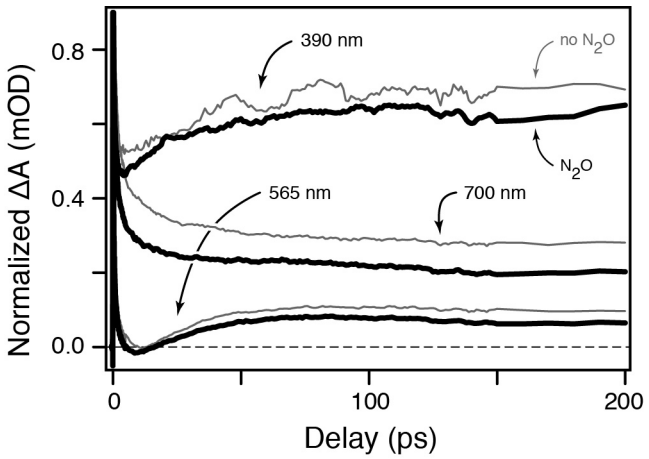

Figure 6.17 Normalized kinetics of DMPT-PFCP in cyclohexane (thin gray lines) and with added N_2O (thick black lines), probing at 390, 565, and 700 nm.

6.7 References

(1) Ward, C. L.; Elles, C. G. Controlling the Excited-State Reaction Dynamics of a Photochromic Molecular Switch with Sequential Two-Photon Excitation. *J. Phys. Chem. Lett.* **2012,** *3*, 2995-3000.

(2) Ward, C. L.; Elles, C. G. Cycloreversion Dynamics of a Photochromic Molecular Switch via One-Photon and Sequential Two-Photon Excitation. *J. Phys. Chem. A* **2014,** *118*, 10011-10019.

(3) Houk, A. L.; Zheldakov, I. L.; Tommey, T. A.; Elles, C. G. Two-Photon Excitation of *trans*-Stilbene: Spectroscopy and Dynamics of Electronically Excited States Above S_1. *J. Phys. Chem. B* **2015,** *119*, 9335-9344.

(4) Houk, A. L.; Allen, S. L.; Bliss, J. R.; Elles, C. G. One- and Two-Photon Absorption Spectroscopy and Quantum Yields of the Cycloreversion Reaction of a Photochromic Molecular Switch. *In Preparation*.

(5) Corredor, C. C.; Belfield, K. D.; Bondar, M. V.; Przhonska, O. V.; Hernandez, F. E.; Kachkovsky, O. D. One- and Two-Photon Photochromism of 3,4-bis-(2,4,5-trimethyl-thiophen-3-yl)furan-2,5-dione. *J. Photochem. Photobiol. A* **2006,** *184*, 177-183.

(6) Ishibashi, Y.; Okuno, K.; Ota, C.; Umesato, T.; Katayama, T.; Murakami, M.; Kobatake, S.; Irie, M.; Miyasaka, H. Multiphoton-Gated Cycloreversion Reactions of Photochromic Diarylethene Derivatives with Low Reaction Yields Upon One-Photon Visible Excitation. *Photochem. Photobiol. Sci.* **2010,** *9*, 172-180.

(7) Mori, K.; Ishibashi, Y.; Matsuda, H.; Ito, S.; Nagasawa, Y.; Nakagawa, H.; Uchida, K.; Yokojima, S.; Nakamura, S.; Irie, M.; Miyasaka, H. One-Color Reversible Control of Photochromic Reactions in a Diarylethene Derivative: Three-Photon Cyclization and Two-Photon Cycloreversion by a Near-Infrared Femtosecond Laser Pulse at 1.28 μm. *J. Am. Chem. Soc.* **2011,** *133*, 2621-2625.

(8) Irie, M.; Fukaminato, T.; Matsuda, K.; Kobatake, S. Photochromism of Diarylethene Molecules and Crystals: Memories, Switches, and Actuators. *Chem. Rev.* **2014,** *114*, 12174-12277.

(9) Larson, E. J.; Friesen, L. A.; Johnson, C. K. An Ultrafast One-Photon and Two-Photon Transient Absorption Study of the Solvent-Dependent Photophysics in All-trans Retinal. *Chem. Phys. Lett.* **1997,** *265*, 161-168.

(10) Larson, E. J.; Pyszczynski, S. J.; Johnson, C. K. Solvent Dependence of Electronic Relaxation in All-trans Retinal Studied by One- and Two-Photon Induced Transient Absorption. *J. Phys. Chem. A* **2001,** *105*, 8136-8144.

(11) Linden, P. A.; Zimmermann, J.; Brixner, T.; Holt, N. E.; Vaswani, H. M.; Hiller, R. G.; Fleming, G. R. Transient Absorption Study of Peridinin and Peridinin−Chlorophyll a−Protein after Two-Photon Excitation. *J. Phys. Chem. B* **2004,** *108*, 10340-10345.

(12) Balkowski, G. M.; Groeneveld, M.; Zhang, H.; Hendrikx, C. C. J.; Polhuis, M.; Zuilhof, H.; Buma, W. J. Femtosecond Spectroscopic Studies of the One- and Two-Photon Excited-State Dynamics of 2,2,17,17-Tetramethyloctadeca-5,9,13-trien-3,7,11,15-tetrayne: A Trimeric Oligodiacetylene. *J. Phys. Chem. A* **2006,** *110*, 11435-11439.

(13) Kosumi, D.; Kusumoto, T.; Fujii, R.; Sugisaki, M.; Iinuma, Y.; Oka, N.; Takaesu, Y.; Taira, T.; Iha, M.; Frank, H. A.; Hashimoto, H. One- and Two-Photon Pump–Probe Optical Spectroscopic Measurements Reveal the S_1 and Intramolecular Charge Transfer States are Distinct in Fucoxanthin. *Chem. Phys. Lett.* **2009,** *483*, 95-100.

(14) Kosumi, D.; Kusumoto, T.; Fujii, R.; Sugisaki, M.; Iinuma, Y.; Oka, N.; Takaesu, Y.; Taira, T.; Iha, M.; Frank, H. A.; Hashimoto, H. Ultrafast S_1 and ICT State Dynamics of a Marine Carotenoid Probed by Femtosecond One- and Two-Photon Pump-Probe Spectroscopy. *J. Lumin.* **2011,** *131*, 515-518.

(15) Ma, L.; Galstyan, G.; Zhang, K.; Kloc, C.; Sun, H.; Soci, C.; Michel-Beyerle, M. E.; Gurzadyan, G. G. Two-Photon-Induced Singlet Fission in Rubrene Single Crystal. *J. Chem. Phys.* **2013,** *138*, 184508.

(16) Pang, Y.; Jones, G. A.; Prantil, M. A.; Fleming, G. R. Unusual Relaxation Pathway from the Two-Photon Excited First Singlet State of Carotenoids. *J. Am. Chem. Soc.* **2010,** *132*, 2264-2273.

(17) Pang, Y.; Prantil, M. A.; Van Tassle, A. J.; Jones, G. A.; Fleming, G. R. Excited-State Dynamics of 8′ -Apo- β -caroten-8′ -al and 7′ ,7′ -Dicyano-7′ -apo- β -carotene Studied by Femtosecond Time-Resolved Infrared Spectroscopy. *J. Phys. Chem. B* **2009,** *113*, 13086-13095.

(18) Moreno, J.; Dobryakov, A. L.; Ioffe, I. N.; Granovsky, A. A.; Hecht, S.; Kovalenko, S. A. Broadband Transient Absorption Spectroscopy with 1- and 2-Photon Excitations: Relaxation Paths and Cross Sections of a Triphenylamine Dye in Solution. *J. Chem. Phys.* **2015,** *143*, 024311.

(19) Moreno, J.; Gerecke, M.; Dobryakov, A. L.; Ioffe, I. N.; Granovsky, A. A.; Bléger, D.; Hecht, S.; Kovalenko, S. A. Two-Photon-Induced versus One-Photon-Induced Isomerization Dynamics of a Bistable Azobenzene Derivative in Solution. *J. Phys. Chem. B* **2015,** *119*, 12281-12288.

(20) Buckup, T.; Weigel, A.; Hauer, J.; Motzkus, M. Ultrafast Multiphoton Transient Absorption of β-Carotene. *Chem. Phys.* **2010,** *373*, 38-44.

(21) Irie, M.; Sakemura, K.; Okinaka, M.; Uchida, K. Photochromism of Dithienylethenes with Electron-Donating Substituents. *J. Org. Chem.* **1995,** *60*, 8305-8309.

(22) Irie, M. Diarylethenes for Memories and Switches. *Chem. Rev.* **2000,** *100*, 1685-1716.

(23) Miyasaka, H.; Murakami, M.; Itaya, A.; Guillaumont, D.; Nakamura, S.; Irie, M. Multiphoton Gated Photochromic Reaction in a Diarylethene Derivative. *J. Am. Chem. Soc.* **2001,** *123*, 753-754.

(24) Miyasaka, H.; Murakami, M.; Okada, T.; Nagata, Y.; Itaya, A.; Kobatake, S.; Irie, M. Picosecond and Femtosecond Laser Photolysis Studies of a Photochromic Diarylethene Derivative: Multiphoton Gated Reaction. *Chem. Phys. Lett.* **2003,** *371*, 40-48.

(25) Murakami, M.; Miyasaka, H.; Okada, T.; Kobatake, S.; Irie, M. Dynamics and Mechanisms of the Multiphoton Gated Photochromic Reaction of Diarylethene Derivatives. *J. Am. Chem. Soc.* **2004,** *126*, 14764-14772.

(26) Ishibashi, Y.; Mukaida, M.; Falkenstrom, M.; Miyasaka, H.; Kobatake, S.; Irie, M. One- and Multi-Photon Cycloreversion Reaction Dynamics of Diarylethene Derivative with Asymmetrical Structure, as Revealed by Ultrafast Laser Spectroscopy. *Phys. Chem. Chem. Phys.* **2009,** *11*, 2640-2648.

(27) Ryo, S.; Ishibashi, Y.; Murakami, M.; Miyasaka, H.; Kobatake, S.; Irie, M. Multiphoton-Gated Photochromic Reaction of Diarylethene Derivatives in PMMA Solid Film. *J. Phys. Org. Chem.* **2007,** *20*, 953-959.

(28) Ishibashi, Y.; Tani, K.; Miyasaka, H.; Kobatake, S.; Irie, M. Picosecond Laser Photolysis Study of Cycloreversion Reaction of a Diarylethene Derivative in Polycrystals: Multiphoton-Gated Reaction. *Chem. Phys. Lett.* **2007,** *437*, 243-247.

(29) Tani, K.; Ishibashi, Y.; Miyasaka, H.; Kobatake, S.; Irie, M. Dynamics of Cyclization, Cycloreversion, and Multiphoton-Gated Reaction of a Photochromic Diarylethene Derivative in Crystalline Phase. *J. Phys. Chem. C* **2008,** *112*, 11150-11157.

(30) Belfield, K. D.; Bondar, M. V.; Corredor , C. C.; Hernandez, F. E.; Przhonska, O. V.; Yao, S. Two-Photon Photochromism of a Diarylethene Enhanced by Förster Resonance Energy Transfer from Two-Photon Absorbing Fluorenes. *ChemPhysChem* **2006,** *7*, 2514-2519.

(31) Corredor, C. C.; Huang, Z.-L.; Belfield, K. D.; Morales, A. R.; Bondar, M. V. Photochromic Polymer Composites for Two-Photon 3D Optical Data Storage. *Chem. Mater.* **2007,** *19*, 5165-5173.

(32) Belfield, K. D.; Bondar, M. V.; Hernandez, F. E.; Masunov, A. E.; Mikhailov, I. A.; Morales, A. R.; Przhonska, O. V.; Yao, S. Two-Photon Absorption Properties of New Fluorene-Based Singlet Oxygen Photosensitizers. *J. Phys. Chem. C* **2009,** *113*, 4706-4711.

(33) Zheldakov, I. L.; Wasylenko, J. M.; Elles, C. G. Excited-State Dynamics and Efficient Triplet Formation in Phenylthiophene Compounds. *Phys. Chem. Chem. Phys.* **2012,** *14*, 6211-6218.

(34) Nagura, C.; Suda, A.; Kawano, H.; Obara, M.; Midorikawa, K. Generation and Characterization of Ultrafast White-Light Continuum in Condensed Media. *Appl. Opt.* **2002,** *41*, 3735-3742.

(35) Buchvarov, I.; Trifonov, A.; Fiebig, T. Toward an Understanding of White-Light Generation in Cubic Media-Polarization Properties Across the Entire Spectral Range. *Opt. Lett.* **2007,** *32*, 1539-1541.

(36) Vivas, M. G.; Siqueira, J. P.; Silva, D. L.; de Boni, L.; Mendonca, C. R. Investigation of the Nonlinear Absorption Spectrum of all-*trans* Retinoic Acid by Using the Steady and Transient Two-Photon Absorption Spectroscopy. *RSC Adv.* **2015,** *5*, 74531-74538.

(37) Sumi, T.; Takagi, Y.; Yagi, A.; Morimoto, M.; Irie, M. Photoirradiation Wavelength Dependence of Cycloreversion Quantum Yields of Diarylethenes. *Chem. Comm.* **2014,** *50*, 3928-3930.

(38) Schütze, M.; Trappe, C.; Kurz, H. Experimental Proof of Saturation in Nonresonant Multiple‐Photon Ionization. *J. Appl. Phys.* **1994,** *76*, 1314-1316.

(39) Charalambidis, D.; Xenakis, D.; Uiterwaal, C. J. G. J.; Maragakis, P.; Jian, Z.; Schröder, H.; Faucher, O.; Lambropoulos, P. Multiphoton Ionization Saturation Intensities and Generalized Cross Sections From ATI Spectra. *J. Phys. B: At. Mol. Opt. Phys.* **1997,** *30*, 1467-1479.

(40) Witzel, B.; Uiterwaal, C. J. G. J.; Schröder, H.; Charalambidis, D.; Kompa, K. L. Analysis of Multiphoton Ionization of Metal Atoms in the Saturation Regime Using Subpicosecond KrF Laser Pulses. *Phys. Rev. A* **1998,** *58*, 3836-3848.

(41) Sauer, M. C.; Arai, S.; Dorfman, L. M. Pulse Radiolysis Studies. VII. The Absorption Spectra and Radiation Chemical Yields of the Solvated Electron in the Aliphatic Alcohols. *J. Chem. Phys.* **1965,** *42*, 708-712.

(42) Jha, K. N.; Bolton, G. L.; Freeman, G. R. Temperature Shifts in the Optical Spectra of Solvated Electrons in Methanol and Ethanol. *J. Phys. Chem.* **1972,** *76*, 3876-3883.

(43) Baxendale, J. H.; Rasburn, E. J. Pulse Radiolysis Study of the Kinetics of Electron Reactions in Liquid n-Hexane at Room Temperature. *J. Chem. Soc., Faraday Trans. 1* **1974,** *70*, 705-717.

(44) Baxendale, J. H.; Bell, C.; Wardman, P. Observations on Solvated Electrons in Aliphatic Hydrocarbons at Room Temperature by Pulse Radiolysis. *J. Chem. Soc., Faraday Trans. 1* **1973,** *69*, 776-786.

(45) Baxendale, J. H. A Pulse Radiolysis Study of Solvated Electrons in Dilute Solutions of Polar Liquids in Nonpolar Solvents. *Can. J. Chem.* **1977,** *55*, 1996-2002.

(46) Hara, M.; Miwa, M.; Takeshita, T.; Watanabe, S. Resonance Two-Photon Ionization of Diarylethene in the Presence of Cyclodextrin. *Int. J. Photoenergy* **2013,** *2013*, 6.

(47) Browne, W. R.; de Jong, J. J. D.; Kudernac, T.; Walko, M.; Lucas, L. N.; Uchida, K.; van Esch, J. H.; Feringa, B. L. Oxidative Electrochemical Switching in Dithienylcyclopentenes, Part 1: Effect of Electronic Perturbation on the Efficiency and Direction of Molecular Switching. *Chem. Eur. J.* **2005,** *11*, 6414-6429.

(48) Logtenberg, H.; Browne, W. R. Electrochemistry of Dithienylethenes and Their Application in Electropolymer Modified Photo- and Redox Switchable Surfaces. *Org. Biomol. Chem.* **2013,** *11*, 233-243.

7. Two-Photon Activation of *p*-Hydroxyphenacyl Phototriggers: Toward Spatially Controlled Release of Diethyl Phosphate and ATP

7.1 Introduction

Photoactivated protecting groups (PPGs) are covalently bound structures that block the normal action of a "caged" compound until the active species is released through photolysis. Using a pulsed light source to selectively release chemical triggers from a PPG enables potentially transformative studies of biological phenomena, both *in vitro* and *in vivo*.[1] Ideally, the active compound is released rapidly and in high yield, while both the protecting group and its photoproducts are biologically inert.[2-4] Beginning with a handful of brief reports describing the release of "caged" nucleotides (cAMP and ATP) from an *o*-nitrobenzyl PPG,[5,6] the search for novel phototriggers has grown into an active field with wide-ranging applications in biology,[5,6] biochemistry,[7,8] and physiology.[9]

The challenge of developing efficient and biologically benign PPGs is complicated by the practical requirement that the chromophore should absorb in the red or near-IR in order to allow better tissue penetration and avoid unintentional photochemical reactions that occur under shorter-wavelength irradiation. However, PPGs designed to absorb at long wavelengths are often severely limited by inefficient photolysis due to the lower excitation energy, as well as limited solubility due to functionalization of the chromophore. As an alternative, therefore, multi-photon excitation has become an increasingly popular method for triggering PPGs at relatively long wavelengths.[10] Multi-photon activation offers the added benefit of spatial control by releasing caged compounds only in the focal volume of a laser, a region as small as 10–100 μm^3, where nonlinear excitation activates the PPG.[11]

Importantly, two-photon excitation (2PE) of a PPG preserves the selectivity of a single chromophore, compared with higher-order multi-photon excitation, which tends to be non-specific. Selective excitation is important for avoiding unwanted photochemistry in the surrounding medium. Depending on the concentration of the caged compound and the quantum efficiency of the uncaging reaction, selective activation of a PPG requires a two-photon absorption cross section (σ_{2PA}) of a few GM or more (1 GM = 10^{-50} $cm^4 \cdot s \cdot molecule^{-1} \cdot photon^{-1}$).[10]

Recent advances in the design, construction, and implementation of new two-photon PPGs have been only moderately successful.[12,13] Although relatively large 2PA cross sections have been achieved, the two-photon quantum yields and fragmentation rates remain low, solubility is still a concern, and most of these novel compounds have not been vetted for biological compatibility.[10] Therefore, rather than proposing a new chromophore, we have examined the two-photon absorption and release properties of *p*-hydroxyphenacyl (*p*HP), a known PPG that meets the requirements of rapid and efficient photolysis following one-photon excitation.[1,7] The *p*HP chromophore is widely adaptable as a phototrigger,[1,7,14-16] and was previously screened for biological compatibility.[2,3,17]

In this chapter, we examine the two-photon activation of *p*HP for the first time. Specifically, we report on the broadband two-photon absorption (2PA) spectroscopy of the *p*HP chromophore, including the parent compound *p*-hydroxyacetophenone (**1**), then demonstrate the feasibility of two-photon activated uncaging of two phosphate derivatives, *p*-hydroxyphenacyl diethyl phosphate (**2**) and *p*-hydroxyphenacyl adenosine triphosphate (**3**), see Scheme 7.1. Photolysis of **2** and **3** is known to efficiently release diethyl phosphate (**4**) and ATP (**5**), respectively, along with the biologically inert photoproduct *p*-hydroxyphenylacetic acid (**6**).[1,18-22]

We also discuss using the deprotonated *p*HP chromophore (pK_a ~ 8) to extend the two-photon excitation spectrum to even longer wavelengths.

Scheme 7.1 Structures of *p*-hydroxyphenacyl compounds.

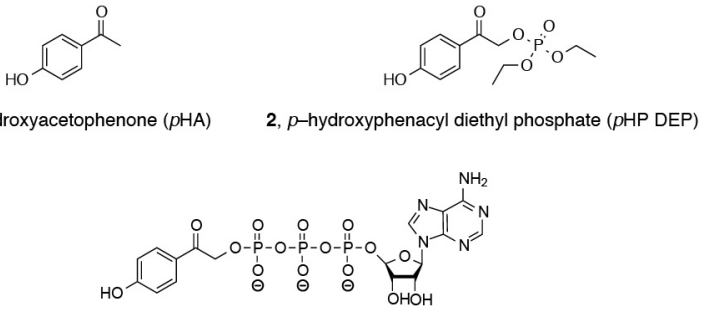

1, *p*–hydroxyacetophenone (*p*HA)

2, *p*–hydroxyphenacyl diethyl phosphate (*p*HP DEP)

3, *p*–hydroxyphenacyl adenosine triphosphate (*p*HP ATP)

7.2 Experimental Methods

The synthesis of **1**, **2**, and **3** (see scheme 7.1) has been described elsewhere.[7,18,23] Here, we measure the broadband two-photon absorption (2PA) spectra of compounds **1** and **2** (as well as the conjugate bases, $\mathbf{1}^-$ and $\mathbf{2}^-$) in methanol, and then monitor the two-photon–induced uncaging reactions of the PPGs **2** and **3** in aqueous solutions. However, the one-photon absorption (1PA) spectra are essentially the same in both solvents. In contrast, we monitor the two-photon–induced uncaging of **2** and **3** dissolved in aqueous solutions using much lower concentrations (~10^{-4} M), because photolysis of the PPG proceeds more rapidly in the presence of water.[7] Although the solubility of compound **3** is sufficiently high to be measured in pure water, we add 5% acetonitrile to improve the solubility of compound **2**. All solvents were used as received without further purification.

We measure broadband 2PA spectra using the pulsed output of a regeneratively amplified Ti:Sapphire laser (Legend Elite HE, Coherent). Briefly, we overlap monochromatic pump and

broadband probe pulses in the sample and measure the attenuation of the probe light as a function of wavelength.[24-27] Absorption only occurs when the two laser pulses overlap in time and space, because neither photon is individually resonant. Scanning the relative delay of the two laser pulses and integrating the transient signal at each wavelength accounts for the temporal dispersion of the broadband probe pulse and eliminates nonresonant contributions, including cross-phase modulation.[28] The integrated transient absorption signal is directly proportional to the absolute 2PA cross section (σ_{2PA}) of the sample at the total energy of the pump and probe photons.[24] Combining the spectra obtained for 2–3 different pump wavelengths gives the 2PA spectrum across a very broad range of excitation energies. All 2PA spectra were measured with parallel relative polarization of the pump and probe light, except where otherwise specified. Details of the experimental setup are described elsewhere.[27]

We monitor the progress of the two-photon–induced uncaging reactions of **2** and **3** by irradiating 1 mL aliquots of each sample with an intense beam of 180 fs laser pulses at 550 nm, while periodically recording the electronic absorption spectrum with a UV-vis spectrophotometer (Thermo Scientific, Evolution 300). The absorption measurements reveal the change in concentration as a function of irradiation time. The sample solution is held in a 1 cm quartz cuvette and continuously mixed with a magnetic stir bar while being irradiated by the laser. The collimated laser beam has a diameter of 230 μm (FWHM) across the entire 1 cm path length of the sample. A collimated beam is necessary to avoid self-focusing and generation of white-light continuum within the sample,[29-31] as observed under tighter focusing conditions. A variable neutral density filter attenuates the laser intensity for power-dependent measurements of the bulk conversion rate. The onset of continuum generation limits the maximum pulse energy to about 10 μJ, which delivers an *average* power (energy/time) of only 10 mW at the 1 kHz repetition rate of

the laser, but a *peak* power of more than 50 MW. The peak intensity (power/area) at the center of the 230 μm diameter laser beam reaches 25 GW/cm^2, which is more than sufficient for nonresonant two-photon absorption by the solute.

7.3 Results

7.3.1 Two-Photon Absorption Spectroscopy

Figure 7.1 compares the one- and two-photon absorption spectra of compounds **1** and **2** in methanol. The broadband 2PA spectrum of compound **1** was obtained across the full two-photon energy range 3.6–6.4 eV using pump pulses at 800, 470, and 370 nm. The 2PA spectrum of **2** was measured over a narrower range (800 and 470 nm pump wavelengths only) because our primary interest is using long-wavelength excitation to trigger the release of caged compounds. Too little sample was available to obtain the 2PA spectrum of **3**.

All of the absorption spectra were measured in methanol because the 2PA measurement requires concentrations of ~0.05 M or higher, which is above the solubility limit of the *p*HP compounds in water. However, the 1PA spectra are essentially the same in methanol and water, with broad absorption bands near 4.5, 5.6, and 6.3 eV. These 1PA bands are a common feature of the *p*HP chromophore.[1,32] Compounds **1** and **2** also have a distinct 2PA band centered near 4.5 eV that closely resembles the 1PA band at the same total excitation energy. In contrast, the higher-energy 2PA bands of compound **1** are much weaker.

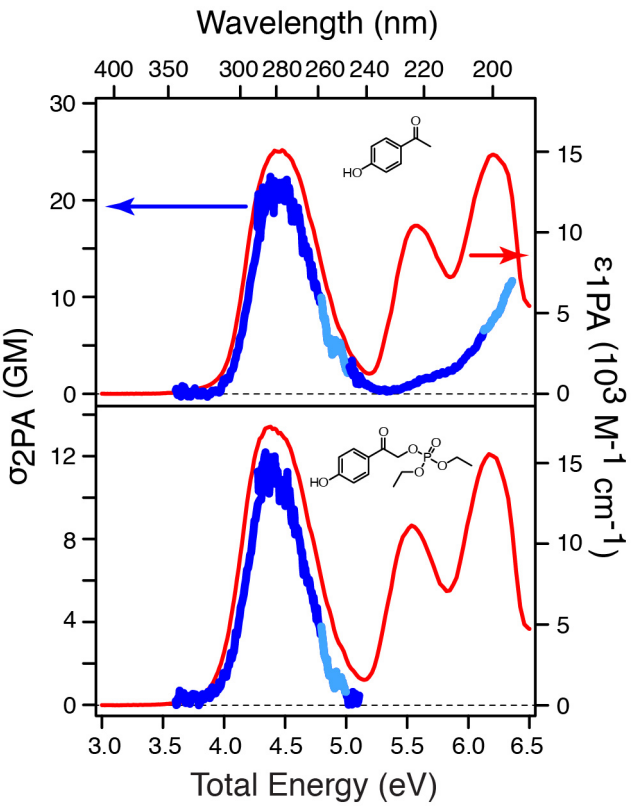

Figure 7.1 Comparison of the 1PA (red) and 2PA (blue) spectra of **1** (top panel; 1.3×10^{-3} M and 0.06 M, respectively) and **2** (bottom panel; 1.9×10^{-3} M and 0.11 M, respectively). All samples are in methanol. The light blue regions indicate where the contributions from solvent Raman scattering have been subtracted from the 2PA spectra.

The maximum cross sections of the lowest-energy 2PA bands of **1** and **2** are σ_{2PA} = 23 ± 11 GM and σ_{2PA} = 11 ± 6 GM, respectively. The estimated uncertainties are 95% confidence limits based on the uncertainties of the experimental parameters of each measurement. The confidence limits are also consistent with the variation that we observe for several independent measurements of the absolute 2PA cross section. Similar to other 2PA measurements, the spatial profile of the excitation laser is the largest source of uncertainty, because the excitation intensity must be known precisely in order to calculate the absolute 2PA cross section from the measured

pump-probe absorption signal.[24] However, the relative uncertainty *across* each broadband 2PA spectrum is much lower than the uncertainty in the absolute 2PA cross sections because we measure all wavelengths simultaneously.

The 2PA spectra in Figure 7.1 were corrected to account for overlapping contributions from stimulated Raman scattering of the probe light by the solvent. recorded with parallel polarization of the pump and probe light. The solvent Raman bands were removed by subtracting the pure solvent signal obtained under identical conditions (see the Appendix). Except for these narrow Raman bands, methanol does not contribute any appreciable signal in the 2PA spectrum below 6.5 eV.

Importantly, the stimulated Raman bands provide a useful reference for measuring the absolute 2PA cross sections, because the two signals have the same dependence on the intensity and spatial overlap of the pump and probe laser beams.[33] The integrated, stimulated Raman cross section that we measure for the C–H stretching bands of pure methanol under the same conditions as in Figure 7.1 (470 nm pump) is about 3.5 times smaller than the previously reported value for spontaneous Raman scattering at a similar pump wavelength (488 nm).[34,35] The discrepancy in Raman cross sections suggests that the spectra in Figure 7.1 may slightly underestimate the absolute 2PA cross sections of the *p*HP chromophore.

The 2PA spectra in Figure 7.1 were recorded with parallel polarization of the pump and probe light. The 2PA cross sections are 2–3 times smaller for perpendicular polarization. The polarization ratio, $r = \sigma_{2PA}(\|)/\sigma_{2PA}(\perp)$, is essentially constant across the entire 2PA spectrum of each compound as shown in Figures 7.7 and 7.9 of the Appendix. We report the average value of the polarization ratio for each compound in Table 7.1.

Table 7.1 One- and two-photon absorption properties of the *p*HP chromophore.[a]

	1	**2**	**1**$^{-}$	**2**$^{-}$
ε_{1PA} (M^{-1} cm^{-1})	15 000 [b]	15 000 [b]	30 000	30 000
σ_{2PA} (GM)	23±11	11±6	32±16	13±8
$\sigma_{2PA}(\|\|)/\sigma_{2PA}(\perp)$	2.5	2.3	~5	–

[a] The uncertainties in parentheses are estimated for 95% confidence limits. [b] Ref. 1.

Figure 7.2 shows the one- and two-photon absorption spectra of the same two compounds under basic conditions, where the phenol functional group is deprotonated (pK_a ~ 8).[21,22] We label the deprotonated compounds **1**$^{-}$ and **2**$^{-}$ to distinguish the different environments. The lowest energy absorption bands of the conjugate bases shift to longer wavelength by ~0.7 eV in both the 1PA and 2PA spectra. Interestingly, the one-photon absorptivity increases by about a factor of two upon deprotonation. The absolute 2PA cross section also increases slightly, to σ_{2PA} = 32±16 GM for **1**$^{-}$ and σ_{2PA} = 13±8 GM for **2**$^{-}$, although the difference is within the range of our experimental uncertainty. As was the case for the protonated compounds, the absolute 2PA cross section is roughly twice as large for the parent chromophore (**1**$^{-}$) compared with the caged phosphate (**2**$^{-}$), although a similar diference is not observed in the 1PA spectra. The one- and two-photon absorption properties of all four species are summarized in Table 7.1.

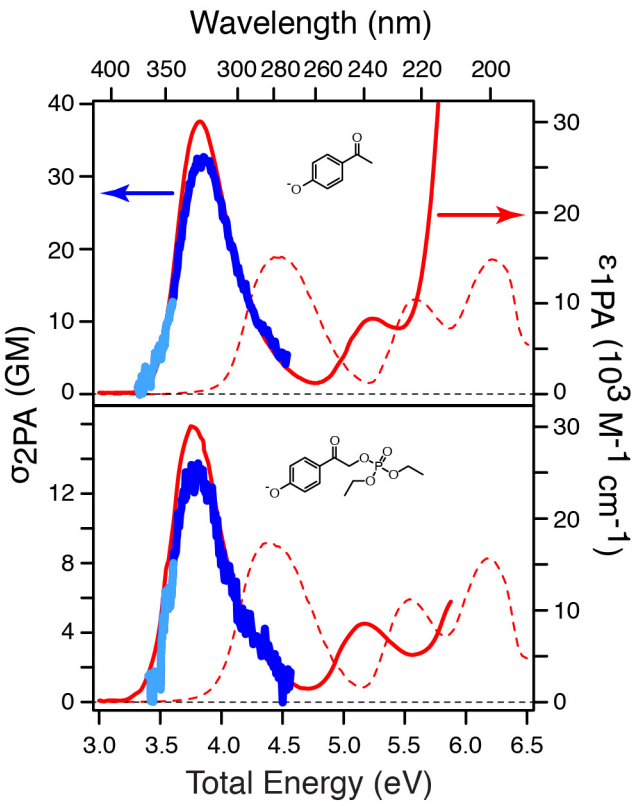

Figure 7.2 Comparison of the 1PA (red) and 2PA (blue) spectra of $\mathbf{1}^-$ (top panel; 6.0×10^{-4} M and 0.06 M, respectively), and of $\mathbf{2}^-$ (bottom panel; 3.3×10^{-4} M and 0.11 M, respectively). All samples are in methanol with ~18 equivalents of NaOH. The light blue regions indicate where the contributions from solvent Raman scattering have been subtracted from the 2PA spectra. For reference, the dashed red lines are the 1PA spectra of **1** and **2** at neutral pH.

7.3.2 Two-Photon Uncaging Efficiency

The photolysis of *p*HP is most efficient in the presence of water,[7] therefore we monitor the uncaging reactions of compounds **2** and **3** in dilute aqueous solutions (~10^{-4} M). Although compound **3** was studied in pure water, we added 5% acetonitrile to the solution of compound **2** in order to improve the solubility. We determine the efficiency of the two-photon–induced *p*HP uncaging reactions by monitoring the absorption spectrum as a function of time under

nonresonant excitation conditions. Recording the linear absorption of the irradiated samples at regular intervals reveals the progress of the uncaging reaction, as shown in Figure 7.3.

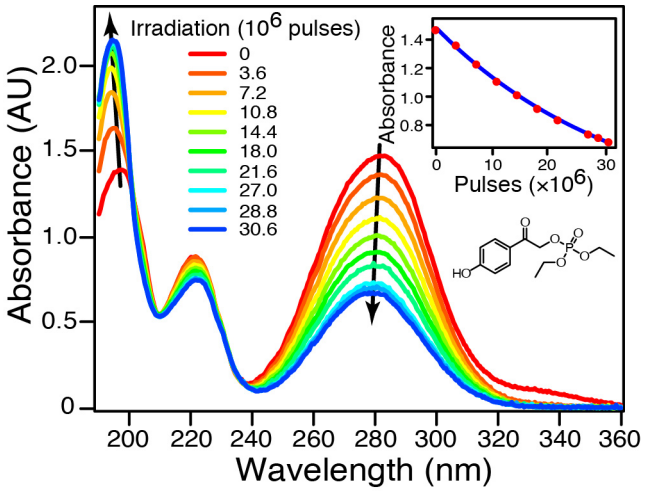

Figure 7.3 Evolution of the absorption spectrum of **2** under irradiation with nonresonant ~100 fs laser pulses at 550 nm. The inset shows the decreasing absorption at 281 nm, including an exponential fit to the data.

The uncaging reactions of **2** and **3** are typically initiated through excitation of the lowest absorption band of the *p*HP chromophore, therefore we use intense, nonresonant later pulses at 550 nm (one-photon equivalent of 275 nm, or 4.5 eV) to induce the two-photon uncaging reactions. Scheme 7.2 shows the well-known photochemistry of **2** and **3** following excitation with a single UV photon. Each compound efficiently releases a caged phosphate (**4** or **5**, respectively), along with the biologically inert *p*-hydroxyphenylacetic acid fragment, **6**.[1,18-22,32] We monitor the progress of the uncaging reaction under the nonresonant excitation conditions by recording the linear absorption spectrum of the irradiated samples at regular intervals.

Scheme 7.2 Photolytic uncaging reactions of the *p*HP chromophore.

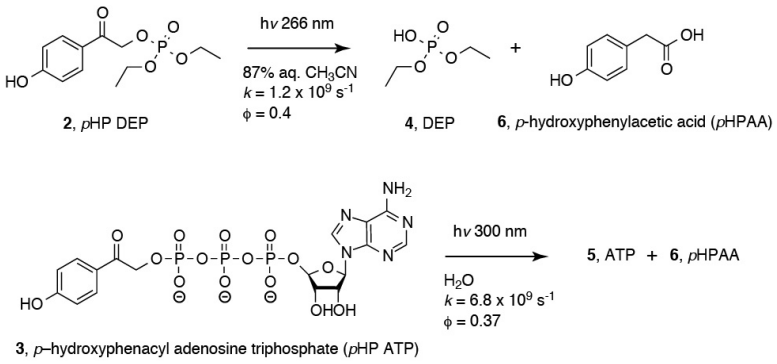

Figure 7.3 shows the evolution of the absorption spectrum for nonresonant irradiation of compound **2**. The absorption spectrum approaches an asymptotic limit that resembles the spectrum of photoproduct **6** (λ_{max} = 275 nm), because the uncaged compound **4** does not have any appreciable absorption in this region.[1,36] In contrast, the asymptotic limit for nonresonant excitation of compound **3** (not shown) has an additional contribution from ATP near 265 nm.

The inset of Figure 7.3 shows the decreasing absorbance of the sample at 280 nm as a function of laser irradiation time. A best fit to the data using a single exponential function with constant offset gives a first-order rate constant of $k_{bulk} = 2.6\times10^{-8}$ per laser pulse. At the 1 kHz repetition rate of our laser, this corresponds to a half-life of 10.7 hours for conversion of the full 1 mL sample. The relatively slow conversion in Figure 7.3 is a consequence of the small fraction of sample that is irradiated by the pulsed laser. The laser irradiates only about 0.17% of the 1 mL sample volume, therefore the overall conversion rate is limited by the small amount of sample that is in the laser volume at any given time. We stir the sample continuously to ensure a uniform concentration throughout the sample cell. Without stirring or diffusion, we estimate that complete conversion of the photocaged compound within the laser volume would take only about 1–2 min. Much shorter conversion times could be achieved with a higher repetition rate of

the laser. We emphasize that this bulk conversion rate is independent of the microscopic photolysis rate, which is of the order 10^9 s^{-1}.[19]

The rate of conversion depends on the excitation rate (excitation events per unit time) and the quantum efficiency of the reaction (fraction of successful uncaging reactions per excitation event). Here, we define the quantum efficiency following two-photon excitation (Φ_{2PA}) as the fraction of molecules that react per two-photon excitation event, rather than per photon, in order to facilitate a comparison with the one-photon conversion efficiency (Φ_{1PA}). The excitation rate depends on the absolute 2PA cross section of the molecule, the concentration, and the laser pulse characteristics. Thus, the conversion rate for irradiation with a pulsed laser is given by Equation 1,

$$\text{Rate} = const \cdot \sigma_{2PA} \cdot \Phi_{2PA} \cdot E^2 \quad (1)$$

Here E is the integrated energy of the incident laser pulses (μJ/pulse). The proportionality constant in Equation 1 is entirely determined by the experimental parameters, including the laser beam diameter, the pulse duration, and the concentration of the sample (see the Appendix).

Measuring the initial conversion rate as a function of increasing intensity, as shown in Figure 7.4 and 7.5, confirms that two-photon activation mechanism for compounds **2** and **3**, respectively. The initial conversion rate is measured in the first 20–30 minutes of irradiation for laser pulse energies ranging from 1 to 10 μJ/pulse. The conversion rates have been corrected to account for a small degree of photoconversion induced by the UV-vis spectrophotometer, as measured using a second sample under the same UV-vis irradiation conditions, but in the absence of laser excitation. As expected, the conversion rate increases quadratically with the laser pulse energy, confirming a two-photon excitation mechanism.

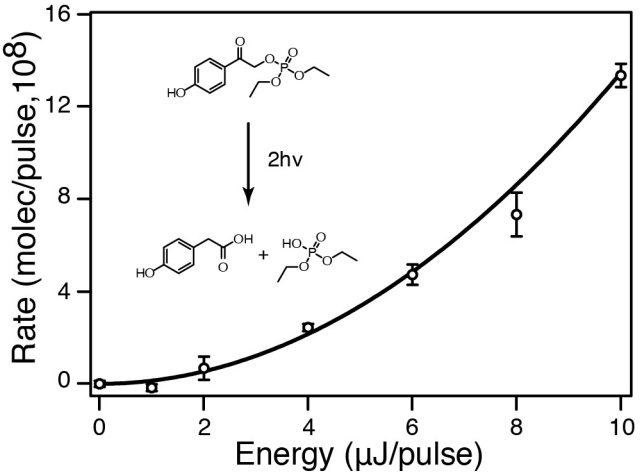

Figure 7.4 Two-photon induced conversion rate as a function of laser intensity (energy per pulse) at 550 nm for compound **2** (9.8×10^{-5} M). The solid line is a fit to the data assuming quadratic power dependence (Equation 1).

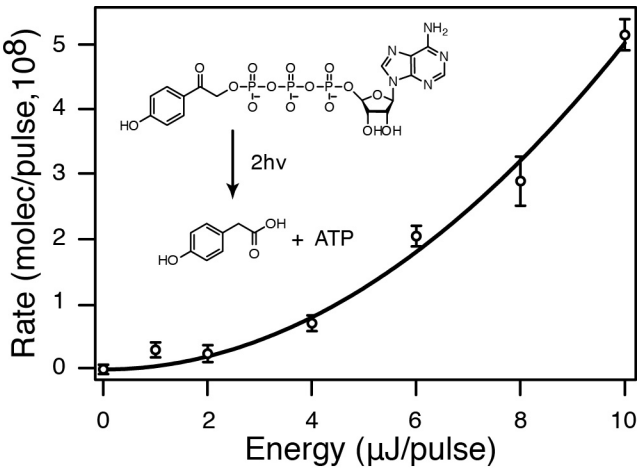

Figure 7.5 Two-photon induced conversion rate as a function of laser intensity (energy per pulse) at 550 nm for compound **3** (6.4×10^{-5} M). The solid line is a fit to the data assuming quadratic power dependence (Equation 1).

Recognizing that the absolute 2PA cross section and two-photon absorption quantum yield are inherent molecular properties, we define an action cross section, $\sigma_{action} = \sigma_{2PA}\Phi_{2PA}$, that combines both quantities and gives a simplified rate equation.

$$\text{Rate} = const \cdot \sigma_{\text{action}} \cdot E^2 \quad (2)$$

The action cross section is the only adjustable parameter in the quadratic fits to the energy-dependent conversion rates in Figures 7.4 and 7.5. The best fits to the data give two-photon action cross sections of 0.53±0.16 GM and 0.28±0.04 GM for compounds **2** and **3**, respectively.

The action cross sections for **2** and **3** are significantly lower than the independently measured absolute 2PA cross sections for the *p*HP chromophore, suggesting relatively low quantum efficiency for the photolysis reaction. For example, using σ_{2PA} = 11 GM from above gives a two-photon quantum efficiency of only Φ_{2PA} = 0.05±0.03 for compound **2**, compared with the one-photon quantum yield of 0.40±0.02.[1]

The discrepancy between the one- and two-photon quantum efficiencies probably reflects incomplete mixing of the sample during irradiation with the laser, which would give a lower than expected bulk conversion rate due to a concentration gradient between the laser focal volume and the bulk solution. In other words, slow mixing compared with the 1 kHz repetition rate of the laser may not fully refresh the sample within the laser volume between laser pulses, causing slower than expected conversion of the full sample. Thus, the values that we obtain represent lower limits for the bulk conversion rates, and probably underestimate the two-photon action cross sections and quantum efficiencies.

An independently measured value for the absolute 2PA cross section of compound **3** is not available for comparison with the measured action cross section, therefore we cannot report a

two-photon reaction quantum yield for that compound. The quantum yields and action cross sections for both compounds are summarized in Table 7.2.

Table 7.2 Photorelease quantum efficiencies.

	2	**3**
Φ_{1PA}[a]	0.40±0.02	0.37±0.01
σ_{action}	>0.53±0.16 GM	>0.28±0.04 GM
Φ_{2PA}	>0.05±0.03	–

[a] From Ref. 7.

7.4 Discussion

7.4.1 Two-Photon Induced Uncaging

The quadratic dependence of the photoconversion rates in Figures 7.4 and 7.5 confirm that nonresonant, two-photon activation of the *p*HP chromophore is possible using a pulsed, visible laser. The absolute 2PA cross section is sufficiently large (>10 GM) to allow selective excitation of the *p*HP chromophore, and therefore selective release of caged compounds. The discrepancy between the one- and two-photon excitation quantum efficiencies is surprising if both excitation methods access the same excited electronic state, although we cannot rule out a difference between the quantum efficiencies, the inconsistency probably reflects incomplete stirring of the sample creating a concentration gradient within the focal volume. Not only do these measurements of the 2PA spectroscopy and quantum efficiencies increase the possibility of spatially and temporally selective photorelease of substrates from the *p*HP PPG at biologically inert wavelengths, but the 2PA spectroscopy also provides new information about the electronic structure of the *p*HP chromophore.

The desire to push the absorption of PPGs from the mid visible range (500–620 nm) to longer wavelengths (550–720 nm) is easily achieved for the *p*HP chromophores by deprotonating the compounds to their respective conjugate bases. The conjugate bases of **1** and **2** display their lowest energy $^{1}\pi\pi^{*}$ transitions at 3.8 eV (Figure 7.2). Recent measurements indicate that the quantum efficiency, although lower in the conjugated bases, is still sufficient for the controlled release of caged compounds under basic conditions.[21,37,38] The 1PA extinction coefficients for the lowest energy bands increase by a factor of two upon deprotonation of the *p*HP chromophores to their respective conjugate bases. A slight increase is also observed for the 2PA transitions, partially offsetting the lower efficiency of the two-photon–induced uncaging reaction of the conjugate bases. The 2PA maxima at 3.8 eV suggest that two-photon excitation of the conjugate bases $\mathbf{1}^{-}$ and $\mathbf{2}^{-}$ with a 650 nm pulsed laser is sufficient for the photorelease of the phosphate substrates and using longer wavelengths would excite the tail of the 2PA band of the conjugate base.

7.4.2 Photoactivated Uncaging Mechanism

The currently accepted mechanism for one-photon uncaging from the *p*HP chromophore involves rapid electronic relaxation within the manifold of singlet excited states, followed by intersystem crossing to a triplet biradical state that ultimately dissociates to give the photoproducts.[1,19,20,36] Although one- and two-photon excitation potentially access different initially excited states, and could therefore lead to different outcomes,[39-42] the similar 1PA and 2PA bands near 4.5 eV suggest that the same excited state may be responsible for both transitions. The similar shifts of the one- and two-photon absorption bands upon deprotonation

support this assertion, as does the polarization dependence of the 2PA spectrum, as described below.

The strong absorption band in the 1PA spectrum of the *p*HP chromophore has been assigned as having primarily $\pi \rightarrow \pi^*$ character, and accesses the L_a-type S_3 ($^1\pi\pi^*$) initially excited state.[32] The two lower-lying singlet states are the L_b-type S_2 ($^1\pi\pi^*$) and S_1 ($^1n\pi^*$), both states have much lower oscillator strength than S_3.[32,43] The weak transition to S_2 is a consequence of the nodal structure for L_a-type transitions,[32,44] whereas symmetry dictates the weak transition strength for S_1. The transition to the lowest-lying $^1n\pi^*$ singlet state is very weak because $n \rightarrow \pi^*$ excitation correlates to a one-photon forbidden ^{1}A" symmetry transition within the C_s point group, but the transition is possible due to coupling with the π orbitals.[32,36]

All of the electronic transitions are two-photon symmetry allowed for the *p*HP compounds studied here, but our 2PA measurements suggest that a transition to the same S_3 ($^1\pi\pi^*$) state dominates the 2PA spectrum. Specifically, we use the 2PA cross sections measured at parallel and perpendicular relative polarizations of the pump and probe beams to determine the 2PA polarization ratios, which gives the character of the two-photon accessible excited states. The 2PA polarization ratio is related to the symmetry of the electronic transition through the spatially averaged two-photon transition dipole tensor, and, in favorable cases, the magnitude of the 2PA polarization ratio reveals the symmetry of the electronically excited state based on symmetry requirements of the transition tensor for the two-photon transition.[45-49] For example, the polarization ratio for molecules belonging to the C_s point group (*e.g.* compound **1**) must be $\geq 4/3$ for totally symmetric transitions that access a final state with A' (rather than A") symmetry. Nontotally symmetric transitions to states with A" symmetry must have a polarization ratio between 1/2 and 4/3. We measure the 2PA cross sections of compounds **1** and **2** to be 2–3 times

smaller for perpendicular, compared with parallel relative polarization, indicating a totally symmetric transition to a state with A' symmetry.

Both the L_a- and L_b-type $^1\pi\pi^*$ transitions of conjugated molecules have A' symmetry, consistent with the polarization ratios that we measure for compound **1**. Although there is no restriction on the polarization ratio for molecules in the lower-symmetry C_1 point group, the polarization ratio for compound **2** reports on the local symmetry of the *p*HP chromophore, which maintains a similar structure as **1**, and therefore will follow a similar trend. Given the relatively large polarization ratio across the spectrum for both **1** and **2** (Table 7.1), we are confident that the strong 2PA band at 4.5 eV accesses a totally symmetric (A') excited state for both compounds, and therefore has little or no contribution from the lower-lying $^1n\pi^*$ state.

7.5 Conclusions

The photochemistry of *p*HP releasing different phosphates, such as ATP and GTP has been thoroughly investigated by a number of research groups.[20,36,50] While there are examples of PPGs that exhibit two-photon induced reactions using longer wavelength excitation[10,13,51-56], most have not been well characterized using one-photon to induce uncaging. Here we have determined the intensity-dependent 2PE-induced release rates of two well-studied caged esters[18,23,57] following irradiation with a Ti:Sapphire pulsed femtosecond laser and we also measured the broadband 2PA spectroscopy of two *p*HP chromophores. Based on the known efficient, rapid release rates, and the demonstrated biocompatibility of *p*HP,[2,3,17] these esters have immediate and wide-ranging applicability as 2PE phototriggers for studies in chemistry and biology.[7,15,16] Furthermore, this study demonstrates the viability of *p*HP as a two-photon activated PPG to spatially control the release of biologically active compounds.

Although the *bulk* conversion rates are rather low for the large (1 mL) samples studied here, controlled release in the small focal volume of a laser beam would be achieved much faster, and could be further accelerated with a higher-repetition rate laser. Our experiments use an amplified Ti:Sapphire laser operating at 1 kHz in order to generate tunable pump pulses and white light probe, but repetition rates up to 100 MHz are possible using Ti:Sapphire oscillators over a narrower wavelength range. Lower pulse energies are easily compensated with tighter focusing conditions in order to achieve comparable conversion rates with excellent spatial resolution when using a higher repetition rate. Shorter pulse durations would also increase the peak intensity, giving increased excitation rates. Conversely, continuous wave (cw) two-photon excitation would not allow for the efficient release of substrates from a *p*HP PPG[58] because the peak intensities necessary for a two-photon excitation process (10-10^{10} W/cm^2) are not easily attained with cw.[51,54,59] Our measurements have peak intensities well within the range needed to induce efficient two-photon uncaging, as well as the *p*HP chromophores we studied have sufficiently large absolute 2PA cross sections (>10 GM) allowing for selective excitation of the *p*HP chromophore to then selectively release bound substrates.

7.6 Appendices

7.6.1 Raman Band Subtraction and Polarization Ratios

The integrated signal we measure for the broadband 2PA spectra of **1**, **2**, $\mathbf{1}^-$, and $\mathbf{2}^-$ in methanol also include a stimulated Raman signal from the pump light dominated by CH_3 stretching modes in methanol. Stimulated Raman contributions from pure methanol are subtracted from the broadband 2PA signal of the molecules to give the full 2PA spectra above. The entire integrated signals obtained for all the molecules in solvent and pure solvents are

below for both relative parallel and perpendicular polarizations of the pump and probe beams (Figures 7.6,7.8, 7.10).

The 2PA parallel and perpendicular polarization measurements are used to determine a polarization ratio, $r = \sigma_{2PA}(\|)/\sigma_{2PA}(\perp)$.[45-47,49] The polarization ratio gives information about the symmetry of the two-photon allowed electronic transitions of the molecules. Molecules that belong to the C_2 point group have $r \geq 4/3$ for totally symmetric transitions with A' character and $r < 4/3$ for nontotally symmetric transitions with A" character.[45-47,49] The measured polarization ratios of the molecules are below (Figures 7.7, 7.9, 7.11). Light gray regions in the spectra of the integrated signals and the polarization ratios indicate stimulated Raman signal and the dark gray regions are areas of small signals, low signal-to-noise resolution, or additional scattering contributions.

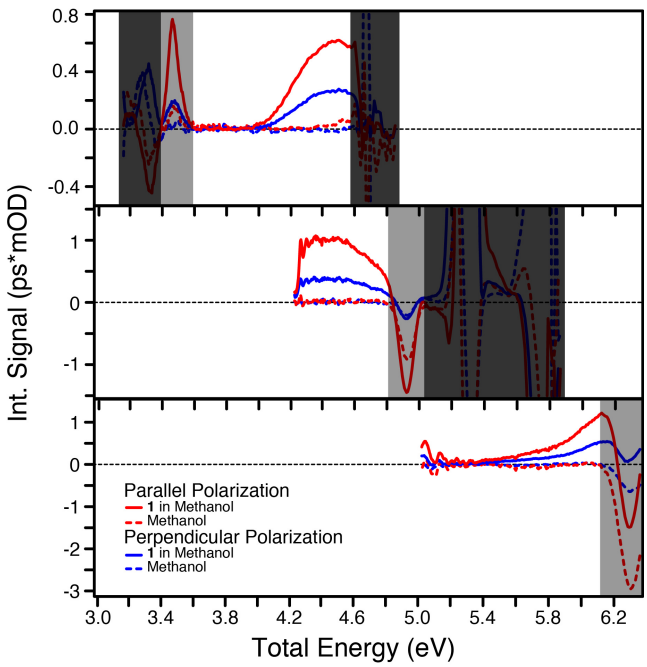

Figure 7.6 **1** in methanol, two-photon absorption (2PA) and stimulated Raman signals integrated in time, plotted against total energy (pump+probe energy). Top row of spectra used a pump excitation of 800 nm, the middle row of spectra used a pump excitation of 470 nm, and the bottom row of spectra used a pump excitation of 370 nm. The light gray boxes indicate the energy range that Raman contributions are present following the excitations listed above and the dark gray boxes indicate areas of either small signals from low probe light signal, low signal-to-noise resolution, or additional scattering contributions (*i.e.* Rayleigh, Stokes, Anti-Stokes scattering).

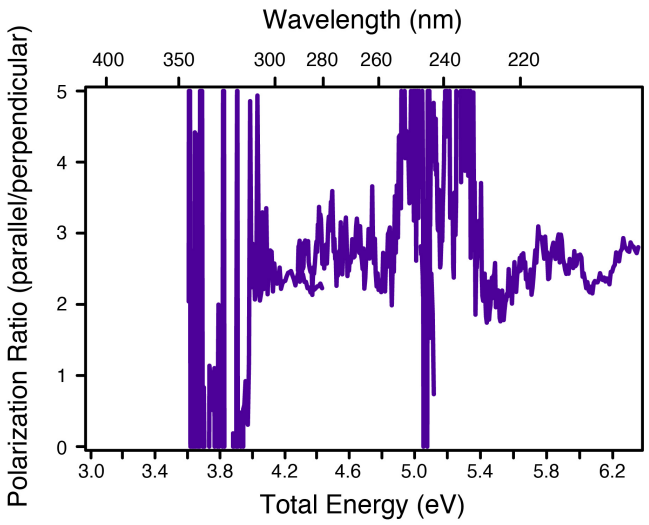

Figure 7.7 **1** in methanol, 2PA parallel/perpendicular polarization ratio, with the Raman contributions subtracted from the 2PA signal.

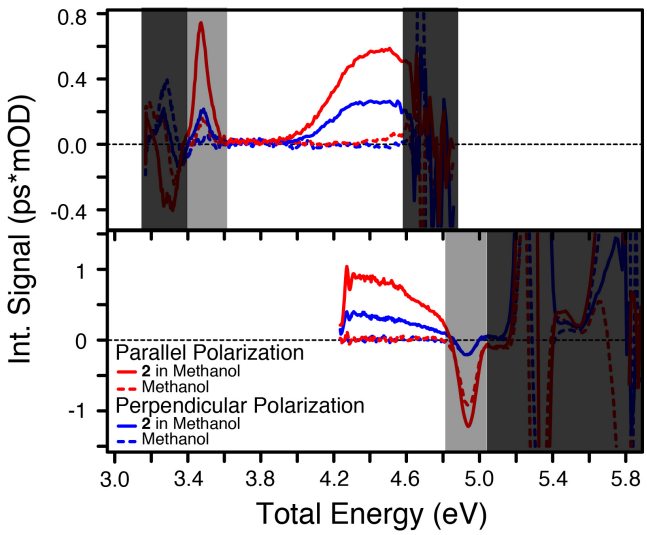

Figure 7.8 **2** in methanol, two-photon absorption (2PA) and stimulated Raman signals integrated in time, plotted against total energy (pump+probe energy). Top row of spectra used a pump excitation of 800 nm and the bottom row of spectra used a pump excitation of 470 nm. The light gray boxes indicate the energy range that Raman contributions are present following the excitations listed above and the dark gray boxes indicate areas of either small signals, low signal-to-noise resolution, or additional scattering contributions (*i.e.* Rayleigh, Stokes, Anti-Stokes scattering).

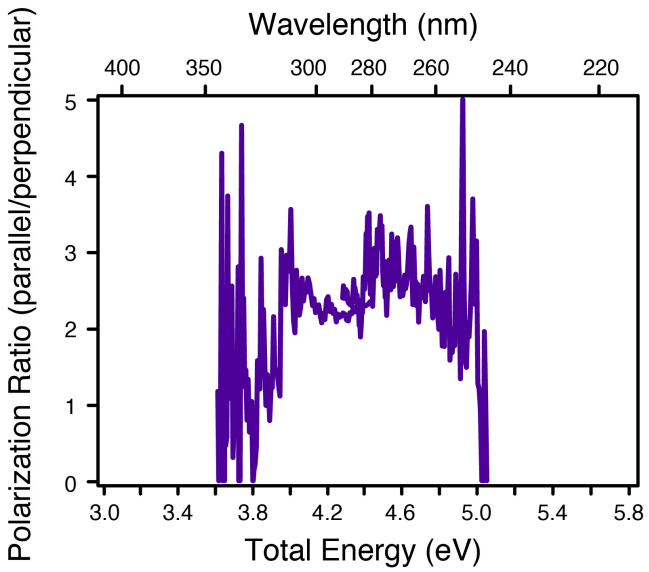

Figure 7.9 **2** in methanol, 2PA parallel/perpendicular polarization ratio, with the Raman contributions subtracted from the 2PA signal.

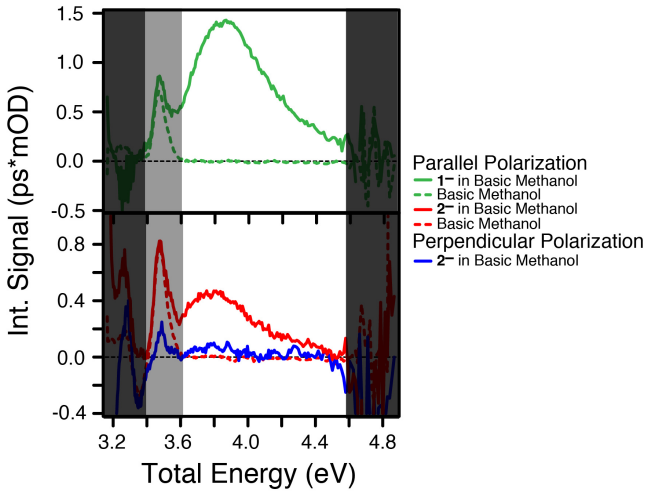

Figure 7.10 (Top) $\mathbf{1}^-$ in basic methanol and (Bottom) $\mathbf{2}^-$ in basic methanol, both excited with 800 nm pump light, two-photon absorption (2PA) and stimulated Raman signals integrated in time, plotted against total energy (pump+probe energy). The light gray boxes indicate the energy range that Raman contributions are present following the excitation listed above and the dark gray boxes indicate areas of either small signals, low signal-to-noise resolution, or additional scattering contributions (*i.e.* Rayleigh, Stokes, Anti-Stokes scattering).

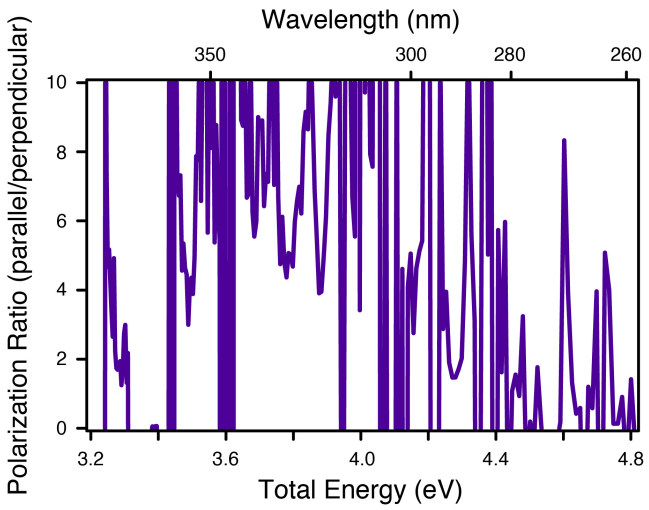

Figure 7.11 $\mathbf{2}^-$ in basic methanol, 2PA parallel/perpendicular polarization ratio, with the Raman contributions subtracted from the 2PA signal.

7.6.2 Stimulated Raman Scattering as an Internal Standard

The stimulated Raman signal of the solvent can be used as an internal standard to more accurately determine the absolute 2PA cross section of the studied molecules.[33] The integrated Raman signal of pure methanol in the time and frequency domain is proportional to the Raman scattering cross section ($d\sigma/d\Omega$) of methanol. The stimulated Raman cross section is given as,

$$\frac{d\sigma}{d\Omega} = -\frac{\ln(10)}{E_{pump}\,\ell\,GF}\,\frac{\hbar\,\omega_{pump}\,\omega_{probe}^2}{8\,\pi^3\,c^2\,N_{solvent}}\int \Delta A(\tau, w)d\tau dw_{Raman} \qquad (3)$$

The absolute 2PA cross is given as,[24]

$$\sigma_{2PA} = \frac{\ln(10)}{E_{pump}\,\ell\,GF}\,\frac{\hbar\,\omega_{pump}}{N_{solvent}}\int \Delta A(\tau)d\tau_{2PA} \qquad (4)$$

Equation 5 uses the determined Gaussian overlap factor (*GF*) from the stimulated Raman cross section measurement of the solvent in Equation 3 and uses the determined *GF* in the absolute 2PA cross section equation to obtain a more accurate absolute 2PA cross section by using the Raman signal as an internal standard.

$$\sigma_{2PA} = -\frac{8\,\pi^3\,c^2\,N_{solvent}}{N_{solute}\,\omega_{probe}^2}\left(\frac{d\sigma}{d\Omega}\right)\frac{\int \Delta A(\tau) d\tau_{2PA}}{\int \Delta A(\tau,w) d\tau dw_{Raman}} \quad (5)$$

The 2PA and Raman cross section parameters are listed in Table 7.3. The determined Raman scattering cross section is compared against the literature spontaneous Raman cross section of methanol to determine accuracy of the measurement (Tables 7.4 and 7.5).[34,35]

Table 7.3 Parameters for the 2PA and Raman cross section measurements.[a,b]

Pump light	370 nm (**1**)	470 nm (**1**)	470 nm (**2**)	800 nm (**1**)[c]	800 nm (**2**)[c]	800 nm (**1**)[c]	800 nm (**1**$^{-}$)[c]	800 nm (**2**)[c]	800 nm (**2**$^{-}$)[c]
E_{pump} (10^{-6}, J/pulse)	1.00 [0.10]	4.54 [0.14]	4.54 [0.14]	1.46 [0.04]	1.46 [0.04]	0.86 [0.03]	0.86 [0.03]	1.42 [0.04]	1.42 [0.04]
GF (cm^{-2})	1330 [40]	236 [21]	236 [21]	335 [28]	335 [28]	793 [106]	793 [106]	431 [41]	431 [41]
ω_{pump} (10^{15}, s^{-1})	5.09	4.01	4.01	2.35	2.35	2.35	2.35	2.35	2.35
ω_{probe} (10^{15}, s^{-1})	3.44	3.49	3.49	2.94	2.94	2.92	2.92	2.92	2.93
N_{solute} (10^{19}, molec/cm^3)	12.4 [0.1]	3.7 [0.7]	6.5 [1.0]	3.7 [0.7]	6.5 [1.0]	3.7 [0.7]	3.7 [0.7]	6.5 [1.0]	3.2 [1.0]
$\int\Delta A(\tau,w)d\tau dw_{Rama}$ (OD)	-0.020 [0.001]	-0.041 [0.001]	-0.041 [0.001]	0.025 [0.001][d]	0.026 [0.001][d]	0.025 [0.001]	0.026 [0.001]	0.028 [0.001]	0.028 [0.001]
$\int\Delta A(\tau)d\tau_{2PA}$ (ps·mOD)	1.19 [0.02]	1.05 [0.02]	0.81 [0.02]	0.62 [0.01]	0.58 [0.01]	0.78 [0.02]	1.42 [0.03]	0.61 [0.01]	0.46 [0.01]

Values in square brackets are reported uncertainties with 95% confidence. [a] Constant parameters for the measurements: ℓ – path length (1 mm); $N_{solvent}$ – number density of the solvent methanol (1.5×10^{22} molec/cm^3); $\hbar$ – Planck's constant; c – Speed of light. [b] Definition of parameters: E_{pump} – incident energy of pump beam; GF – Gaussian overlap factor of pump and probe beams; ω_{pump} – angular frequency of the pump beam; ω_{probe} – angular frequency of the stimulated Raman band in the probe beam; N_{solute} – number density of the solute; $\int\Delta A(\tau,w)d\tau dw_{Raman}$ – integrated stimulated Raman band in the time and frequency domain; $\int\Delta A(\tau)d\tau_{2PA}$ – integrated 2PA signal in the time domain. [c] Signal is the Stokes stimulated Raman scattering signal. [d] Raman and 2PA cross-sections were determined using the Raman contribution in the data set of the sample because of a diminished Raman signal from the pure solvent data set, likely due to a change in the overlap of the pump and probe beams.

Table 7.4 Measured Raman cross sections of pure methanol and basic methanol.

Pump Light	Experiment					Literature
	370 nm (**1**)	470 nm (**1**)	470 nm (**2**)	800 nm ($\mathbf{1}^-$)[a]	800 nm ($\mathbf{2}^-$)[a]	488 nm[b]
Raman Cross Section (10^{-30} cm^2/molec·ser)	13 [3]	1.7 [0.4]	1.7 [0.4]	0.69 [0.21]	0.84 [0.20]	5.7 [0.6]
2PA Cross Section of Solute from Raman Internal Standard (GM)	3.8 [1.1] @ 6.12 eV	87 [25] @ 4.50 eV	38 [11] @ 4.50 eV	265 [76] @ 3.85 eV	91 [35] @ 3.85 eV	–
2PA Cross-Section of Solute from Measured Parameters (GM)	6.0 [2.7] @ 6.12 eV	26 [12] @ 4.50 eV	11 [6] @ 4.50 eV	32 [16] @ 3.85 eV	13 [8] @ 3.85 eV	–

Values in square brackets are reported uncertainties with 95% confidence. [a] Signal is the Stokes stimulated Raman scattering signal. [b] Refs. 34,35.

Table 7.5 Measured Raman cross sections of pure methanol and basic methanol.

Pump Light	Experiment						Literature
	800 nm (**1**)[a]	800 nm (**2**)[a]	800 nm (**1**)[a]	800 nm (**2**)[a]	800 nm ($\mathbf{1}^-$)[a]	800 nm ($\mathbf{2}^-$)[a]	488 nm[b]
Raman Cross Section (10^{-30} cm^2/molec·ser)	0.92 [0.23][c]	0.94 [0.23][c]	0.65 [0.20]	0.82 [0.20]	0.69 [0.21]	0.84 [0.20]	5.7 [0.6]
2PA Cross Section of Solute from Raman Internal Standard (GM)	121 [37][c] @ 4.50 eV	63 [19][c] @ 4.50 eV	155 [44] @ 4.50 eV	61 [23] @ 4.50 eV	265 [76] @ 3.85 eV	91 [35] @ 3.85 eV	–
2PA Cross Section of Solute from Measured Parameters (GM)	20 [9] @ 4.50 eV	11 [5] @ 4.50 eV	18 [9] @ 4.50 eV	9 [4] @ 4.50 eV	32 [16] @ 3.85 eV	13 [8] @ 3.85 eV	–

Values in square brackets are reported uncertainties with 95% confidence. [a] Signal is the Stokes stimulated Raman scattering signal. [b] Refs. 34,35. [c] Raman and 2PA cross sections were determined using the Raman contribution in the data set of the sample because of a diminished Raman signal from the pure solvent data set, likely due to a change in the overlap of the pump and probe beams.

7.6.3 Determination of the Two-Photon Action Cross Section

The two-photon action cross section (σ_{action}) is the product of the two-photon reaction quantum yield (Φ_{2PA}) and the absolute 2PA cross section (σ_{2PA}). The Φ_{2PA} is the measurement of the number of molecules converted per absorption event.

$$\Phi_{2PA} = \frac{\text{molecules converted}}{\text{photon absorption event}} \quad (6)$$

Equation 7 gives the change in irradiance through the path length, ℓ, of the sample when only a two-photon absorption process occurs, where I is the irradiance in the r and z cylindrical coordinates and in time, t, and β is the 2PA coefficient (proportional to σ_{2PA}), N is the number density of the sample, and λ, is the pump wavelength.

$$\frac{\partial I(r,t,z)}{\partial z} = -\beta I(r,t,z)^2 = -\sigma_{2PA} N \left(\frac{\lambda}{hc}\right) I(r,t,z)^2 \quad (7)$$

Using Equation 7 the transmitted irradiance can be determined and is given by Equation 8, where I_0 is the incident irradiance.

$$I(r,t) = \frac{I_0(r,t)}{1+\beta \ell I_0(r,t)} \quad (8)$$

Which can be rewritten as, when $\beta \ell I_0(r,t) \ll 1$,

$$\Delta I = I_0(r,t) - I(r,t) \cong \beta \ell I_0^2(r,t) \quad (9)$$

The total difference in energy, ΔE, is the difference of the total incident energy, E_0, and the energy as a function of position in the path length of the sample, $E(z)$. In Equation 10 ΔE is determined by integrating the difference in irradiance, ΔI, over the time, t, and transverse coordinates, r.

$$\Delta E = E_0 - E(z) = \iint \Delta I \, dr \, dt \quad (10)$$

The incident pulse shape $I_0(r,t)$ is approximated to be Gaussian functions in t and r in Equation 11; where, ρ is the pulse width, τ is the pulse duration, I_0 is the peak irradiance and is given in Equation 12, and E is the integrated pulse energy.

$$I_0(r,t) = I_0 e^{-r^2/2\rho^2} e^{-t^2/2\tau^2} \quad (11)$$

$$I_0 = \frac{E}{(2\pi)^{3/2}\rho^2\tau} \quad (12)$$

Ultimately, ΔE is equal to Equation 13 when Equations 11 and 13 are plugged into Equation 10 and using the relation of β to σ_{2PA} in Equation 7.

$$\Delta E = \frac{\sigma_{2\mathrm{PA}} N \ell E^2}{8\pi^{3/2}\rho^2\tau}\left(\frac{\lambda}{hc}\right) \tag{13}$$

The two-photon excitation rate (Rate, molecules converted per laser pulse) is related to ΔE,

$$\mathrm{Rate} = \frac{\Delta E}{\left(\frac{hc}{\lambda}\right)}\Phi_{2\mathrm{PA}} = \frac{N\ell}{8\pi^{3/2}\rho^2\tau}\left(\frac{\lambda}{hc}\right)^2 E^2\sigma_{2\mathrm{PA}}\Phi_{2\mathrm{PA}} \tag{14}$$

Equation 15 is given in terms of the full width at half maximum (FWHM) of ρ and τ.

$$\mathrm{Rate} = \frac{(2\ln 2)^{3/2} N\ell}{\pi^{3/2}\rho_{FWHM}^2\tau_{FWHM}}\left(\frac{\lambda}{hc}\right)^2 E^2\sigma_{2\mathrm{PA}}\Phi_{2\mathrm{PA}} = \mathrm{constant}\, E^2\sigma_{\mathrm{action}} \tag{15}$$

The two-photon excitation rate is proportional to the product of the two-photon action cross section (σ_{action}) and the square of the integrated energy (E) of the laser pulse (Equation 15), where σ_{action} is the product of the $\sigma_{2\mathrm{PA}}$ and $\Phi_{2\mathrm{PA}}$. The parameters for the two-photon action cross section measurements are listed in Table 7.6.

Table 7.6 Parameters of two-photon action cross sections.[a,b]

Pump light, λ	550 nm (**2**)	550 nm (**3**)
N (10^{19}, molec/cm^3)	5.9 [1.7]	3.8 [0.4]
ℓ (cm)	1.000 [0.002]	1.000 [0.002]
ρ_{FWHM} (10^{-3}, cm)	22.9 [0.8]	22.9 [0.8]
τ_{FWHM} (10^{-15}, s)	87.7 [6.1]	87.7 [6.1]
σ_{action} (GM)	0.53 [0.16]	0.28 [0.04]

Values in square brackets are reported uncertainties with 95% confidence. [a] Constant parameters for the measurements: h – Planck's constant; c – speed of light. [b] Definition of parameters: N – number density of the solute in solution; ℓ – path length; ρ_{FWHM} – full width at half maximum of the beam diameter; τ_{FWHM} – full width at half maximum of the pulse duration; σ_{action} – two-photon action cross section, $\sigma_{\mathrm{action}} = \sigma_{2\mathrm{PA}}\Phi_{2\mathrm{PA}}$.

7.7 References

(1) Klán, P.; Ŝolomek, T.; Bochet, C. G.; Blanc, A.; Givens, R.; Rubina, M.; Popik, V.; Kostikov, A.; Wirz, J. Photoremovable Protecting Groups in Chemistry and Biology: Reaction Mechanisms and Efficacy. *Chem. Rev.* **2013,** *113*, 119-191.

(2) Kötting, C.; Gerwert, K. Time-Resolved FTIR Studies Provide Activation Free Energy, Activation Enthalpy and Activation Entropy for GTPase Reactions. *Chem. Phys.* **2004,** *307*, 227-232.

(3) Kötting, C.; Kallenbach, A.; Suveyzdis, Y.; Wittinghofer, A.; Gerwert, K. The GAP Arginine Finger Movement into the Catalytic Site of Ras Increases the Activation Entropy. *Proc. Natl. Acad. Sci. U.S.A.* **2008,** *105*, 6260-6265.

(4) Kilic, F.; Kashikar, N. D.; Schmidt, R.; Alvarez, L.; Dai, L.; Weyand, I.; Wiesner, B.; Goodwin, N.; Hagen, V.; Kaupp, U. B. Caged Progesterone: A New Tool for Studying Rapid Nongenomic Actions of Progesterone. *J. Am. Chem. Soc.* **2009,** *131*, 4027-4030.

(5) Engels, J.; Schlaeger, E. J. Synthesis, Structure, and Reactivity of Adenosine Cyclic 3',5'-Phosphate Benzyl Triesters. *J. Med. Chem.* **1977,** *20*, 907-911.

(6) Kaplan, J. H.; Forbush, B.; Hoffman, J. F. Rapid Photolytic Release of Adenosine 5'-Triphosphate from a Protected Analog: Utilization by the Na:K Pump of Human Red Blood Cell Ghosts. *Biochemistry* **1978,** *17*, 1929-1935.

(7) Goeldner, M.; Givens, R. S., *Dynamics Studies in Biology*. Wiley-VCH: Weinheim, Germany, 2006.

(8) Syberg, F.; Suveyzdis, Y.; Kötting, C.; Gerwert, K.; Hofmann, E. Time-Resolved Fourier Transform Infrared Spectroscopy of the Nucleotide-Binding Domain from the ATP-Binding

Cassette Transporter MsbA: ATP Hydrolysis is the Rate-Limiting Step in the Catalytic Cycle. *J. Biol. Chem.* **2012,** *287*, 23923-23931.

(9) Ellis-Davies, G. C. R. Caged Compounds: Photorelease Technology for Control of Cellular Chemistry and Physiology. *Nat. Methods* **2007,** *4*, 619-628.

(10) Bort, G.; Gallavardin, T.; Ogden, D.; Dalko, P. I. From One-Photon to Two-Photon Probes: "Caged" Compounds, Actuators, and Photoswitches. *Angew. Chem. Int. Ed.* **2013,** *52*, 4526-4537.

(11) Olson, J. P.; Kwon, H.-B.; Takasaki, K. T.; Chiu, C. Q.; Higley, M. J.; Sabatini, B. L.; Ellis-Davies, G. C. R. Optically Selective Two-Photon Uncaging of Glutamate at 900 nm. *J. Am. Chem. Soc.* **2013,** *135*, 5954-5957.

(12) Warther, D.; Gug, S.; Specht, A.; Bolze, F.; Nicoud, J.-F.; Mourot, A.; Goeldner, M. Two-Photon Uncaging: New Prospects in Neuroscience and Cellular Biology. *Bioorg. Med. Chem.* **2010,** *18*, 7753-7758.

(13) Salierno, M.; Marceca, E.; Peterka, D. S.; Yuste, R.; Etchenique, R. A Fast Ruthenium Polypyridine Cage Complex Photoreleases Glutamate with Visible or IR Light in One and Two Photon Regimes. *J. Inorg. Biochem.* **2010,** *104*, 418-422.

(14) Givens, R. S.; Rubina, M.; Wirz, J. Applications of *p*-Hydroxyphenacyl (*p*HP) and Coumarin-4-ylmethyl Photoremovable Protecting Groups. *Photochem. Photobio. Sci.* **2012,** *11*, 472-488.

(15) Kötting, C.; Suveyzdis, Y.; Bojja, R. S.; Metzler-Nolte, N.; Gerwert, K. Label-Free Screening of Drug-Protein Interactions by Time-Resolved Fourier Transform Infrared Spectroscopic Assays Exemplified by Ras Interactions. *Appl. Spectrosc.* **2010,** *64*, 967-972.

(16) Kötting, C.; Güldenhaupt, J.; Gerwert, K. Time-Resolved FTIR Spectroscopy for Monitoring Protein Dynamics Exemplified by Functional Studies of Ras Protein Bound to a Lipid Bilayer. *Chem. Phys.* **2012,** *396*, 72-83.

(17) Du, X.; Frei, H.; Kim, S. H. The Mechanism of GTP Hydrolysis by Ras Probed by Fourier Transform Infrared Spectroscopy. *J. Biol. Chem.* **2000,** *275*, 8492-8500.

(18) Park, C.-H.; Givens, R. S. New Photoactivated Protecting Groups. 6. *p*-Hydroxyphenacyl: A Phototrigger for Chemical and Biochemical Probes. *J. Am. Chem. Soc.* **1997,** *119*, 2453-2463.

(19) Conrad, P. G.; Givens, R. S.; Hellrung, B.; Rajesh, C. S.; Ramseier, M.; Wirz, J. *p*-Hydroxyphenacyl Phototriggers: The Reactive Excited State of Phosphate Photorelease. *J. Am. Chem. Soc.* **2000,** *122*, 9346-9347.

(20) Givens, R. S.; Heger, D.; Hellrung, B.; Kamdzhilov, Y.; Mac, M.; Conrad, P. G.; Cope, E.; Lee, J. I.; Mata-Segreda, J. F.; Schowen, R. L.; Wirz, J. The Photo-Favorskii Reaction of *p*-Hydroxyphenacyl Compounds is Initiated by Water-Assisted, Adiabatic Extrusion of a Triplet Biradical. *J. Am. Chem. Soc.* **2008,** *130*, 3307-3309.

(21) Givens, R. S.; Stensrud, K.; Conrad, P. G.; Yousef, A. L.; Perera, C.; Senadheera, S. N.; Heger, D.; Wirz, J. *p*-Hydroxyphenacyl Photoremovable Protecting Groups - Robust Photochemistry Despite Substituent Diversity. *Can. J. Chem.* **2011,** *89*, 364-384.

(22) Klíčová, Ĺ.; Šebej, P.; Šolomek, T.; Hellrung, B.; Slavíček, P.; Klán, P.; Heger, D.; Wirz, J. Adiabatic Triplet State Tautomerization of p-Hydroxyacetophenone in Aqueous Solution. *J. Phys. Chem. A* **2012,** *116*, 2935-2944.

(23) Givens, R. S.; Park, C.-H. p-Hydroxyphenacyl ATP[1]: A New Phototrigger. *Tetrahedron Lett.* **1996,** *37*, 6259-6262.

(24) Elles, C. G.; Rivera, C. A.; Zhang, Y.; Pieniazek, P. A.; Bradforth, S. E. Electronic Structure of Liquid Water from Polarization-Dependent Two-Photon Absorption Spectroscopy. *J. Chem. Phys.* **2009,** *130*, 084501.

(25) Belfield, K. D.; Bondar, M. V.; Hernandez, F. E.; Masunov, A. E.; Mikhailov, I. A.; Morales, A. R.; Przhonska, O. V.; Yao, S. Two-Photon Absorption Properties of New Fluorene-Based Singlet Oxygen Photosensitizers. *J. Phys. Chem. C* **2009,** *113*, 4706-4711.

(26) Yamaguchi, S.; Tahara, T. Two-Photon Absorption Spectrum of all-*trans* Retinal. *Chem. Phys. Lett.* **2003,** *376*, 237-243.

(27) Houk, A. L.; Zheldakov, I. L.; Tommey, T. A.; Elles, C. G. Two-Photon Excitation of *trans*-Stilbene: Spectroscopy and Dynamics of Electronically Excited States Above S_1. *J. Phys. Chem. B* **2015,** *119*, 9335-9344.

(28) Kovalenko, S. A.; Dobryakov, A. L.; Ruthmann, J.; Ernsting, N. P. Femtosecond Spectroscopy of Condensed Phases with Chirped Supercontinuum Probing. *Phys. Rev. A* **1999,** *59*, 2369-2384.

(29) Brodeur, A.; Chin, S. L. Ultrafast White-Light Continuum Generation and Self-Focusing in Transparent Condensed Media. *J. Opt. Soc. Am. B* **1999,** *16*, 637-650.

(30) Nagura, C.; Suda, A.; Kawano, H.; Obara, M.; Midorikawa, K. Generation and Characterization of Ultrafast White-Light Continuum in Condensed Media. *Appl. Opt.* **2002,** *41*, 3735-3742.

(31) Buchvarov, I.; Trifonov, A.; Fiebig, T. Toward an Understanding of White-Light Generation in Cubic Media-Polarization Properties Across the Entire Spectral Range. *Opt. Lett.* **2007,** *32*, 1539-1541.

(32) Ma, C.; Kwok, W. M.; Chan, W. S.; Zuo, P.; Wai Kan, J. T.; Toy, P. H.; Phillips, D. L. Ultrafast Time-Resolved Study of Photophysical Processes Involved in the Photodeprotection of *p*-Hydroxyphenacyl Caged Phototrigger Compounds. *J. Am. Chem. Soc.* **2005,** *127*, 1463-1472.

(33) Isobe, K.; Kawano, H.; Suda, A.; Kumagai, A.; Miyawaki, A.; Midorikawa, K. Simultaneous Imaging of Two-Photon Absorption and Stimulated Raman Scattering by Spatial Overlap Modulation Nonlinear Optical Microscopy. *Biomed. Opt. Express* **2013,** *4*, 1548-1558.

(34) Colles, M. J.; Griffiths, J. E. Relative and Absolute Raman Scattering Cross Sections in Liquids. *J. Chem. Phys.* **1972,** *56*, 3384-3391.

(35) Griffiths, J. E. Raman Scattering Cross Sections in Strongly Interacting Liquid Systems: CH_3OH, C_2H_5OH, *i*-C_3H_7OH, $(CH_3)_2CO$, H_2O, and D_2O. *J. Chem. Phys.* **1974,** *60*, 2556-2557.

(36) Ma, C.; Kwok, W. M.; Chan, W. S.; Du, Y.; Kan, J. T. W.; Toy, P. H.; Phillips, D. L. Ultrafast Time-Resolved Transient Absorption and Resonance Raman Spectroscopy Study of the Photodeprotection and Rearrangement Reactions of *p*-Hydroxyphenacyl Caged Phosphates. *J. Am. Chem. Soc.* **2006,** *128*, 2558-2570.

(37) Stensrud, K. F.; Heger, D.; Sebej, P.; Wirz, J.; Givens, R. S. Fluorinated Photoremovable Protecting Groups: The Influence of Fluoro Substituents on the Photo-Favorskii Rearrangement. *Photochem. Photobiol. Sci.* **2008,** *7*, 614-624.

(38) Stensrud, K.; Noh, J.; Kandler, K.; Wirz, J.; Heger, D.; Givens, R. S. Competing Pathways in the Photo-Favorskii Rearrangement and Release of Esters: Studies on Fluorinated p-Hydroxyphenacyl-Caged GABA and Glutamate Phototriggers. *J. Org. Chem.* **2009,** *74*, 5219-5227.

(39) Pang, Y.; Jones, G. A.; Prantil, M. A.; Fleming, G. R. Unusual Relaxation Pathway from the Two-Photon Excited First Singlet State of Carotenoids. *J. Am. Chem. Soc.* **2010,** *132*, 2264-2273.

(40) Buckup, T.; Weigel, A.; Hauer, J.; Motzkus, M. Ultrafast Multiphoton Transient Absorption of β-Carotene. *Chem. Phys.* **2010,** *373*, 38-44.

(41) Ishibashi, Y.; Okuno, K.; Ota, C.; Umesato, T.; Katayama, T.; Murakami, M.; Kobatake, S.; Irie, M.; Miyasaka, H. Multiphoton-Gated Cycloreversion Reactions of Photochromic Diarylethene Derivatives with Low Reaction Yields Upon One-Photon Visible Excitation. *Photochem. Photobiol. Sci.* **2010,** *9*, 172-180.

(42) Moreno, J.; Dobryakov, A. L.; Ioffe, I. N.; Granovsky, A. A.; Hecht, S.; Kovalenko, S. A. Broadband Transient Absorption Spectroscopy with 1- and 2-Photon Excitations: Relaxation Paths and Cross Sections of a Triphenylamine Dye in Solution. *J. Chem. Phys.* **2015,** *143*, 024311.

(43) Yang, Y. L.; Ho, Y.-C.; Dyakov, Y. A.; Hsu, W.-H.; Ni, C.-K.; Sun, Y.-L.; Tsai, W.-C.; Hu, W.-P. Effects of Intramolecular Hydrogen Bonding on the Excited State Dynamics of Phenol Chromophores. *Phys. Chem. Chem. Phys.* **2013,** *15*, 7182-7190.

(44) Platt, J. R. Classification of Spectra of Cata‐Condensed Hydrocarbons. *J. Chem. Phys.* **1949,** *17*, 484-495.

(45) Monson, P. R.; McClain, W. M. Polarization Dependence of the Two-Photon Absorption of Tumbling Molecules with Application to Liquid 1-Chloronaphthalene and Benzene. *J. Chem. Phys.* **1970,** *53*, 29-37.

(46) McClain, W. M. Excited State Symmetry Assignment Through Polarized Two-Photon Absorption Studies of Fluids. *J. Chem. Phys.* **1971,** *55*, 2789-2796.

(47) Monson, P. R.; McClain, W. M. Complete Polarization Study of the Two-Photon Absorption of Liquid 1-Chloronaphthalene. *J. Chem. Phys.* **1972,** *56*, 4817-4825.

(48) McClain, W. M. Two-Photon Molecular Spectroscopy. *Acc. Chem. Res.* **1974,** *7*, 129-135.

(49) Wirth, M. J.; Koskelo, A.; Sanders, M. J. Molecular Symmetry and Two-Photon Spectroscopy. *Appl. Spectrosc.* **1981,** *35*, 14-21.

(50) Chen, X.; Ma, C.; Kwok, W. M.; Guan, X.; Du, Y.; Phillips, D. L. A Theoretical Investigation of p-Hydroxyphenacyl Caged Phototrigger Compounds: An Examination of the Excited State Photochemistry of *p*-Hydroxyphenacyl Acetate. *J. Phys. Chem. A* **2006,** *110*, 12406-12413.

(51) Gug, S.; Charon, S.; Specht, A.; Alarcon, K.; Ogden, D.; Zietz, B.; Leonard, J.; Haacke, S.; Bolze, F.; Nicoud, J. F.; Goeldner, M. Photolabile Glutamate Protecting Group with High One- and Two-Photon Uncaging Efficiencies. *ChemBioChem* **2008,** *9*, 1303-1307.

(52) Gug, S.; Bolze, F.; Specht, A.; Bourgogne, C.; Goeldner, M.; Nicoud, J.-F. Molecular Engineering of Photoremovable Protecting Groups for Two-Photon Uncaging. *Angew. Chem. Int. Ed.* **2008,** *47*, 9525-9529.

(53) Fino, E.; Araya, R.; Peterka, D. S.; Salierno, M.; Etchenique, R.; Yuste, R. RuBi-Glutamate: Two-Photon and Visible-Light Photoactivation of Neurons and Dendritic Spines. *Front. Neural Circuits* **2009,** *3*.

(54) Abate-Pella, D.; Zeliadt, N. A.; Ochocki, J. D.; Warmka, J. K.; Dore, T. M.; Blank, D. A.; Wattenberg, E. V.; Distefano, M. D. Photochemical Modulation of Ras-Mediated Signal Transduction Using Caged Farnesyltransferase Inhibitors: Activation by One- and Two-Photon Excitation. *ChemBioChem* **2012,** *13*, 1009-1016.

(55) Donato, L.; Mourot, A.; Davenport, C. M.; Herbivo, C.; Warther, D.; Leonard, J.; Bolze, F.; Nicoud, J. F.; Kramer, R. H.; Goeldner, M.; Specht, A. Water-Soluble, Donor-Acceptor Biphenyl Derivatives in the 2-(*o*-nitrophenyl)propyl Series: Highly Efficient Two-Photon Uncaging of the Neurotransmitter ɣ-aminobutyric acid at λ=800 nm. *Angew. Chem. Int. Ed.* **2012,** *51*, 1840-1843.

(56) Specht, A.; Bolze, F.; Donato, L.; Herbivo, C.; Charon, S.; Warther, D.; Gug, S.; Nicoud, J.-F.; Goeldner, M. The Donor-Acceptor Biphenyl Platform: A Versatile Chromophore for the Engineering of Highly Efficient Two-Photon Sensitive Photoremovable Protecting Groups. *Photochem. Photobiol. Sci.* **2012,** *11*, 578-586.

(57) Givens, R. S.; Weber, J. F. W.; Jung, A. H.; Park, C.-H., New Photoprotecting Groups: Desyl and p-Hydroxyphenacyl Phosphate and Carboxylate Esters. In *Methods in Enzymology*, Gerard, M., Ed. Academic Press: 1998; Vol. 291, pp 1-29.

(58) Pickens, C. J.; Gee, K. R. Photolabile Thymidine Cleavable with a 532 Nanometer Laser. *Tetrahedron Lett.* **2011,** *52*, 4989-4991.

(59) Cepraga, C.; Gallavardin, T.; Marotte, S.; Lanoe, P. H.; Mulatier, J. C.; Lerouge, F.; Parola, S.; Lindgren, M.; Baldeck, P. L.; Marvel, J.; Maury, O.; Monnereau, C.; Favier, A.; Andraud, C.; Leverrier, Y.; Charreyre, M. T. Biocompatible Well-Defined Chromophore-Polymer Conjugates for Photodynamic Therapy and Two-Photon Imaging. *Polym. Chem.* **2013,** *4*, 61-67.

8. Conclusions

In this dissertation we have used nonlinear excitation, namely two-photon excitation to measure the electronic spectroscopy, excited-state dynamics, and reaction quantum yields of photoactivated molecules. The photoactivated molecules studied include two photochromic molecules, stilbene and 1,2-bis(2,4-dimethyl-5-phenyl-3-thienyl)perfluoro-cyclopentene (DMPT-PFCP), in addition to a phototrigger molecule, *para*-hydroxyphenacyl (*p*HP). By studying higher-lying excited electronic states of photoactivated molecules, we gain insight into the behavior of these states. Additionally, we can use nonlinear excitation to control the photochemical reaction pathways of these photoactivated molecules.

The one- and two-photon absorption spectroscopy provides the excited-state energies of the higher-lying one- and two-photon accessible states. The excited-state dynamics from S_1 following linear excitation are well studied for these photochromic molecules, but much less is known about the dynamics from higher-lying excited states following nonlinear excitation. The excited state dynamics shows the photochromic molecules relax on the order of hundreds of femtoseconds to S_1 following two-photon excitation to higher-lying states, but once on S_1 the same dynamics are observed as with linear excitation.[1] However, ionization induced by excitation with more than two photons opens up a different reaction pathway, which can be used to control the photochemical reaction of these photochromic molecules. The nonlinear excitation process also affects the reaction quantum yields of the photoactivated molecules.

Stilbene is an ideal model photochromic system because this molecule undergoes photoisomerization and photocyclization.[2-6] The complementary spectroscopy and dynamics measurements of stilbene from S_1 have been studied extensively.[2-6] Our one- and two-photon absorption spectroscopy measurements of the stilbene series, consisting of *trans*-stilbene, *cis*-

stilbene, and phenanthrene, indicate we access different excited states with one and two photons for different symmetry point groups. We then excited higher-lying two-photon accessible states of *trans*-stilbene, which induces very fast dynamics from S_N to S_1 and the potential energy surface of S_1 dictates the long time dynamics to the ground S_0 state.[1] Further dynamics measurements following two-photon excitation with better time resolution and/or a better measure of the vibrational dynamics can provide added insight into the structural relaxation and isomerization dynamics of *trans*-stilbene from higher-lying excited states. The ionization of *trans*-stilbene with more than two photons can also be investigated to determine if additional reaction pathways are accessed by these higher-lying excited states.

DMPT-PFCP is a more complicated photochromic model system that reversibly undergoes cyclization and cycloreversion following irradiation with light, from the open-ring isomer to the closed-ring isomer and vice versa, respectively.[4,7] We measured the spectroscopy, quantum yields, and excited-state dynamics of the closed-ring isomer of DMPT-PFCP to investigate the cycloreversion reaction under one- and two-photon excitation. The electronic spectroscopy of the closed-ring isomer has a strong absorption at 3.3 eV in both the one- and two-photon absorption spectra. However, measuring the quantum yields following linear and nonlinear excitation with a total energy of 3.3 eV give reaction yields of ~1.5% and ~16%, respectively; which is not consistent if the same reaction pathways are accessed with one and two photons. The excited-state dynamics measurements revealed distinct differences following linear and nonlinear excitation, as well as with low and high intensity light, indicating a different reaction pathway is accessed under high intensity nonlinear excitation. We have provided evidence of an ionization pathway being accessed following nonlinear excitation with high intensity light, which may explain the order of magnitude increase in the quantum yield

following nonlinear excitation. We have suggested the 2+ cation of the closed-ring isomer undergoes the cycloreversion reaction to produce more open-ring isomer molecules, but the spectroelectrochemistry of DMPT-PFCP would provide spectroscopic information about the 1+ and 2+ cations. Additional electron quenching experiments with N_2O or another quencher of the quantum yields and dynamics following nonlinear excitation will give further evidence for the ionization mechanism under these excitation conditions.

The phototrigger we studied, *p*HP photochemically releases substrates quickly and efficiently in aqueous media and produces only one major photoproduct.[8-14] The lowest energy absorption bands in the UV are the same for one- and two-photon absorption of the protonated *p*HP compounds. For the deprotonated *p*HP compounds the lowest energy absorption bands are red-shifted and are the same for one- and two-photon absorption. *p*HP has previously been shown to photochemically release a substrate with linear excitation[8-14] and we have demonstrated the same release following two-photon excitation. Measuring the two-photon induced release of substrates from deprotonated *p*HP compounds would provide a means of releasing substrates with visible to near-IR light rather than with UV light.

The two-photon absorption spectroscopy, dynamics, and quantum yield measurements presented in this dissertation are useful for a wide range of applications. These nonlinear measurements of the photochromic molecules studied here can provide fundamental molecular information about applications from optical data storage to three-dimensional microfabrication. For the phototrigger molecules these measurements can be utilized for applications ranging from two-photon fluorescence microscopy to drug delivery. The nonlinear measurements presented in this dissertation provide fundamental information about the two-photon accessible excited states of these photochromic and phototrigger molecule and this information can be used to improve

two-photon excitation applications. Computational studies of two-photon accessible excited states can provide spectroscopic information about the photoactivated molecules, ranging from the excited-state energies to the character of the excited states. Transient Raman spectroscopy can be used to obtain any vibrational information about the higher-lying excited states of these photoactivated molecules. Studying the two-photon absorption spectroscopy, dynamics, and quantum yields of the photochromic molecules in the solid phase can provide additional information about the higher-lying excited states without complications from solvents.

This dissertation used nonlinear excitation, specifically two-photon excitation to study higher-lying excited states to develop a better fundamental understanding of these states. The nonlinear spectroscopy research on photoactivated molecules in this dissertation provides complimentary information about two-photon accessible exited states, excited-state dynamics, and reaction quantum yields. These nonlinear measurements answer fundamental questions about the higher-lying excited states of these photoactivated molecules. Additionally, we have demonstrated that nonlinear excitation can be used to selectively control the outcome of photochemical reactions. This research also provides spectroscopic benchmarks for further experimental and computational studies of the character and energies of the two-photon accessible states of these photochromic and phototrigger molecules.

8.1 References

(1) Houk, A. L.; Zheldakov, I. L.; Tommey, T. A.; Elles, C. G. Two-Photon Excitation of *trans*-Stilbene: Spectroscopy and Dynamics of Electronically Excited States Above S_1. *J. Phys. Chem. B* **2015,** *119*, 9335-9344.

(2) Waldeck, D. H. Photoisomerization Dynamics of Stilbenes. *Chem. Rev.* **1991,** *91*, 415-436.

(3) Meier, H. The Photochemistry of Stilbenoid Compounds and Their Role in Materials Technology. *Angew. Chem. Int. Ed. Engl.* **1992,** *31*, 1399-1420.

(4) Irie, M. Diarylethenes for Memories and Switches. *Chem. Rev.* **2000,** *100*, 1685-1716.

(5) Kay, E. R.; Leigh, D. A.; Zerbetto, F. Synthetic Molecular Motors and Mechanical Machines. *Angew. Chem. Int. Ed.* **2007,** *46*, 72-191.

(6) Budyka, M. F. Diarylethylene Photoisomerization and Photocyclization Mechanisms. *Russ. Chem. Rev.* **2012,** *81*, 477-493.

(7) Irie, M.; Fukaminato, T.; Matsuda, K.; Kobatake, S. Photochromism of Diarylethene Molecules and Crystals: Memories, Switches, and Actuators. *Chem. Rev.* **2014,** *114*, 12174-12277.

(8) Goeldner, M.; Givens, R. S., *Dynamics Studies in Biology*. Wiley-VCH: Weinheim, Germany, 2006.

(9) Klán, P.; Ŝolomek, T.; Bochet, C. G.; Blanc, A.; Givens, R.; Rubina, M.; Popik, V.; Kostikov, A.; Wirz, J. Photoremovable Protecting Groups in Chemistry and Biology: Reaction Mechanisms and Efficacy. *Chem. Rev.* **2013,** *113*, 119-191.

(10) Park, C.-H.; Givens, R. S. New Photoactivated Protecting Groups. 6. *p*-Hydroxyphenacyl: A Phototrigger for Chemical and Biochemical Probes. *J. Am. Chem. Soc.* **1997,** *119*, 2453-2463.

(11) Conrad, P. G.; Givens, R. S.; Hellrung, B.; Rajesh, C. S.; Ramseier, M.; Wirz, J. *p*-Hydroxyphenacyl Phototriggers: The Reactive Excited State of Phosphate Photorelease. *J. Am. Chem. Soc.* **2000,** *122*, 9346-9347.

(12) Givens, R. S.; Heger, D.; Hellrung, B.; Kamdzhilov, Y.; Mac, M.; Conrad, P. G.; Cope, E.; Lee, J. I.; Mata-Segreda, J. F.; Schowen, R. L.; Wirz, J. The Photo-Favorskii Reaction of *p*-Hydroxyphenacyl Compounds is Initiated by Water-Assisted, Adiabatic Extrusion of a Triplet Biradical. *J. Am. Chem. Soc.* **2008,** *130*, 3307-3309.

(13) Givens, R. S.; Stensrud, K.; Conrad, P. G.; Yousef, A. L.; Perera, C.; Senadheera, S. N.; Heger, D.; Wirz, J. *p*-Hydroxyphenacyl Photoremovable Protecting Groups - Robust Photochemistry Despite Substituent Diversity. *Can. J. Chem.* **2011,** *89*, 364-384.

(14) Klíčová, Ĺ.; Šebej, P.; Šolomek, T.; Hellrung, B.; Slavíček, P.; Klán, P.; Heger, D.; Wirz, J. Adiabatic Triplet State Tautomerization of p-Hydroxyacetophenone in Aqueous Solution. *J. Phys. Chem. A* **2012,** *116*, 2935-2944.